Contents

Chapter 3: Accurate Relativistic Calculations Including QED Contributions for Few-Electron Systems

W. R. Johnson[a] *, K. T. Cheng[b] † and M. H. Chen[b] ‡

[a]Department of Physics, 225 Nieuwland Science Hall
University of Notre Dame, Notre Dame, IN 46556 USA

[b]University of California
Lawrence Livermore National Laboratory
Livermore, CA 94550 USA

ABSTRACT

Relativistic calculations of energy levels of few-electron atoms, including the Breit interaction and radiative corrections, are treated using two different methods: many-body perturbation theory and the configuration-interaction method. The point of departure of both methods is the no-pair Hamiltonian, which is briefly discussed. To set a foundation for few-electron calculations, the Dirac equation is reviewed and radiative corrections to energy levels of one-electron ions are discussed. Second-, third-, and all-order many-body perturbation theory, is applied to ground states of helium and helium-like ions and to low-lying states of lithium and lithium-like ions. Corrections from the Breit interaction are included in these studies. The relativistic configuration-interaction method, including the Breit interaction, is applied to excited states of few-electron atoms and ions. Radiative corrections to $n = 2$ states of highly-charged lithium-like ions are discussed in detail.

1. INTRODUCTION

Although the proper point of departure for relativistic atomic structure calculations is quantum electrodynamics (QED), very few atomic structure calculations have been carried out entirely within the QED framework. Indeed, almost all relativistic calculations of the structure of many-electron atoms are based on some variant of the Hamiltonian introduced a half century ago by Brown and Ravenhall [1] to understand the helium fine structure. By decoupling the electron and radiation fields in QED to order α (the fine-structure constant) using a contact transformation, Brown and Ravenhall obtained a relativistic momentum-space Hamiltonian in which the electron-electron Coulomb interaction was surrounded by positive-energy projection operators. Owing to the fact that contributions from virtual electron-positron pairs are automatically projected out of

*email: johnson@nd.edu
†email: ktcheng@llnl.gov
‡email: chen7@llnl.gov

the Brown-Ravenhall Hamiltonian, it has become known as the *no-pair* Hamiltonian. A configuration-space version of the no-pair Hamiltonian was given by Mittleman [2, 3, 4], who showed how to incorporate the Breit interaction and lowest-order radiative corrections. An alternative derivation of the configuration-space no-pair Hamiltonian starting from the Bethe-Salpeter formulation of QED was given by Sucher [5].

Later, in Sec. 4, we will give a detailed discussion of the need for the no-pair Hamiltonian in relativistic calculations, its limitations, and its relation to QED. To establish a foundation for our studies of few-electron systems, we start in Sec. 2 with a discussion of the one-electron central-field Dirac equation and radiative corrections to one-electron atoms. In Sec. 3 we describe many-body perturbation theory (MBPT) calculations of few-electron atoms, and finally, in Sec. 4 we turn to relativistic configuration-interaction (RCI) calculations.

2. CENTRAL-FIELD DIRAC EQUATION

As a lowest-order approximation, we assume that each electron in an atom moves in the field of the nucleus, which is described by a potential $V_{\rm nuc}(r)$, and a spherically symmetric potential $U(r)$ that accounts approximately for the remaining bound electrons. The wave functions ϕ_k describing possible states of the electron satisfy the one-electron Dirac equation

$$h\,\phi_k = [h_0 + U(r)]\,\phi_k = \epsilon_k \phi_k, \tag{1}$$

where the eigenvalue ϵ_k is the electron energy and h_0 is the Dirac Hamiltonian,

$$h_0 = c\,\boldsymbol{\alpha}\cdot\boldsymbol{p} + mc^2\beta + V_{\rm nuc}(r); \tag{2}$$

$\boldsymbol{\alpha}$ and β being 4×4 Dirac matrices,

$$\boldsymbol{\alpha} = \begin{pmatrix} 0 & \boldsymbol{\sigma} \\ \boldsymbol{\sigma} & 0 \end{pmatrix}, \qquad \beta = \begin{pmatrix} I & 0 \\ 0 & -I \end{pmatrix}. \tag{3}$$

In the above equation, I is the 2×2 identity matrix and $\boldsymbol{\sigma} = (\sigma_x, \sigma_y, \sigma_z)$ are Pauli matrices,

$$I = \begin{pmatrix} 1 & 0 \\ 0 & 1 \end{pmatrix}, \quad \sigma_x = \begin{pmatrix} 0 & 1 \\ 1 & 0 \end{pmatrix}, \quad \sigma_y = \begin{pmatrix} 0 & -i \\ i & 0 \end{pmatrix}, \quad \sigma_z = \begin{pmatrix} 1 & 0 \\ 0 & -1 \end{pmatrix}. \tag{4}$$

(Later, when making comparisons with nonrelativistic calculations, we subtract the electron rest energy mc^2 from ϵ_k.) The choice of the potential $U(r)$ is more or less arbitrary; one important choice being the (Dirac) Hartree-Fock potential. Eigenstates of Eq. (1) fall into three classes: bound states with $-mc^2 < \epsilon_k < mc^2$, continuum states with $\epsilon_k > mc^2$, and "negative energy" (positron) states $\epsilon_k \le -mc^2$. Since contributions from virtual electron-positron pairs are projected out of the no-pair Hamiltonian, we will be concerned primarily with bound and continuum electron states.

The total angular momentum is given by $\boldsymbol{J} = \boldsymbol{L} + \boldsymbol{S}$, where $\boldsymbol{L}$ is the orbital angular momentum, and $\boldsymbol{S}$ is the 4×4 spin angular momentum matrix,

$$\boldsymbol{S} = \frac{1}{2}\begin{pmatrix} \boldsymbol{\sigma} & 0 \\ 0 & \boldsymbol{\sigma} \end{pmatrix}, \tag{5}$$

in units $\hbar = 1$. It is an elementary exercise to show that $\boldsymbol{J}$ commutes with the Dirac Hamiltonian h, provided the potential U is isotropic. We may, therefore, classify eigenstates of h according to the eigenvalues of energy, J^2 and J_z. Eigenstates of J^2 and J_z are easily constructed using the two-component representation of $\boldsymbol{S}$. They are the spherical spinors defined in the following subsection.

2.1. Spherical Spinors

We combine spherical harmonics $Y_{lm}(\theta, \phi)$, which are eigenstates of L^2 and L_z, with two-component spinors, χ_μ, which are eigenstates of S^2 and S_z, to form spherical spinors, which are eigenstates of J^2 and J_z. The spherical spinors are denoted by $\Omega_{jlm}(\theta, \phi)$ and are defined by the equation

$$\Omega_{j\,lm}(\theta, \phi) = \sum_\mu C(l, 1/2, j; m-\mu, \mu, m) Y_{l\,m-\mu}(\theta, \phi)\chi_\mu \,. \tag{6}$$

where $C(j_1, j_2, j_3; m_1, m_2, m_3)$ is a Clebsch-Gordan coefficient [6]. The two-component spinors χ_μ with $\mu = \pm 1/2$ are

$$\chi_{1/2} = \begin{pmatrix} 1 \\ 0 \end{pmatrix} \quad \text{and} \quad \chi_{-1/2} = \begin{pmatrix} 0 \\ 1 \end{pmatrix}. \tag{7}$$

From the discussion above, we obtain the following two-component representations of spherical spinors for the two possible values, $j = l \pm 1/2$:

$$\Omega_{l+1/2\ l\ m}(\theta, \phi) = \begin{pmatrix} \sqrt{\frac{l+m+1/2}{2l+1}}\, Y_{l\ m-1/2}(\theta, \phi) \\ \sqrt{\frac{l-m+1/2}{2l+1}}\, Y_{l\ m+1/2}(\theta, \phi) \end{pmatrix}, \tag{8}$$

$$\Omega_{l-1/2\ l\ m}(\theta, \phi) = \begin{pmatrix} -\sqrt{\frac{l-m+1/2}{2l+1}}\, Y_{l\ m-1/2}(\theta, \phi) \\ \sqrt{\frac{l+m+1/2}{2l+1}}\, Y_{l\ m+1/2}(\theta, \phi) \end{pmatrix}. \tag{9}$$

Spherical spinors are eigenfunctions of $\boldsymbol{\sigma} \cdot \boldsymbol{L}$ and, therefore, of the operator

$$K = -1 - \boldsymbol{\sigma} \cdot \boldsymbol{L}.$$

The eigenvalue equation for K is

$$K\Omega_{jlm}(\theta, \phi) = \kappa\ \Omega_{jlm}(\theta, \phi)\,, \tag{10}$$

where the (integer) eigenvalues are $\kappa = -l - 1$ for $j = l + 1/2$, and $\kappa = l$ for $j = l - 1/2$. These values can be summarized as $\kappa = \mp(j + 1/2)$ for $j = l \pm 1/2$. The value of κ determines both j and l. Consequently, the more compact notation, $\Omega_{\kappa m} \equiv \Omega_{jlm}$ can be used. Spherical spinors satisfy the orthogonality relations

$$\int_0^\pi \sin\theta d\theta \int_0^{2\pi} d\phi\, \Omega^\dagger_{\kappa' m'}(\theta, \phi)\Omega_{\kappa m}(\theta, \phi) = \delta_{\kappa' \kappa}\delta_{m' m}\,. \tag{11}$$

The parity operator P maps $\boldsymbol{r} \to -\boldsymbol{r}$. In spherical coordinates, the operator P transforms $\phi \to \phi + \pi$ and $\theta \to \pi - \theta$. Under a parity transformation,

$$PY_{lm}(\theta, \phi) = Y_{lm}(\pi - \theta, \phi + \pi) = (-1)^l Y_{lm}(\theta, \phi)\,. \tag{12}$$

It follows that the spherical spinors are eigenfunctions of P having eigenvalues $\pi = (-1)^l$. The two spinors $\Omega_{\kappa m}(\theta,\phi)$ and $\Omega_{-\kappa m}(\theta,\phi)$, corresponding to the same value of j, have values of l differing by one unit and, therefore, have opposite parity. Spherical spinors transform as

$$\boldsymbol{\sigma}\cdot\hat{\boldsymbol{r}}\,\Omega_{\kappa m}(\theta,\phi) = -\Omega_{-\kappa m}(\theta,\phi)\,, \tag{13}$$

under the operator $\boldsymbol{\sigma}\cdot\hat{\boldsymbol{r}}$, where $\hat{\boldsymbol{r}} = \boldsymbol{r}/r$.

Now, let us consider the operator $\boldsymbol{\sigma}\cdot\boldsymbol{p}$. Using Eq. (13), it follows that

$$\boldsymbol{\sigma}\cdot\boldsymbol{p} = \boldsymbol{\sigma}\cdot\hat{\boldsymbol{r}}\;\boldsymbol{\sigma}\cdot\hat{\boldsymbol{r}}\;\boldsymbol{\sigma}\cdot\boldsymbol{p} = -i\,\boldsymbol{\sigma}\cdot\hat{\boldsymbol{r}}\left[i\,\hat{\boldsymbol{r}}\cdot\boldsymbol{p} - \frac{\boldsymbol{\sigma}\cdot(\boldsymbol{r}\times\boldsymbol{p})}{r}\right]. \tag{14}$$

In deriving this equation, we have made use of the identity

$$\boldsymbol{\sigma}\cdot\boldsymbol{A}\;\boldsymbol{\sigma}\cdot\boldsymbol{B} = \boldsymbol{A}\cdot\boldsymbol{B} + i\,\boldsymbol{\sigma}\cdot(\boldsymbol{A}\times\boldsymbol{B})\,.$$

From Eq. (14), it follows that

$$\boldsymbol{\sigma}\cdot\boldsymbol{p}\;f(r)\;\Omega_{\kappa m}(\theta,\phi) = i\left(\frac{df}{dr} + \frac{\kappa+1}{r}f\right)\;\Omega_{-\kappa m}(\theta,\phi)\,, \tag{15}$$

again in units $\hbar = 1$. The identities (13) and (15) are important in the reduction of the central-field Dirac equation to radial form.

2.2. Separation of Dirac Equation

Solutions to the Dirac equation in a spherically symmetric potential $U(r)$ for a state with energy ϵ and angular momentum quantum numbers $(\kappa\, m)$ take the form

$$\phi_{\kappa m}(\boldsymbol{r}) = \frac{1}{r}\begin{pmatrix} iP_\kappa(r) & \Omega_{\kappa m}(\hat{r}) \\ Q_\kappa(r) & \Omega_{-\kappa m}(\hat{r}) \end{pmatrix}. \tag{16}$$

We find, with the help of the identities (13,15), that the radial functions $P_\kappa(r)$ and $Q_\kappa(r)$ satisfy the coupled first-order differential equations:

$$(V + mc^2)\,P_\kappa + c\left(\frac{d}{dr} - \frac{\kappa}{r}\right)Q_\kappa \;=\; \epsilon\,P_\kappa \tag{17}$$

$$-c\left(\frac{d}{dr} + \frac{\kappa}{r}\right)P_\kappa + (V - mc^2)\,Q_\kappa \;=\; \epsilon\,Q_\kappa \tag{18}$$

where $V(r) = V_{\rm nuc}(r) + U(r)$. The normalization condition for the orbital $\phi_{\kappa m}(\boldsymbol{r})$,

$$\int \phi^\dagger_{\kappa m}(\boldsymbol{r})\phi_{\kappa m}(\boldsymbol{r})\,d^3r = 1, \tag{19}$$

becomes

$$\int_0^\infty [\,P^2_\kappa(r) + Q^2_\kappa(r)\,]\,dr = 1, \tag{20}$$

when expressed in terms of the radial functions $P_\kappa(r)$ and $Q_\kappa(r)$. The radial eigenfunctions and their associated eigenvalues, ϵ, can be determined analytically for a Coulomb potential. In most other cases, however, the eigenvalue problem must be solved numerically.

2.3. Bound-State Coulomb Wave Functions

In this subsection, we discuss analytical solutions to the radial Dirac equations (17) and (18) for the special case $V(r) = -Z/r$. (We adopt atomic units where $\hbar = e = m = 1$ in this section and in the sequel.) As a first step in our analysis, we examine these equations at large values of r. Retaining only dominant terms as $r \to \infty$, we find

$$c\,\frac{dQ_\kappa}{dr} = (\epsilon - c^2)P_\kappa\,, \tag{21}$$

$$c\,\frac{dP_\kappa}{dr} = -(\epsilon + c^2)Q_\kappa\,, \tag{22}$$

in atomic units. This pair of equations can be converted into the second-order equation

$$c^2\frac{d^2P_\kappa}{dr^2} + (\epsilon^2 - c^4)P_\kappa = 0, \tag{23}$$

which has two linearly independent solutions, $e^{\pm\lambda r}$, with $\lambda = \sqrt{c^2 - \epsilon^2/c^2}$. The physically acceptable solution is

$$P_\kappa(r) = e^{-\lambda r}\,. \tag{24}$$

The corresponding solution Q_κ is given by

$$Q_\kappa(r) = \sqrt{\frac{c^2-\epsilon}{c^2+\epsilon}}\;e^{-\lambda r}. \tag{25}$$

Factoring the asymptotic behavior, we express the radial functions in the form

$$P_\kappa = \sqrt{1+\epsilon/c^2}\;e^{-\lambda r}(F_1 + F_2)\,, \tag{26}$$

$$Q_\kappa = \sqrt{1-\epsilon/c^2}\;e^{-\lambda r}(F_1 - F_2)\,. \tag{27}$$

Substituting this *ansatz* into (17) and (18), we find that the functions F_1 and F_2 satisfy the coupled equations

$$\frac{dF_1}{dx} = \frac{\epsilon Z}{c^2\lambda x}F_1 + \left(\frac{Z}{\lambda x} - \frac{\kappa}{x}\right)F_2\,, \tag{28}$$

$$\frac{dF_2}{dx} = -\left(\frac{Z}{\lambda x} + \frac{\kappa}{x}\right)F_1 + \left(1 - \frac{\epsilon Z}{c^2\lambda x}\right)F_2\,, \tag{29}$$

where $x = 2\lambda r$.

We seek solutions to Eqs. (28,29) that have the limiting forms $F_1 = a_1 x^\gamma$ and $F_2 = a_2 x^\gamma$ as $x \to 0$. Substituting these expressions into (28) and (29) and retaining only the most singular terms, we find:

$$\frac{a_2}{a_1} = \frac{\gamma - \epsilon Z/c^2\lambda}{-\kappa + Z/\lambda} = \frac{-\kappa - Z/\lambda}{\gamma + \epsilon Z/c^2\lambda}. \tag{30}$$

Clearing fractions in the right-hand equality, leads to the result $\gamma^2 = \kappa^2 - Z^2/c^2 = \kappa^2 - \alpha^2 Z^2$. Here, we have used the fact that $c = 1/\alpha$ in atomic units. The physically

acceptable value of γ is given by the positive square root, $\gamma = \sqrt{\kappa^2 - \alpha^2 Z^2}$. Next, we use Eq. (28) to express F_2 in terms of F_1,

$$F_2 = \frac{1}{-\kappa + Z/\lambda}\left[x\frac{dF_1}{dx} - \frac{\epsilon Z}{c^2\lambda}\,F_1\right]. \tag{31}$$

This equation, in turn, can be used to eliminate F_2 from Eq. (29), leading to

$$x\frac{d^2F_1}{dx^2} + (1-x)\frac{dF_1}{dx} - \left(\frac{\gamma^2}{x^2} - \frac{\epsilon Z}{c^2\lambda}\right)F_1 = 0\,. \tag{32}$$

Finally, we write

$$F_1(x) = x^\gamma F(x)\,, \tag{33}$$

and find that the function $F(x)$ satisfies Kummer's equation,

$$x\frac{d^2F}{dx^2} + (b-x)\frac{dF}{dx} - aF = 0\,, \tag{34}$$

where $a = \gamma - \epsilon Z/c^2\lambda$, and $b = 2\gamma + 1$. The solutions to Eq. (34) that are regular at the origin are the confluent hypergeometric functions [7, chap. VI]:

$$\begin{aligned} F(a,b,x) &= 1 + \frac{a}{b}x + \frac{a(a+1)}{b(b+1)}\frac{x^2}{2!} + \frac{a(a+1)(a+2)}{b(b+1)(b+2)}\frac{x^3}{3!} \\ &\quad + \cdots + \frac{a(a+1)\cdots(a+k-1)}{b(b+1)\cdots(b+k-1)}\frac{x^k}{k!} + \cdots\,. \end{aligned} \tag{35}$$

Therefore,

$$F_1(x) = x^\gamma\, F(a,b,x)\,. \tag{36}$$

The function $F_2(x)$ can also be expressed in terms of confluent hypergeometric functions. Using Eq. (31), we find

$$F_2(x) = \frac{x^\gamma}{(-\kappa + Z/\lambda)}\left(x\frac{dF}{dx} + aF\right) = \frac{(\gamma - \epsilon Z/c^2\lambda)}{(-\kappa + Z/\lambda)}x^\gamma F(a+1,b,x)\,. \tag{37}$$

Combining these results, we obtain the following expressions for the radial Dirac functions:

$$\begin{aligned} P_\kappa(r) &= \sqrt{1+\epsilon/c^2}\,e^{-x/2}x^\gamma[(-\kappa + Z/\lambda)F(a,b,x) \\ &\qquad + (\gamma - \epsilon Z/c^2\lambda)F(a+1,b,x)\big], \end{aligned} \tag{38}$$

$$\begin{aligned} Q_\kappa(r) &= \sqrt{1-\epsilon/c^2}\,e^{-x/2}x^\gamma[(-\kappa + Z/\lambda)F(a,b,x) \\ &\qquad - (\gamma - \epsilon Z/c^2\lambda)F(a+1,b,x)\big]. \end{aligned} \tag{39}$$

These solutions have yet to be normalized.

We now turn to the eigenvalue problem. First, we examine the behavior of the radial functions at large r. We find:

$$F(a,b,x) \;\rightarrow\; \frac{\Gamma(b)}{\Gamma(a)}\, e^x x^{a-b}[1+O(|x|^{-1})]\,, \tag{40}$$

$$aF(a+1,b,x) \;\rightarrow\; \frac{\Gamma(b)}{\Gamma(a)}\, e^x x^{a+1-b}[1+O(|x|^{-1})]\,. \tag{41}$$

The resulting radial wave function, therefore, grows exponentially unless the coefficient of the exponential in Eqs. (40) and (41) vanishes. It follows that the radial wave functions are normalizable if, and only if, the coefficient of the exponential in Eqs. (40) and (41) vanishes. This occurs at the poles of $\Gamma(a)$, which are located at the points $a = -n_r$, where $n_r = 0, -1, -2, \cdots$. We define the principal quantum number n through the relation, $n = k + n_r$, where $k = |\kappa| = j + 1/2$. The eigenvalue equation $a = -(n-k)$ can, therefore, be written

$$\epsilon Z/c^2\lambda = \gamma + n - k\,. \tag{42}$$

The case $a = -n_r = 0$ requires special attention. In this case, one can solve the eigenvalue equation to find $k = Z/\lambda$. From this, it follows that the two factors $-\kappa + Z/\lambda$ and $\gamma - \epsilon Z/c^2\lambda$ in Eqs. (38) and (39) vanish for $\kappa = k > 0$. Non-trivial states with $n_r = 0$ occur only for $\kappa < 0$. Therefore, for a given value of $n > 0$ there are $2n-1$ possible eigenfunctions: n eigenfunctions with $\kappa = -1, -2, \cdots -n$, and $n-1$ eigenfunctions with $\kappa = 1, 2, \cdots n-1$.

Solving the eigenvalue equation for ϵ, we obtain

$$\epsilon_{n\kappa} = \frac{c^2}{\sqrt{1 + \frac{\alpha^2 Z^2}{(\gamma+n-k)^2}}}\,. \tag{43}$$

It is interesting to note that the Dirac energy levels depend only on $k = |\kappa|$. Those levels having the same values of n and j, but different values of ℓ are degenerate. Thus, for example, the $2s_{1/2}$ and $2p_{1/2}$ levels in hydrogen-like ions are degenerate. By contrast, levels with the same value of n and ℓ but different values of j, such as the $2p_{1/2}$ and $2p_{3/2}$ levels, have different energies. The separation between two such levels is the fine-structure interval. Expanding (43) in powers of αZ, we find

$$\epsilon_{n\kappa} = c^2 - \frac{Z^2}{2n^2} - \frac{\alpha^2 Z^4}{2n^3}\left(\frac{1}{k} - \frac{3}{4n}\right) + \;\cdots\,. \tag{44}$$

The first term in this expansion is just the electron's rest energy (mc^2) expressed in atomic units. The second term is precisely the nonrelativistic Coulomb-field binding energy. The third term is the leading fine-structure correction. The fine-structure energy difference between the $2p_{3/2}$ and $2p_{1/2}$ levels in hydrogen is predicted by this formula to be

$$\Delta\epsilon_{2p} = \frac{\alpha^2}{32}\,\text{a.u.} = 0.3652\,\text{cm}^{-1}\,,$$

in close agreement with the measured separation 0.3659 cm^{-1}. The separation of the $2s_{1/2}$ and $2p_{1/2}$ levels in hydrogen is measured to be $0.0354\,\mathrm{cm}^{-1}$. The degeneracy between these two levels predicted by the Dirac equation is lifted by the Lamb-shift, discussed in the following subsection.

Let us introduce the (non-integer) parameter $N = Z/\lambda = (\gamma + n - k)c^2/\epsilon$. From (43), we find $N = \sqrt{n^2 - 2(n-k)(k-\gamma)}$. Thus, $N = n$ when $n = k$. With this definition, the coefficients of the hypergeometric functions in Eqs. (38) and (39) can be written

$$(-\kappa + Z/\lambda) = (N - \kappa)\,, \tag{45}$$
$$(\gamma - \epsilon Z/c^2\lambda) = -(n-k)\,. \tag{46}$$

Introducing the normalization factor

$$N_{n\kappa} = \frac{1}{N\,\Gamma(2\gamma+1)}\sqrt{\frac{Z\,\Gamma(2\gamma+1+n-k)}{2\,(n-k)!\,(N-\kappa)}}\,, \tag{47}$$

we can write the radial Dirac Coulomb wave functions as

$$P_{n\kappa}(r) = \sqrt{1+\epsilon_{n\kappa}/c^2}\,N_{n\kappa}e^{-x/2}x^{\gamma}\left[(N-\kappa)F(-n+k,2\gamma+1,x)\right.$$
$$\left.-\,(n-k)F(-n+k+1,2\gamma+1,x)\right]\,, \tag{48}$$
$$Q_{n\kappa}(r) = \sqrt{1-\epsilon_{n\kappa}/c^2}\,N_{n\kappa}e^{-x/2}x^{\gamma}\left[(N-\kappa)F(-n+k,2\gamma+1,x)\right.$$
$$\left.+\,(n-k)F(-n+k+1,2\gamma+1,x)\right]\,. \tag{49}$$

These functions satisfy the normalization condition (20). It should be noted that the ratio of the scale factors in (48) and (49) is $\sqrt{(1-\epsilon_{n\kappa}/c^2)/(1+\epsilon_{n\kappa}/c^2)} \approx \alpha Z/2n$. Thus, $Q_{n\kappa}(r)$ is several orders of magnitude smaller than $P_{n\kappa}(r)$ for $Z = 1$. For this reason, $P_{n\kappa}$ and $Q_{n\kappa}$ are referred to as the large and small components of the radial Dirac wave function, respectively.

As a specific example, let us consider the $1s_{1/2}$ ground state of an electron in a hydrogen-like ion with nuclear charge Z. For this state, $n = 1$, $\kappa = -1$, $k = 1$, $\gamma = \sqrt{1-\alpha^2Z^2}$, $\epsilon_{n\kappa}/c^2 = \gamma$, $N = 1$, $\lambda = Z$ and $x = 2Zr$. Therefore,

$$P_{1-1}(r) = \sqrt{\frac{1+\gamma}{2}}\sqrt{\frac{2Z}{\Gamma(2\gamma+1)}}\,(2Zr)^{\gamma}e^{-Zr}\,,$$
$$Q_{1-1}(r) = \sqrt{\frac{1-\gamma}{2}}\sqrt{\frac{2Z}{\Gamma(2\gamma+1)}}\,(2Zr)^{\gamma}e^{-Zr}\,.$$

2.4. QED Corrections to One-Electron Energy Levels

The energy difference between the $2s_{1/2}$ and $2p_{1/2}$ levels in hydrogen and in hydrogen-like ions (the Lamb shift) includes contributions from radiative corrections, reduced mass, nuclear recoil, and finite nuclear size. These corrections are discussed here and in the following two subsections.

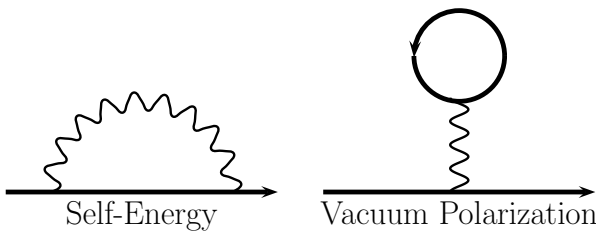

Figure 1. Feynman diagrams representing the one-loop self-energy and vacuum-polarization corrections. Heavy lines represent bound-electrons and wavy lines represent virtual photons.

Self Energy

The largest contribution to the Lamb shift in one-electron atoms or ions arises from the electron self-energy and can be expressed in terms of a slowly varying functions $F(nlj,\, \alpha Z)$ and $G(nlj,\, \alpha Z)$ through

$$\Delta E_{\rm SE} = \left(\frac{\alpha}{\pi}\right) \frac{\alpha^2 Z^4}{n^3}\; F_{\rm SE}(nlj,\, \alpha Z) + \left(\frac{\alpha}{\pi}\right)^2 \frac{\alpha^2 Z^4}{n^3}\; G_{\rm SE}(nlj, \alpha Z),\ \text{(a.u.)}, \tag{50}$$

where $F_{\rm SE}(nlj,\, \alpha Z)$ gives the one-loop correction illustrated in the left panel of Fig. 1, and $G_{\rm SE}(nlj,\, \alpha Z)$ gives the much smaller two-loop self-energy corrections. For low Z, it is common to expand the functions F and G in powers of αZ, however, the convergence of such expansions is poor and it is necessary to resort to numerical evaluation to obtain reliable values for intermediate and high Z. One can write

$$\begin{aligned} F_{\rm SE}(nlj, \alpha Z) = \frac{4}{3} \Bigg\{ & \left[\ln(\alpha Z)^{-2} + \frac{11}{24}\right] \delta_{l0} + L_{nl} - \frac{3 C_{lj}}{8(2l+1)} + \alpha Z\, A_5 \\ & + (\alpha Z)^2 \left[A_{61} \ln(\alpha Z)^{-2} + A_{62} \ln^2(\alpha Z)^{-2} + H(\alpha Z)\right] \Bigg\}, \end{aligned} \tag{51}$$

where the term L_{nl} on the first line is the Bethe logarithm,

$$L_{nl} = \begin{cases} -2.984128556 & \text{for } 1s \\ -2.811768893 & \text{for } 2s \\ 0.030016709 & \text{for } 2p \end{cases}$$

The coefficient C_{lj} on the first line of Eq. (51) is

$$C_{lj} = \begin{cases} 1/(l+1) & \text{for } j = l + 1/2 \\ -1/l & \text{for } j = l - 1/2 \end{cases}$$

The remaining coefficients of the "confirmed" radiative corrections are

$$\begin{aligned} A_5 &= 3\pi \left[1 + \frac{11}{128} - \frac{1}{2}\ln 2\right] \delta_{l0} \\ A_{61} &= \begin{cases} 7\ln 2 - 63/80 & \text{for } 1s \\ 4\ln 2 + 67/40 & \text{for } 2s \\ 103/240 & \text{for } 2p_{1/2} \\ 29/120 & \text{for } 2p_{3/2} \end{cases} \\ A_{62} &= -\frac{3}{4}\,\delta_{l0}. \end{aligned}$$

The function $H(\alpha Z)$ in Eq. (51) gives the remainder of $F_{\rm SE}(nlj,\,\alpha Z)$ not represented by the analytical expressions above. It can be inferred from the precise numerical values given by Jentschura et al. [8] for Z from 1 to 5 and from Mohr [9, 10, 11, 12] and Mohr and Kim [13] for higher Z. Finite nuclear size corrections to $F_{\rm SE}(nlj,\,\alpha Z)$ have been accurately evaluated by Mohr and Soff [14]. A similar expansion for the much smaller two-loop corrections $G_{\rm SE}(nlj,\,\alpha Z)$ is given in Refs. [15, 16]. The leading term in that expansion is

$$\begin{aligned} G_{\rm SE}(nlj,0) &= \frac{C_{lj}}{2l+1}\left[\frac{197}{144} + \frac{\pi^2}{12} - \frac{\pi^2}{2}\ln(2) + \frac{3}{4}\,\zeta(3)\right] \\ &\quad + \left[-\frac{4819}{1296} - \frac{49\pi^2}{108} + 2\pi^2\ln(2) - 3\,\zeta(3)\right]\delta_{l0}\,, \end{aligned} \tag{52}$$

where $\zeta(n)$ is Riemann's zeta function.

Vacuum Polarization

The next largest correction to the Lamb shift is the vacuum polarization correction illustrated by the Feynman diagram given in the right panel of Fig. 1. We write the vacuum-polarization correction as

$$\Delta E_{\rm VP} = \left(\frac{\alpha}{\pi}\right)\frac{\alpha^2 Z^4}{n^3}\,F_{\rm VP}(nlj,\,\alpha Z) + \left(\frac{\alpha}{\pi}\right)^2\frac{\alpha^2 Z^4}{n^3}\,G_{\rm VP}(nlj,\,\alpha Z).$$

The dominant contribution to $F_{\rm VP}$ can be obtained as the expectation value of the Uehling potential [17]

$$\delta V(r) = -\frac{2\alpha Z}{3\pi r}\int_1^\infty dt\sqrt{t^2-1}\left(\frac{1}{t^2} + \frac{1}{2t^4}\right)e^{-2ctr}. \tag{53}$$

The expectation value of the Uehling potential leads to

$$F_{\rm VP}(nlj,0) = -\frac{4}{15}\,\delta_{l0}.$$

Corrections to $F_{\rm VP}(nlj,\alpha Z)$ of order $(\alpha Z)^n$ with $n \geq 1$ have been considered by Wichmann and Kroll [18] and lead to an expansion similar to that given above for the self-energy. Coefficients of higher-order terms in the Uehling and Wichmann and Kroll potentials are given, for example, in Ref. [16].

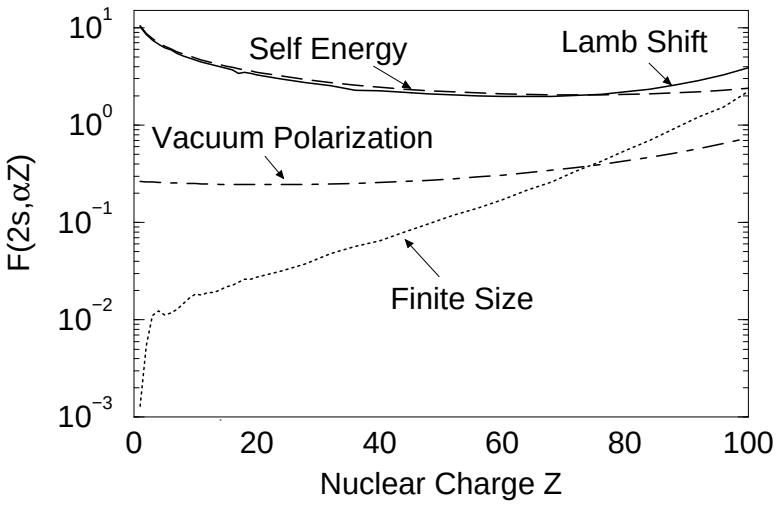

Figure 2. The three dominant contributions to the slowly varying function $F(2s, \alpha Z)$ for the Lamb shift of $2s$ states of highly-charged hydrogen-like ions; self-energy, vacuum polarization, and finite nuclear size, are given along the isoelectronic sequence.

Two-loop vacuum-polarization corrections can be expressed in terms of a slowly varying function $G_{\rm VP}(nlj, \alpha Z)$ of the type introduced in Eq. (50), leading to [19]

$$G_{\rm VP}(nlj, 0) = -\frac{82}{81}\,\delta_{l0}. \tag{54}$$

The relative sizes of the dominant contributions to the slowly varying function $F(2s, \alpha Z)$ for the Lamb shift of $2s$ states of highly-charged hydrogen-like ions; self-energy, vacuum polarization, and finite nuclear size, are shown in Fig. 2.

2.5. Reduced Mass and Relativistic Recoil

Reduction of the two-body electron-nucleus Schrödinger equation to center of mass coordinates leads to an equivalent one-body problem where the electron mass is replaced by the reduced mass $\mu = mM/(M + m)$. The effect of this replacement is to scale the infinite-mass Rydberg constant by μ/m. The corresponding shift of energy from the infinite-mass value E_{nl} is

$$\Delta_{RM} E_{nl} = \left(\frac{M}{M+m} - 1\right) E_{nl} = -\frac{m}{M+m}\; E_{nl}\,. \quad \text{(nonrelativistic)} \tag{55}$$

The relativistic generalization of the above expression, which has been considered in Refs. [20–23] is difficult in as much as there is no proper relativistic two-body Hamiltonian. One starting point for the discussion of the relativistic electron-nuclear two-body problem is the effective Hamiltonian

$$H_{\rm eff} = Mc^2 + \frac{p^2}{2M} + c\,\boldsymbol{\alpha}\cdot\boldsymbol{p} + mc^2\beta - \frac{Z}{r} + \frac{Z}{r}\frac{(\boldsymbol{\alpha}\cdot\boldsymbol{p} + \boldsymbol{\alpha}\cdot\hat{\boldsymbol{r}}\;\boldsymbol{p}\cdot\hat{\boldsymbol{r}})}{M}, \tag{56}$$

which contains the rest energy of the electron and nucleus, the kinetic energies of the nucleus and the electron, together with electrostatic and magnetostatic interactions between the electron and nucleus. The energy from this expression accurate to order $(\alpha Z)^4$ and to order m/M is

$$E_{nk} = (M+m)c^2 + \mu[f(nk) - 1] - \frac{m}{2M}\frac{\alpha^4 Z^4}{4n^4},$$

where

$$f(nk) = \left[1 + \frac{\alpha^2 Z^2}{(n-k+\gamma)^2}\right]^{-1/2}.$$

This expression gives the dominant recoil corrections

$$\Delta_{RM} E_{n\kappa} = -\frac{m}{M+m} E_{n\kappa} - \frac{m}{2M}\frac{\alpha^4 Z^4}{4n^4} \quad \text{(relativistic)}, \tag{57}$$

where it is understood that the rest energy $(M+m)c^2$ is omitted in $E_{n\kappa}$.

A further relativistic reduced mass correction obtained from QED was given by Lathrup et al. [24] and can be expressed as

$$F_{\rm RM}(nlj, \alpha Z) = \begin{cases} -\frac{m}{M}\left[4\ln(\alpha Z)^{-2} + 4L_{ns} + \frac{6}{5}\right] & \text{for } ns_{1/2} \\ -\frac{m}{M}\left[4L_{np} - \frac{1}{3}\right] & \text{for } np_{1/2} \\ -\frac{m}{M}\left[4L_{np} + \frac{1}{6}\right] & \text{for } np_{3/2} \end{cases}, \tag{58}$$

in terms of the slowly varying function $F(nlj, \alpha Z)$ introduced previously.

An additional radiative correction that depends on the finite mass of the nucleus, referred to as a "radiative recoil correction", was given in [25] and [26]. The leading terms in the radiative recoil correction are

$$F_{\rm RR}(nlj, \alpha Z) = \begin{cases} \frac{mZ}{M}\left[\frac{1}{3}\ln(\alpha Z)^{-2} + \frac{8}{3}L_{1s} + \frac{62}{9} + \frac{14}{3}\ln(2)\right] & \text{for } 1s \\ -\frac{mZ}{M}\left[\frac{1}{3}\ln(\alpha Z)^{-2} + \frac{8}{3}L_{2s} + \frac{187}{18}\right] & \text{for } 2s \\ \frac{mZ}{M}\left[\frac{8}{3}L_{2p} - \frac{7}{18}\right] & \text{for } 2p \end{cases}. \tag{59}$$

An up to date discussion of the relativistic reduced mass and recoil corrections can be found in the review article of Eides et al. [16].

2.6. Finite Nuclear Size

The finite size of the nuclear charge distribution modifies the nuclear potential near the nucleus. If one assumes a spherically symmetric nuclear charge distribution, $\rho_{\rm nuc}(r)$, the corresponding nuclear potential is

$$V_{\rm nuc}(r) = -4\pi \int_0^\infty \frac{r'^2 \rho_{\rm nuc}(r')}{r_>}\, dr', \tag{60}$$

Table 1
Finite nuclear size corrections $\Delta\epsilon_{n\kappa}$ to energies of $n = 1$ and $n = 2$ states of hydrogen ($R = 1.04$ fm) and hydrogen-like uranium ($R = 7.25$ fm).

State	H (cm^{-1})	U^{91+} (eV)
$1s_{1/2}$	0.0000339	272.657
$2s_{1/2}$	0.0000042	51.995
$2p_{1/2}$	0.0	5.960
$2p_{3/2}$	0.0	0.000

where $r_> = \max(r, r')$. Assuming a uniform distribution of nuclear charge over a sphere of radius R, one finds

$$V_{\rm nuc}(r) = \begin{cases} -\dfrac{Z}{R}\left(\dfrac{3}{2} - \dfrac{r^2}{2R^2}\right), & \text{for } r \le R, \\ -\dfrac{Z}{r}, & \text{for } r > R. \end{cases} \tag{61}$$

The root-mean-square radius $R_{\rm rms}$ for this uniform distribution is $R_{\rm rms} = \sqrt{3/5}\,R$. A fit to nuclear radii obtained in electron-nucleus scattering experiments and muonic x-ray measurements led to the empirical formula [27]

$$R_{\rm rms} = 0.836A^{1/3} + 0.570\ (0.05)\ \text{fm} \quad A > 9, \tag{62}$$

where A is the atomic mass number. Treating the finite size corrections to the Coulomb potential as a perturbation, one finds that the correction to the energy of a level with quantum numbers $(n,\ \kappa)$ of a hydrogen-like ions is

$$\begin{aligned} \Delta\epsilon_{n\kappa} &= \frac{3Z}{\gamma(2\gamma+1)(2\gamma+3)} N_{n\kappa}^2 \left(\frac{2ZR}{N}\right)^{2\gamma} \\ &\quad \times \left[(N-\kappa)^2 + (n-k)^2 - 2\frac{\gamma+n-k}{N}(N-\kappa)(n-k)\right]. \end{aligned} \tag{63}$$

In Table 1, we give the corrections to $n = 1$ and $n = 2$ states of hydrogen and hydrogen-like uranium. The correction are seen to be most important for $ns_{1/2}$ and $np_{1/2}$ states; they grow approximately as R^2Z^4 for these states and fall off roughly as n^{-3}.

The behavior of wave functions near the nucleus, which is influenced by details of the nuclear charge distribution, is important in calculations of hyperfine constants and amplitudes of parity nonconserving transitions. The basic orbitals in such calculations are obtained from self-consistent field calculations in which $\rho_{\rm nuc}(r)$ is assumed to be a Fermi (or Woods-Saxon) distribution

$$\rho_{\rm nuc}(r) = \frac{\rho_0}{1 + \exp[(r-C)/a]}. \tag{64}$$

In this formula, C is the 50% fall-off radius of the distribution, and a is related to the 90%–10% fall-off distance t by $t = 4\ln(3)\,a$. (This potential is used in most of the

calculations presented in this chapter with the value of $t = 2.3$ fm.) The corresponding nuclear potential is

$$V_{\rm nuc}(r) = \begin{cases} -\dfrac{Z}{\mathcal{N}\,C}\left[\left(\dfrac{3}{2} - \dfrac{r^2}{2\,C^2} + \dfrac{\pi^2\,a^2}{2\,C^2} + \dfrac{3\,a^2}{C^2}\,P_2\right) + \dfrac{6\,a^3}{C^2 r}\,(S_3 - P_3)\right], & \text{for } r \le C, \\ -\dfrac{Z}{\mathcal{N}\,r}\left[1 + \dfrac{\pi^2\,a^2}{C^2} + \dfrac{6\,a^3}{C^3}\,(S_3 - P_3) - \dfrac{3\,r a^2}{C^3} P_2\right], & \text{for } r > C, \end{cases} \tag{65}$$

where

$$S_k = \sum_{n=1}^{\infty} \frac{(-1)^{n-1}}{k^n}\ \exp\left[-n\,C/a\right], \tag{66}$$

$$P_k = \sum_{n=1}^{\infty} \frac{(-1)^{n-1}}{k^n}\ \exp\left[-n\,(r-C)/a\right]. \tag{67}$$

Here,

$$\mathcal{N} = 1 + \frac{\pi^2\,a^2}{C^2} + \frac{6\,a^3}{C^3}\,S_3. \tag{68}$$

The root-mean-square radius of the nuclear charge distribution is related to the 50% fall off radius C by

$$R_{\rm rms} = C\,\sqrt{\frac{3}{5}\left(\frac{\mathcal{M}}{\mathcal{N}}\right)}, \tag{69}$$

with

$$\mathcal{M} = 1 + \frac{10\,\pi^2\,a^2}{3\,C^2} + \frac{7\pi^4 a^4}{3\,C^4} + \frac{120\,a^5}{C^5}\,S_5. \tag{70}$$

2.7. Summary for Radiative Corrections in Hydrogenic Ions

There have been numerous experimental studies of radiative corrections to levels in hydrogen-like ions, all confirming to a high degree of accuracy the analysis described in the previous three subsections. As a specific example, we compare results of measurements of the $1s$ Lamb shift [differences between experimental energies and the Dirac-Coulomb energies given in Eq. (43)] for hydrogen and hydrogen-like ions with theoretical predictions from Johnson and Soff [27] in Fig. 3. The monograph of Beyer et al. [28] contains references to the experimental data presented in this figure together with other similar comparisons.

3. MANY-BODY PERTURBATION THEORY

Now let us turn to the many-body perturbation theory treatment of atoms with more than one electron. As discussed in the introduction, our approach is the no-pair Hamiltonian, which is given by

$$H^{\rm (n.p.)} = \sum_i h_0(i) + \frac{1}{2}\sum_{i\ne j} \Lambda_+(ij)\left(\frac{1}{r_{ij}}\right)\Lambda_+(ij) \tag{71}$$

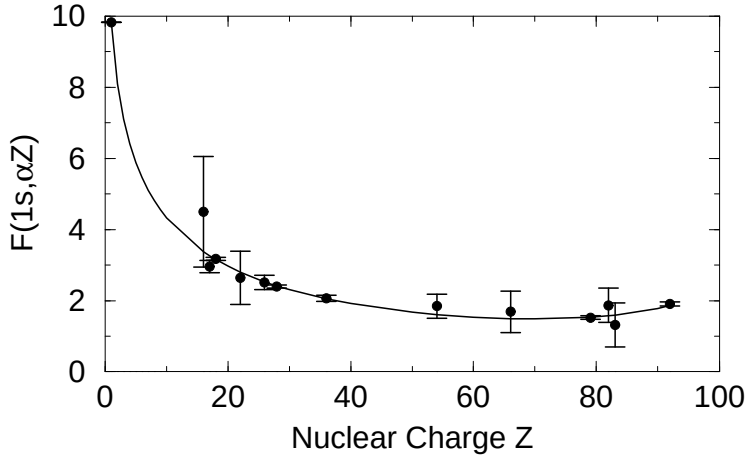

Figure 3. Comparison of theory and experiment for the $1s$ Lamb shift along the hydrogen isoelectronic sequence. The slight rise at high Z is due to finite nuclear size.

in configuration-space, where Λ_+ is a positive-energy projection operator:

$$\Lambda_+(ij) = \sum_{\substack{\epsilon_k > -mc^2 \\ \epsilon_l > -mc^2}} \phi_k(\boldsymbol{r}_i)\, \phi_k^\dagger(\boldsymbol{r}'_i)\; \phi_l(\boldsymbol{r}_j)\, \phi_l^\dagger(\boldsymbol{r}'_j).$$

For simplicity, we write only the Coulomb interaction in (71); however, to obtain correct two-electron fine structure intervals it is also necessary to include the Breit interaction b_{ij}, discussed in the following subsection.

It should be noted that the projection operator Λ_+ and, consequently, the no-pair Hamiltonian depends on the background potential U. One finds however that energies obtained from the no-pair Hamiltonian are only weakly dependent on the potential and that small differences between calculations starting from different potentials can be accounted for in terms of omitted negative-energy corrections. We elaborate on this point in Sec. 4.

To bypass the complicated issue of constructing Λ_+ in configuration space, we work with the second-quantized version of the no-pair Hamiltonian,

$$H^{(\mathrm{n.p.})} = H_0 + V_I \tag{72}$$

$$H_0 = \sum_{ij} \epsilon_i\; a_i^\dagger a_i \tag{73}$$

$$V_I = \frac{1}{2} \sum_{ijkl} v_{ijkl}\; a_i^\dagger a_j^\dagger a_l a_k - \sum_{ij} U_{ij}\; a_i^\dagger a_j\,. \tag{74}$$

In this expression, a_i and $a_j^\dagger$ designate electron annihilation and creation operators, respectively. The projection operators in Eq. (71) are implemented by simply restricting the indices i, j, k, l to bound states and positive-energy continuum states, omitting contributions from negative-energy states entirely. In Eq. (74), the quantity ϵ_i is the eigenvalue

of the Dirac equation corresponding to state ϕ_i, the quantity

$$v_{ijkl} = \left\langle ij \left| \frac{1}{r_{12}} \right| kl \right\rangle \equiv \int\int d^3r_1 d^3r_2 \; \frac{1}{r_{12}} \; \phi_i^\dagger(\boldsymbol{r}_1)\phi_k(\boldsymbol{r}_1) \; \phi_j^\dagger(\boldsymbol{r}_2)\phi_l(\boldsymbol{r}_2) \tag{75}$$

is the two-particle matrix element of the Coulomb (or Coulomb + Breit) interaction, and the quantity

$$U_{ij} = \int d^3r \; \phi_i^\dagger(\boldsymbol{r}) \, U(r) \, \phi_j(\boldsymbol{r}), \tag{76}$$

is a one-particle matrix element of the background potential $U(r)$.

If we treat V_I as a perturbation, then the lowest-order many-electron state vector for an N-electron atom in which the quantum states a, b, c, $\cdots$ are occupied is

$$\Psi_0 = a_a^\dagger a_b^\dagger a_c^\dagger \cdots |0\rangle. \tag{77}$$

This state vector, which is the second-quantized counterpart of a configuration space Slater determinant wave function, is a solution of the equation

$$H_0 \Psi_0 = E^{(0)} \Psi_0 \tag{78}$$

corresponding to energy

$$E^{(0)} = \epsilon_a + \epsilon_b + \epsilon_c + \cdots \; . \tag{79}$$

The first-order correction to the energy from V_I is easily found to be

$$E^{(1)} = \langle \Psi_0 \, | V_I | \, \Psi_0 \rangle = \frac{1}{2} \sum_{ab} \left(v_{abab} - v_{abba} \right) - \sum_a U_{aa}, \tag{80}$$

where the sums run over occupied states. We introduce the notation $\tilde{v}_{ijkl} = v_{ijkl} - v_{ijlk}$ to designate anti-symmetrized two-electron matrix elements, and note that

$$\sum_b \left(v_{ibjb} - v_{ibbj} \right) \equiv \sum_b \tilde{v}_{ibjb} = \left(V_{\rm HF} \right)_{ij}$$

where $\left(V_{\rm HF} \right)_{ij}$, is the matrix element of the (non-local) Hartree-Fock potential, conventionally defined through the relation

$$\begin{aligned} V_{HF} \; \phi_b(\boldsymbol{r}) \; = \; & \sum_a \left\{ \int \frac{d^3r'}{|\boldsymbol{r} - \boldsymbol{r}'|} \left[\phi_a^\dagger(\boldsymbol{r}') \phi_a(\boldsymbol{r}') \right] \phi_b(\boldsymbol{r}) \right. \\ & \left. - \int \frac{d^3r'}{|\boldsymbol{r} - \boldsymbol{r}'|} \left[\phi_a^\dagger(\boldsymbol{r}') \phi_b(\boldsymbol{r}') \right] \phi_a(\boldsymbol{r}) \right\}. \end{aligned} \tag{81}$$

It follows that

$$E^{(1)} = \sum_a \left[\frac{1}{2} V_{\rm HF} - U \right]_{aa}. \tag{82}$$

If we choose the background potential to be the Hartree-Fock potential, $U = V_{\rm HF}$, then we find that the energy through first-order is

$$E^{(0)} + E^{(1)} = \sum_a \left[\epsilon_a - \frac{1}{2} \sum_a \left(V_{\rm HF} \right)_{aa} \right] = \sum_a \left[(h_0)_{aa} + \frac{1}{2} \sum_b \tilde{v}_{abab} \right] . \tag{83}$$

The sum on the right hand side of this expression is precisely the expectation value of the Hamiltonian in the independent-particle approximation. Since the sum on the right-hand side of Eq. (83) is the starting point for a variational treatment of the (Dirac) Hartree-Fock approximation, it follows that choosing $U = V_{\rm HF}$ leads to $E^{(0)} + E^{(1)} = E_{\rm HF}$.

3.1. Breit Interaction

The Breit interaction [29, p. 170] is that part of the interaction between electrons mediated by exchange of transverse photons. The lowest-order energy shift associated with the exchange of a transverse photon between two electrons in states a and b is

$$\begin{aligned} B^{(1)} &= -\frac{1}{2\pi^2} \int d^3 r_1 \int d^3 r_2 \int d^3 k \, e^{i \boldsymbol{k} \cdot (\boldsymbol{r}_1 - \boldsymbol{r}_2)} \Big(\delta_{ij} - k_i k_j / |\boldsymbol{k}|^2 \Big) \\ &\quad \times \left[\frac{1}{\boldsymbol{k}^2} \phi_a^\dagger(\boldsymbol{r}_1) \alpha_i \phi_a(\boldsymbol{r}_1) \phi_b^\dagger(\boldsymbol{r}_2) \alpha_j \phi_b(\boldsymbol{r}_2) \right. \\ &\quad \left. - \frac{1}{\boldsymbol{k}^2 - k_0^2} \phi_a^\dagger(\boldsymbol{r}_1) \alpha_i \phi_b(\boldsymbol{r}_1) \phi_b^\dagger(\boldsymbol{r}_2) \alpha_j \phi_a(\boldsymbol{r}_2) \right] , \end{aligned} \tag{84}$$

where $k_0 = |\epsilon_a - \epsilon_b|/c$. The integral over d^3k above can be carried out leading to $B^{(1)} = b_{abab} - b_{abba}$, the difference between direct b_{abab} and exchange b_{abba} matrix elements of the "frequency-dependent" Breit operator

$$b_{12}(k_0) = - \frac{\boldsymbol{\alpha}_1 \cdot \boldsymbol{\alpha}_2}{r_{12}} \cos(k_0 \, r_{12}) + \boldsymbol{\alpha}_1 \cdot \boldsymbol{\nabla}_1 \; \boldsymbol{\alpha}_2 \cdot \boldsymbol{\nabla}_2 \left[\frac{\cos(k_0 \, r_{12}) - 1}{k_0^2 \, r_{12}} \right] . \tag{85}$$

In the direct matrix element b_{abab}, where $k_0 = 0$, the frequency-dependent Breit interaction reduces to its limiting static form:

$$\lim_{k_0 \to 0} b_{12}(k_0) = b_{12} = - \frac{\boldsymbol{\alpha}_1 \cdot \boldsymbol{\alpha}_2}{r_{12}} + \frac{\boldsymbol{\alpha}_1 \cdot \boldsymbol{\alpha}_2 - (\boldsymbol{\alpha}_1 \cdot \hat{\boldsymbol{r}}_{12}) (\boldsymbol{\alpha}_2 \cdot \hat{\boldsymbol{r}}_{12})}{2 r_{12}} \tag{86}$$

The first term on the right-hand side of Eq. (86) is also referred to as the "unretarded" Breit interaction since it arises in the Feynman gauge as the unretarded current-current interaction; the second term, which arises from the retardation correction to the charge-charge interaction in the Feynman gauge is referred to as the "retardation" correction. To summarize, direct matrix elements of the frequency-dependent Breit interaction b_{ijij} are evaluated using the static limit, whereas exchange matrix elements b_{ijji} are evaluated using Eq. (85) with $k_0 = |\epsilon_i - \epsilon_j|/c$. It was shown by Mittleman [4] that the form of the "frequency-dependent" Breit operator appropriate for evaluating off-diagonal matrix elements b_{ijkl} is

$$b_{12}(k_0) \to \frac{1}{2} \, b_{12}(|\epsilon_i - \epsilon_k|/c) + \frac{1}{2} \, b_{12}(|\epsilon_j - \epsilon_l|/c) \; . \tag{87}$$

Differences between the frequency-dependent Breit interaction and its static limit given in Eq. (86) are of relative order $\alpha^2 Z^2$, and therefore important primarily for highly-charged ions.

The correction to the many-electron Hamiltonian of Eq. (74) from the Breit interaction is

$$B_I = \frac{1}{2}\sum_{ijkl} b_{ijkl}\; a_i^\dagger a_j^\dagger a_l a_k. \tag{88}$$

The corresponding first-order Breit correction to the energy of a closed-shell atom is $B^{(1)} = \frac{1}{2}\sum_{ab} \tilde{b}_{abab}$.

3.2. Second- and Third-Order MBPT for Closed-Shell Atoms

The rules of perturbation theory associated with the relativistic no-pair Hamiltonian are identical to the well-known rules of nonrelativistic many-body perturbation theory, except for the restriction to positive-energy states. The nonrelativistic rules are explained in great detail, for example, in Lindgren and Morrison [30]. Let us start with a closed-shell system such as helium or beryllium in its ground state, and choose the background potential to be the Hartree-Fock potential. Expanding the energy in powers of V_I as

$$E = E^{(0)} + E^{(1)} + E^{(2)} + \cdots = \sum_a \left[\epsilon_a - \frac{1}{2}\left(V_{\rm HF}\right)_{aa}\right] + E^{(2)} + \cdots\;, \tag{89}$$

we find after a straight-forward application of Rayleigh-Schrödinger perturbation theory

$$E^{(2)} = -\frac{1}{2}\sum_{abmn} \frac{v_{abmn}\tilde{v}_{mnab}}{\epsilon_m + \epsilon_n - \epsilon_a - \epsilon_b} \tag{90}$$

$$\begin{aligned} E^{(3)} = & \sum_{abcmnr} \frac{\tilde{v}_{acnr}\tilde{v}_{nmba}\tilde{v}_{rbmc}}{(\epsilon_n + \epsilon_m - \epsilon_a - \epsilon_b)(\epsilon_r + \epsilon_n - \epsilon_a - \epsilon_c)} \\ & + \frac{1}{2}\sum_{abcdmn} \frac{\tilde{v}_{cdmn}v_{nmba}v_{badc}}{(\epsilon_n + \epsilon_m - \epsilon_a - \epsilon_b)(\epsilon_n + \epsilon_m - \epsilon_c - \epsilon_d)} \\ & + \frac{1}{2}\sum_{abmnrs} \frac{\tilde{v}_{absr}v_{nmba}v_{rsnm}}{(\epsilon_n + \epsilon_m - \epsilon_a - \epsilon_b)(\epsilon_r + \epsilon_s - \epsilon_a - \epsilon_b)}. \end{aligned} \tag{91}$$

In the above equations, we denote sums over occupied levels by letters (a, b, $\cdots$) at the beginning of the alphabet, virtual states by letters (m, n, $\cdots$) in the middle of the alphabet. Later, we use indices i or j to designate sums over both occupied and virtual states. The restriction to positive-energy states in the no-pair Hamiltonian leads to the restriction that virtual states be bound states and positive-energy continuum states in the expressions for the second- and third-order energy. Owing to the relatively small size of the Breit interaction, only terms linear in b_{ijkl} are important for most applications. The second-order correction $B^{(2)}$ from one Breit and one Coulomb interaction is easily found to be

$$B^{(2)} = -\sum_{abmn} \frac{b_{abmn}\tilde{v}_{mnab}}{\epsilon_m + \epsilon_n - \epsilon_a - \epsilon_b} \tag{92}$$

from Eq. (90). The term $B^{(3)}$ linear in the Breit interaction and quadratic in the Coulomb interaction can be obtained by replacing v_{ijkl} by $v_{ijkl} + b_{ijkl}$ in Eq. (91), and linearizing the resulting expression in b_{ijkl}.

To evaluate the multiple sums in the expressions above, we first do a reduction to sums of radial integrals and then use make use of finite basis sets to put the resulting expressions into a form suitable for numerical evaluation.

3.3. Angular Reduction of the Coulomb Interaction

The first step in reducing the MBPT expressions into a form suitable for numerical evaluation is a decomposition of the Coulomb integrals v_{ijkl} into sums of products of angular momentum coupling coefficients and radial integrals. To accomplish this decomposition, we first expand the kernel of the Coulomb integrals $1/r_{12}$ as

$$\frac{1}{r_{12}} = \sum_{LM} (-1)^M C_{LM}(\hat{r}_1) C_{L-M}(\hat{r}_2) \frac{r_<^L}{r_>^{L+1}}, \tag{93}$$

where $r_< = \min(r_1, r_2)$ and $r_> = \max(r_1, r_2)$, and where $C_{LM}(\hat{r})$ is the normalized spherical harmonic,

$$C_{LM}(\hat{r}) = \sqrt{\frac{4\pi}{2L+1}}\, Y_{LM}(\hat{r}).$$

With the aid of this expansion, one finds

$$v_{abcd} = \sum_L J_L(abcd)\, X_L(abcd), \tag{94}$$

where the dependence on magnetic quantum numbers is entirely contained in

$$J_L(abcd) = \sum_M (-1)^{j_a+j_b+L-m_a-m_b-M} \begin{pmatrix} j_a & L & j_c \\ -m_a & M & m_c \end{pmatrix} \begin{pmatrix} j_b & L & j_d \\ -m_b & -M & m_d \end{pmatrix}, \tag{95}$$

where the round brackets designate Wigner three-j symbols [6], and where

$$X_L(abcd) = (-1)^L \langle a \| C_L \| c \rangle \langle b \| C_L \| d \rangle R_L(abcd). \tag{96}$$

The coefficient $\langle a \| C_L \| c \rangle$ is a reduced matrix element of $C_{LM}(\hat{r})$, given by

$$\langle a \| C_L \| b \rangle = \sqrt{(2j_a+1)(2j_b+1)}\; (-1)^{j_a+1/2} \begin{pmatrix} j_a & j_b & L \\ -1/2 & 1/2 & 0 \end{pmatrix}, \tag{97}$$

when $l_a + l_b + L$ is even. When $l_a + l_b + L$ is odd, $\langle a \| C_L \| b \rangle$ vanishes. The quantity $R_L(abcd)$ in Eq. (96) is a relativistic Slater Integral defined by

$$R_L(abcd) = \int_0^\infty \int_0^\infty dr_1 dr_2\; \frac{r_<^L}{r_>^{L+1}} \left[P_a(r_1) P_c(r_1) + Q_a(r_1) Q_c(r_1) \right] \times \left[P_b(r_2) P_d(r_2) + Q_b(r_2) Q_d(r_2) \right]. \tag{98}$$

The factor $J(abcd)$ in Eq. (94) contains the entire dependence on magnetic quantum numbers. With the aid of the identity

$$J_L(abdc) = -[L]\sum_K \left\{ \begin{array}{ccc} j_a & j_d & K \\ j_b & j_c & L \end{array} \right\} J_K(abcd), \tag{99}$$

where we have introduced the notation $[L] = 2L + 1$, the anti-symmetrized Coulomb matrix elements may be written

$$\tilde{v}_{abcd} = \sum_L J_L(abcd)\, Z_L(abcd), \tag{100}$$

with

$$Z_L(abcd) = X_L(abcd) + [L]\sum_K \left\{ \begin{array}{ccc} j_a & j_d & K \\ j_b & j_c & L \end{array} \right\} X_K(abdc). \tag{101}$$

Substituting (94) and (100) into Eq. (90) and carrying out the sums over magnetic quantum numbers, one can express the second-order energy in terms of radial integrals as

$$E^{(2)} = -\frac{1}{2}\sum_L \frac{1}{[L]} \sum_{abmn} \frac{Z_L(mnab)X_L(mnab)}{\epsilon_m + \epsilon_n - \epsilon_a - \epsilon_b}. \tag{102}$$

Similarly, the third-order energy can be written

$$\begin{aligned} E^{(3)} \;=\; & \sum_L \frac{1}{[L]^2} \sum_{abcmnr} (-1)^{j_a+j_b+j_c+j_m+j_n+j_r+L+1} \\ & \times \frac{Z_L(acnr)Z_L(mnba)Z_L(rbcm)}{(\epsilon_m + \epsilon_n - \epsilon_a - \epsilon_b)(\epsilon_r + \epsilon_n - \epsilon_a - \epsilon_c)} \\ & + \frac{1}{2}\sum_{\substack{abcdmn \\ L_1L_2L_3}} (-1)^{j_a+j_b+j_c+j_d} \left\{ \begin{array}{ccc} L_1 & L_2 & L_3 \\ j_b & j_d & j_n \end{array} \right\} \left\{ \begin{array}{ccc} L_1 & L_2 & L_3 \\ j_a & j_c & j_m \end{array} \right\} \\ & \times \frac{Z_{L_1}(dcnm)X_{L_2}(nmba)X_{L_3}(badc)}{(\epsilon_n + \epsilon_m - \epsilon_a - \epsilon_b)(\epsilon_n + \epsilon_m - \epsilon_c - \epsilon_d)} \\ & + \frac{1}{2}\sum_{\substack{abmnrs \\ L_1L_2L_3}} (-1)^{j_a+j_b+j_m+j_n} \left\{ \begin{array}{ccc} L_1 & L_2 & L_3 \\ j_n & j_r & j_b \end{array} \right\} \left\{ \begin{array}{ccc} L_1 & L_2 & L_3 \\ j_m & j_s & j_a \end{array} \right\} \\ & \times \frac{Z_{L_1}(basr)X_{L_2}(nmba)X_{L_3}(rsnm)}{(\epsilon_n + \epsilon_m - \epsilon_a - \epsilon_b)(\epsilon_r + \epsilon_s - \epsilon_a - \epsilon_b)}. \end{aligned} \tag{103}$$

To evaluate the sums over virtual states in Eqs. (102) and (103), we make use of the B-spline basis functions described later in this section.

3.4. Angular Reduction of the Breit Interaction

As shown in detail in Ref. [31], the matrix elements of the first term in (86), the unretarded Breit interaction,

$$m_{ijkl} = \int\!\!\int d^3r_1 d^3r_2 \; \frac{1}{r_{12}} \; \phi_i^\dagger(\boldsymbol{r}_1)\, \boldsymbol{\alpha}_1\, \phi_k(\boldsymbol{r}_1) \cdot \phi_j^\dagger(\boldsymbol{r}_2)\, \boldsymbol{\alpha}_2\, \phi_l(\boldsymbol{r}_2) \tag{104}$$

can be decomposed in a spherical basis as

$$m_{ijkl} = \sum_L J_L(ijkl)\,[M_L(ijkl) + N_L(ijkl)]\,, \tag{105}$$

where $J_L(ijkl)$ is the angular-momentum factor given in Eq. (95), and where

$$M_L(ijkl) = (-1)^L \langle i\|C_L\|k\rangle\langle j\|C_L\|l\rangle \left[\frac{L+1}{2L+3}\int_0^\infty dr_1 \int_0^\infty dr_2\ \frac{r_<^{L+1}}{r_>^{L+2}}\ Q_{ik}(r_1)Q_{jl}(r_2) + \frac{L}{2L-1}\int_0^\infty dr_1 \int_0^\infty dr_2\ \frac{r_<^{L-1}}{r_>^{L}}\ P_{ik}(r_1)P_{jl}(r_2)\right], \tag{106}$$

and

$$\begin{aligned} N_L(ijkl) &= (-1)^{L+1}\langle -i\|C_L\|k\rangle\langle -j\|C_L\|l\rangle \\ &\quad \times \frac{(\kappa_i+\kappa_k)(\kappa_j+\kappa_l)}{L(L+1)}\int_0^\infty dr_1 \int_0^\infty dr_2\ \frac{r_<^{L}}{r_>^{L+1}}\ V_{ik}(r_1)V_{jl}(r_2), \end{aligned} \tag{107}$$

where we have introduced

$$P_{ik}(r) = U_{ik}(r) + \frac{\kappa_k - \kappa_i}{L}\ V_{ik}(r), \tag{108}$$

$$Q_{ik}(r) = -U_{ik}(r) + \frac{\kappa_k - \kappa_i}{L+1}\ V_{ik}(r), \tag{109}$$

$$U_{ik}(r) = P_i(r)Q_k(r) - Q_i(r)P_k(r), \tag{110}$$

$$V_{ik}(r) = P_i(r)Q_k(r) + Q_i(r)P_k(r). \tag{111}$$

We use the notation $\langle -i\|C_L\|j\rangle$ in Eq. (107) to designate the reduced matrix element defined in Eq. (97) with $\kappa_i \to -\kappa_i$.

The matrix element of the retardation part of the Breit interaction takes a similar form, the details being given in [32]. We find

$$r_{ijkl} = \sum_L J_L(ijkl)\ O_L(ijkl), \tag{112}$$

with

$$\begin{aligned} O_L(ijkl) &= (-1)^{L+1}\langle i\|C_L\|k\rangle\langle j\|C_L\|l\rangle \\ &\quad \times \left[\frac{(L+1)^2}{(2L+1)(2L+3)}\int_0^\infty dr_1 \int_0^\infty dr_2\ \frac{r_<^{L+1}}{r_>^{L+2}}\ Q_{ik}(r_1)Q_{jl}(r_2)\right. \\ &\quad + \frac{L^2}{(2L+1)(2L-1)}\int_0^\infty dr_1 \int_0^\infty dr_2\ \frac{r_<^{L-1}}{r_>^{L}}\ P_{ik}(r_1)P_{jl}(r_2) \\ &\quad + \frac{L(L+1)}{2(2L+1)}\int_0^\infty dr_1 \int_0^{r_1} dr_2\ \left(\frac{r_<^{L-1}}{r_>^{L}} - \frac{r_<^{L+1}}{r_>^{L+2}}\right) Q_{ik}(r_1)P_{jl}(r_2) \\ &\quad \left. + \frac{L(L+1)}{2(2L+1)}\int_0^\infty dr_1 \int_{r_1}^\infty dr_2\ \left(\frac{r_<^{L-1}}{r_>^{L}} - \frac{r_<^{L+1}}{r_>^{L+2}}\right) P_{ik}(r_1)Q_{jl}(r_2)\right]. \end{aligned} \tag{113}$$

Matrix elements of the frequency-dependent Breit interaction $b_{12}(k_0)$ are somewhat more complicated; they can be evaluated using the formulas given above with the following replacements:

(a) In Eqs. (106), (107) and in the first two lines of Eq. (113) replace expressions of the form

$$\frac{r_<^K}{r_>^{K+1}} \to -k_0\,(2K+1)\,j_K(k_0 r_<)\,y_K(k_0 r_>),$$

where $j_K(x)$ and $y_K(x)$ are spherical Bessel and Hankel functions, respectively, and

(b) replace the last two lines of Eq. (113) by

$$\frac{L(L+1)}{(2L+1)}\int_0^\infty dr_1 \int_0^{r_1} dr_2 \Bigg\{ -2\left[k_0 j_{L-1}(k_0\,r_2)\,y_{L+1}(k_0\,r_1) + \frac{2L+1}{k_0^2}\,\frac{r_2^{L-1}}{r_1^{L+2}}\right] \times Q_{ik}(r_1)P_{jl}(r_2) - 2\,k_0 j_{L+1}(k_0\,r_2)\,y_{L-1}(k_0\,r_1)P_{ik}(r_1)Q_{jl}(r_2)\Bigg\}.$$

3.5. B-Spline Basis Sets

To carry out the sums over states in the MBPT expressions introduced in the previous two subsections, it is convenient to employ finite bases set methods. In the calculations presented in this section and the next, we make use of basis functions constructed as linear combinations of B-splines [33]. Other possible choices of basis functions for relativistic problems are discussed later, in Sec. 4.1. In as much as we are considering correlation corrections to atomic bound states which have limited size, we consider finite-range basis functions. We, therefore, restrict our attention to a finite (but large) cavity of radius R. To study the ground-state or low-lying excited states of ions, the radius of this cavity is chosen to be $R \approx 40/Z_{\rm ion}$ a.u., where $Z_{\rm ion}$ is the ionic charge. For such large cavities, the results of correlation calculations are independent of the cavity radius. We require that the large component of the radial wave function vanish at the origin [$P_\kappa(0) = 0$] and that Massachusetts Institute of Technology (MIT) bag model [34] boundary conditions [$P_\kappa(R) = Q_\kappa(R)$] be satisfied at the cavity boundary. The bag model boundary conditions damp the radial Dirac wave function outside the cavity in such a way that the often discussed difficulty leading to the Klein paradox [35, p. 102] is avoided. The spectrum of the Dirac equation in a cavity is discrete but infinite.

Next, we expand the solutions to the radial Dirac equation in a finite basis. This basis is chosen to be a set of n B-splines of order k. Following deBoor [33], we divide the interval $[0, R]$ into segments. The end points of these segments are given by the knot sequence $\{t_i\}$, $i = 1, 2, \cdots, n+k$. The B-splines of order k, $B_{i,k}(r)$, on this knot sequence are defined recursively by the relations,

$$B_{i,1}(r) = \begin{cases} 1, & t_i \le r < t_{i+1}, \\ 0, & \text{otherwise}, \end{cases} \tag{114}$$

and

$$B_{i,k}(r) = \frac{r - t_i}{t_{i+k-1} - t_i} B_{i,k-1}(r) + \frac{t_{i+k} - r}{t_{i+k} - t_{i+1}} B_{i+1,k-1}(r)\ . \tag{115}$$

The function $B_{i,k}(r)$ is a piecewise polynomial of degree $k-1$ inside the interval $t_i \le r < t_{i+k}$ and $B_{i,k}(r)$ vanishes outside this interval. The knots defining our grid have k-fold

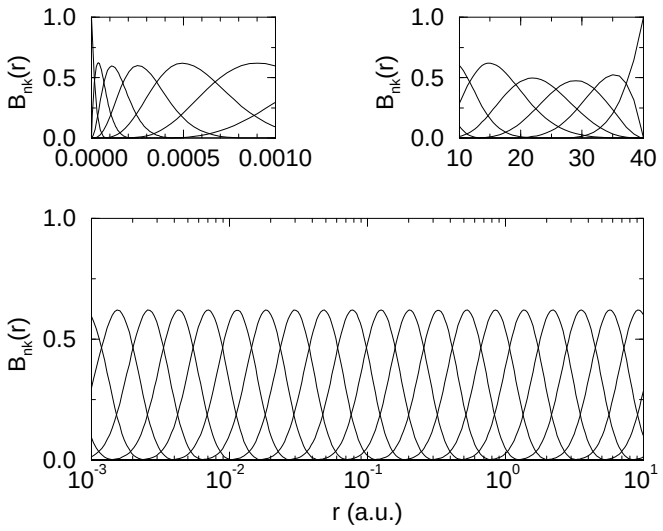

Figure 4. The $n = 30$ B-splines of order $k = 6$ are used to cover the interval 0 to 40 on an "atomic" grid. Note that the splines sum to 1 at each point.

multiplicity at the endpoints 0 and R; *i.e.* $t_1 = t_2 = \cdots = t_k = 0$ and $t_{n+1} = t_{n+2} = \cdots = t_{n+k} = R$. The knots $t_{k+1}, t_{k+2}, \cdots, t_n$ are distributed on an exponential scale between 0 and R. In Fig. 4, we show 30 B-splines of order k covering the interval $r = 0 - 40$ a.u. This set of B-splines could be used as a basis set for expanding radial wave functions.

The set of B-splines of order k on the knot sequence $\{t_i\}$ forms a complete basis for piecewise polynomials of degree $k-1$ on the interval spanned by the knot sequence. We represent the solution to the radial Dirac equation as a linear combination of these B-splines and work with the B-spline representation of the wave functions rather than the wave functions themselves.

The radial Dirac wave functions $P_\kappa(r)$, $Q_\kappa(r)$ satisfies the variational equation $\delta S = 0$, where

$$\begin{aligned} S &= \frac{1}{2}\int_0^R \Big\{ cP_\kappa(r)\left(\frac{d}{dr} - \frac{\kappa}{r}\right) Q_\kappa(r) - cQ_\kappa(r)\left(\frac{d}{dr} + \frac{\kappa}{r}\right) P_\kappa(r) \\ &\quad + V(r)\left[P_\kappa^2(r) + Q_\kappa^2(r)\right] + mc^2\left[P_\kappa^2(r) - Q_\kappa^2(r)\right]\Big\} \\ &\quad - \frac{1}{2}\,\epsilon \int_0^R \left[P_\kappa^2(r) + Q_\kappa^2(r)\right] dr \,. \end{aligned} \tag{116}$$

The parameter ϵ is a Lagrange multiplier introduced to insure that the normalization constraint

$$\int_0^R \left[P_\kappa^2(r) + Q_\kappa^2(r)\right] = 1\,, \tag{117}$$

is satisfied. The variational principle $\delta S = 0$ leads to the radial Dirac equations.

We expand $P_\kappa(r)$ and $Q_\kappa(r)$ in terms of B-splines of order k as

$$P_\kappa(r) = \sum_{i=1}^{n} p_i\, B_i(r), \quad Q_\kappa(r) = \sum_{i=1}^{n} q_i\, B_i(r). \tag{118}$$

The subscript k has been omitted from $B_{i,k}(r)$ for notational simplicity. The action S becomes a quadratic function of the expansion coefficients (p_i, q_i) when the expansions (118) are substituted into the action integral. The variational principle then leads to a system of linear equations for the expansion coefficients,

$$\frac{\partial S}{\partial p_i} = 0, \quad \frac{\partial S}{\partial q_i} = 0, \quad i = 1, \cdots, n\,. \tag{119}$$

The resulting equations can be written in the form of an $2n \times 2n$ symmetric generalized eigenvalue equation,

$$Av = \epsilon Bv\ , \tag{120}$$

where v is the vector of expansion coefficients,

$$v = (p_1, p_2, \cdots, q_1, q_2, \cdots)\ . \tag{121}$$

The $2n \times 2n$ matrices A and B are given by[1]

$$A = \begin{bmatrix} (V) + mc^2(C) & c\,[(D) + (\kappa/r)] \\ -c\,[(D) + (\kappa/r)] & (V) - mc^2(C) \end{bmatrix}, \qquad B = \begin{bmatrix} (C) & 0 \\ 0 & (C) \end{bmatrix} \tag{122}$$

in terms of the following $n \times n$ matrices:

$$(C)_{ij} = \int_0^R B_i(r) B_j(r) dr \qquad (D)_{ij} = \int_0^R B_i(r) \frac{d}{dr} B_j(r) dr \tag{123}$$

$$(V)_{ij} = \int_0^R B_i(r) V(r) B_j(r) dr \qquad (\kappa/r)_{ij} = \int_0^R B_i(r) \frac{\kappa}{r} B_j(r) dr \tag{124}$$

It should be mentioned that the matrices A and B are diagonally dominant banded matrices. The solution to the eigenvalue problem for such matrices is numerically stable. Routines from the LAPACK library [37] can be used to obtain the eigenvalues and eigenvectors numerically.

Solving the $2n$ dimensional generalized eigenvalue equation, one obtains $2n$ real eigenvalues ϵ^λ and $2n$ eigenvectors v^λ. The eigenvectors satisfy the orthogonality relations,

$$\sum_{i,j} v_i^\lambda B_{ij} v_j^\mu = \delta_{\lambda\mu}\ , \tag{125}$$

which leads to the orthogonality relations

$$\int_0^R [P_\kappa^\lambda(r) P_\kappa^\mu(r) + Q_\kappa^\lambda(r) Q_\kappa^\mu(r)] dr = \delta_{\lambda\mu}, \tag{126}$$

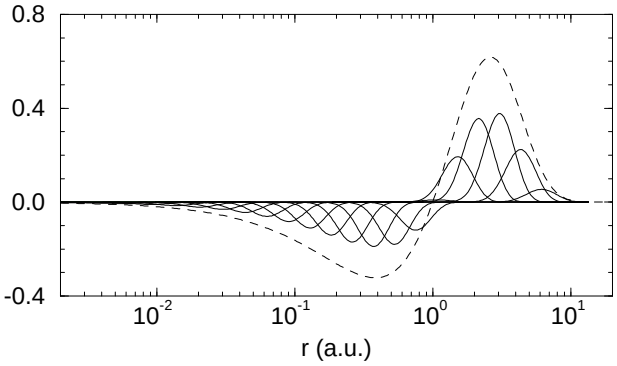

Figure 5. B-spline decomposition of the large-component radial function for a $2s_{1/2}$ state in a Coulomb field with $Z = 2$ obtained using $n = 30$ B-splines of order $k = 6$. The dashed curve is the resulting function $P_{2s_{1/2}}(r)$.

for the corresponding radial wave functions.

In Fig. 5, we show the B-spline decomposition of the large-component radial wave function $P_{2s_{1/2}}(r)$ for the $2s_{1/2}$ state in a Coulomb potential with $Z = 2$ obtained using $n = 30$ splines of order $k = 6$.

The cavity spectrum is complete in the space of piecewise polynomials of degree $k - 1$ and, therefore, can be used instead of the real spectrum to evaluate correlation corrections to states confined to the cavity. The spectrum splits into two distinct equal halves, the lower energy half of the spectrum with $\epsilon^\lambda < -mc^2$ represents the positron states and the upper half represents electron bound and continuum states. In evaluating the sums over states in the MBPT expressions for $E^{(2)}$ and $E^{(3)}$ in Eqs. (102) and (103), we of course omit contributions from the lower half of the spectrum.

Since the cavity boundary is chosen to be far larger than the atomic radius, the lower few bound states are precisely represented in the B-spline basis. The quality of the numerically generated B-spline spectrum can be tested by using it to evaluate sum rules. It is found [36], for example, that the generalized Thomas Reiche-Kuhn (TRK) sum rule is satisfied to parts in 10^7 using 40 splines of order 7 for a given κ and to parts in 10^9 using 50 splines of order 9.

3.6. Ground-State of He-like ions

Now, let us consider the helium ground state. As a first step, we solve the Hartree-Fock equation

$$[h_0 + V_{\rm HF}]\,\phi_{1s} = \epsilon_{1s}\phi_{1s},$$

[1]The modifications to the matrix A needed to ensure that the boundary conditions are satisfied are given in [36].

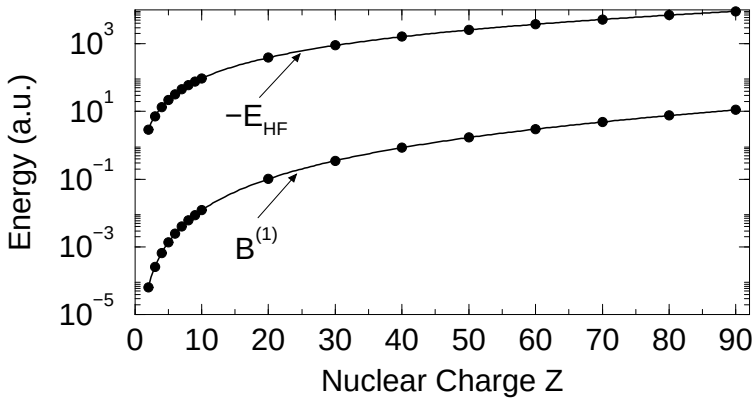

Figure 6. The (Dirac) Hartree-Fock energy $-E_{\rm HF}$ and the first order Breit correction $B^{(1)}$ are given for helium-like ions. $-E_{\rm HF}$ grows approximately as Z^2 and $B^{(1)}$ grows approximately as Z^3 for large Z.

where

$$\begin{aligned} V_{\rm HF}\,\phi_b &= \sum_a \left[\int d^3r'\,\frac{\phi_a^\dagger(\boldsymbol{r}')\phi_a(\boldsymbol{r}')}{|\boldsymbol{r}-\boldsymbol{r}'|}\;\phi_b(\boldsymbol{r}) - \int d^3r'\,\frac{\phi_a^\dagger(\boldsymbol{r}')\phi_b(\boldsymbol{r}')}{|\boldsymbol{r}-\boldsymbol{r}'|}\;\phi_a(\boldsymbol{r})\right] \\ &= 2v_0(1s,1s,r)\;\phi_b(\boldsymbol{r}) - \frac{1}{2l+1}v_l(1s,b,r)\;\phi_{1s}(\boldsymbol{r}). \end{aligned} \tag{127}$$

Here, $v_l(a,b,r)$ is the multipole potential

$$v_l(a,b,r) = \int_0^\infty \frac{r_<^l}{r_>^{l+1}}\left[P_a(r')P_b(r') + Q_a(r')Q_b(r')\right]dr'.$$

For the $(1s)^2$ helium ground state, the HF Potential reduces to

$$V_{\rm HF}\phi_{1s} = v_0(1s,1s,r)\phi_{1s}(\boldsymbol{r}).$$

Solving the HF equation, we find $\epsilon_{1s} = 0.9179907$ a.u.. The resulting lowest-order energy is $E^{(0)} = 2\epsilon_{1s} = -1.8359814$ a.u., and the first-order correction is $E^{(1)} = -\langle 1s|v_0(1s,1s,r)|1s\rangle = -1.0258319$ a.u., giving a total through first-order $E_{\rm HF} = E^{(0)} + E^{(1)} = -2.8618133$ a.u.. The helium binding energy is the difference between the energy of the atom and the energy of the ion with one electron removed. The latter, which is given by Eq. (43), is $E_{\rm ion} = -2.0001069$ a.u., leading to a theoretical value $E_{\rm bind} = -0.8617064$ a.u. in the Hartree-Fock (first-order) approximation. This is in only fair agreement with the experimental binding energy $E_{\rm expt} = -0.9035704$ a.u.. (The HF energy, which grows approximately as Z^2 for large Z, is plotted in Fig. 6 where we also show the lowest-order Breit correction for comparison.)

To go further, we must evaluate the higher-order corrections. Setting $a = b = 1s$ in

Table 2
Partial wave contributions (a.u.) to the second-order ground-state energy $E^{(2)}$ in helium.

L	term	L	term
0	-0.0134991	5	-0.0001675
1	-0.0189775	6	-0.0000876
2	-0.0031927	7	-0.0000500
3	-0.0009326	8	-0.0000306
4	-0.0003618	9–∞	-0.0000743
		Total	-0.0373736

Eq. (102), we obtain the following simple expression for the second-order energy:

$$E^{(2)} = -\sum_L \left[\frac{2L}{[L]^2} \sum_{mn} \frac{R^2_L(1s,1s,m\kappa,n\kappa)}{\epsilon_{m\kappa}+\epsilon_{n\kappa}-2\epsilon_{1s}}\bigg|_{\kappa=L} + \frac{2L+2}{[L]^2} \sum_{mn} \frac{R^2_L(1s,1s,m\kappa,n\kappa)}{\epsilon_{m\kappa}+\epsilon_{n\kappa}-2\epsilon_{1s}}\bigg|_{\kappa=-L-1} \right]. \tag{128}$$

Taking the radial wave functions and energies for states $n\kappa$ from the B-spline basis set, we may easily carry out the double sums in (128). The partial-wave contributions to $E^{(2)}$ from terms in square bracket are listed in Table 2. These terms fall-off approximately as L^{-4} for large L and may easily be extrapolated. We find $E^{(2)} = -0.0373736$ a.u., leading to a binding energy of -0.8990800 a.u., differing from experiment by 0.5%.

The third-order energy is evaluated in a similar way, leading to $E^{(3)} = -0.0036756$ a.u., and a binding energy $E^{(0)} + E^{(1)} + E^{(2)} + E^{(3)} - E_{\rm ion} = -0.9027556$ a.u., within 0.1% of experiment. Plots of the second- and third-order correlation energy along the helium isoelectronic sequence are presented in Fig. 7, where it is seen that $E^{(2)}$ remains approximately constant. Although difficult to see in the graph, $E^{(3)}$ has its largest magnitude (about 10% of $E^{(2)}$ for $Z = 2$ and decreases approximately as $1/Z$ for larger Z. To go further in our study of helium-like ions, we turn to all-order methods.

3.7. Breit Interaction for the Helium Ground State

The Breit interaction in second-quantized form, written in normal order relative to a closed-shell core is

$$B = \frac{1}{2}\sum_{ijkl} b_{ijkl}\, :a_i^\dagger a_j^\dagger a_l a_k: + \frac{1}{2}\sum_{ab} \tilde{b}_{abab}, \tag{129}$$

where $b_{ijkl} = m_{ijkl} + r_{ijkl}$ is the sum of the magnetic and retardation matrix elements. The lowest-order Breit correction for a closed-shell atom is, consequently,

$$B^{(1)} = \langle \Psi_0 \,|B|\, \Psi_0 \rangle = \frac{1}{2}\sum_{ab} \tilde{b}_{abab} \equiv -\frac{1}{2}\sum_{ab} b_{abba}, \tag{130}$$

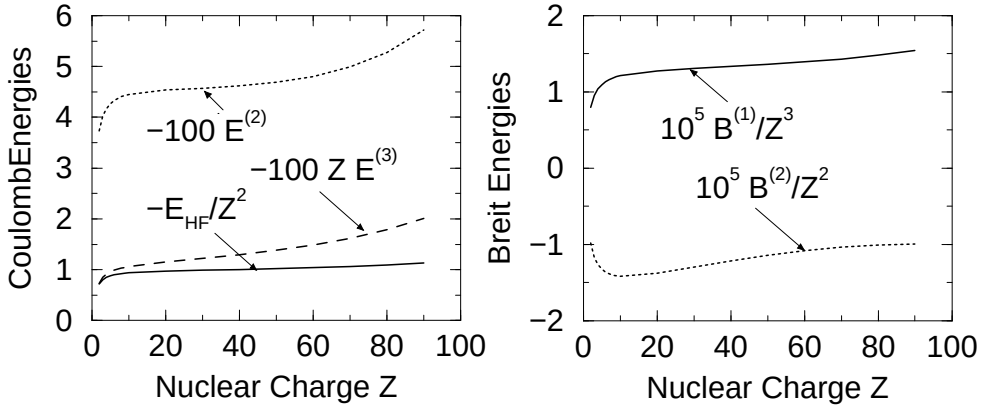

Figure 7. In the left panel, we give the scaled HF energies, $-E_{\rm HF}/Z^2$, second-order Coulomb energies $-100E^{(2)}$, and scaled third-order Coulomb energies $-100ZE^{(3)}$ for the $(1s)^2$ ground states of helium-like ions. In the right panel we give scaled values of first- and second-order ground-state Breit energies $10^5\,B^{(1)}/Z^3$ and $10^5\,B^{(2)}/Z^2$ along the helium isoelectronic sequence.

where we have made use of the fact that the direct part of the Breit matrix element b_{abab} vanishes when summed over closed shells. The Breit matrix element takes a particularly simple form for helium or helium-like ions, where we find

$$B^{(1)} = \frac{16}{3}\int_0^\infty dr \int_0^\infty dr'\, \frac{r_<}{r_>^2}\,[P_{1s}(r)Q_{1s}(r)]\,[P_{1s}(r')Q_{1s}(r')]\,.$$

The first-order Breit correction, which grows approximately as Z^3, is compared with the Hartree-Fock energy for helium-like ions in Fig. 6.

Owing to its small size, the dominant correlation corrections to the Breit interaction are those associated with one Breit and many Coulomb terms. As mentioned earlier, these dominant corrections can be obtained from MBPT formulas such as those in Eqs. (102) and (103) by substituting $v_{ijkl} \to v_{ijkl} + b_{ijkl}$ and linearizing in b_{ijkl}. The second-order (one Breit–one Coulomb) correlation energy from Eq. (92) is

$$B^{(2)} = -\sum_L \frac{1}{[L]} \sum_{abmn} \frac{B_L(abmn)Z_L(abmn)}{\epsilon_m + \epsilon_n - \epsilon_a - \epsilon_b}, \tag{131}$$

where $B_L(abmn) = M_L(abmn) + N_L(abmn) + O_L(abmn)$; M_L and N_L from the magnetic current-current interaction and O_L from retardation.

We find that for the ground states of helium-like ions, the second-order retardation correction is smaller than the second-order magnetic contribution by a factor of about 4 and has an opposite sign. We plot scaled values of the first- and second-order Breit interaction for the ground states of helium-like ions in the right panel of Fig. 7. It is interesting to note that the second-order Breit energy is larger in magnitude than the second-order Coulomb energy for $Z > 70$.

3.8. Single-Double (SD) Equations

To go further, we turn to so-called "all-order" methods. We start by considering relativistic calculations of type carried out by Lindroth [38] and Blundell et al. [39], which account for all possible single and double excitations of the ground-state helium HF wave function. These calculations have the potential of giving an exact helium ground-state energy.

Following [30], we write the no-pair Hamiltonian in normal order with respect to the $(1s)^2$ closed shell. Thus, $H^{(\mathrm{n.p.})} = H_0 + V_0 + V_1 + V_2$ with

$$\begin{aligned} H_0 &= \sum_i \epsilon_i \; a_i^\dagger a_i \\ V_0 &= \sum_a \left[\frac{1}{2}\left(V_{\mathrm{HF}}\right)_{aa} - U_{aa}\right] \\ V_1 &= \sum_{ij} \left[\left(V_{\mathrm{HF}}\right)_{ij} - U_{ij}\right] :a_i^\dagger a_j: \\ V_2 &= \sum_{ijkl} v_{ijkl} \, :a_i^\dagger a_j^\dagger a_l a_k:, \end{aligned} \tag{132}$$

where the operators sandwiched between the colons $:\cdots:$ are in normal order with respect to the closed atomic core. To simplify the calculation, we choose $U = V_{\mathrm{HF}}$, the ground-state Hartree-Fock potential. With this choice, V_1 vanishes. The state vector for the ground-state of a helium-like ion is taken to be the sum of all possible single or double excitations of the $(1s)^2$ HF core:

$$|\Psi\rangle = \left[1 + \sum_{am} \rho_{ma} \; a_m^\dagger a_a + \sum_{mnab} \rho_{mnab} \; a_m^\dagger a_n^\dagger a_a a_b\right] |\Psi_0\rangle. \tag{133}$$

This wave function satisfies the Schrödinger equation

$$(H_0 + V_0 + V_2)|\Psi\rangle = E|\Psi\rangle. \tag{134}$$

Left-multiplying by $\langle\Psi_0|$ and assuming the intermediate-normalization condition

$$\langle\Psi_0|\Psi\rangle = 1,$$

we find

$$\delta E \equiv E - E_{\mathrm{HF}} = \langle\Psi_0|V_2|\Psi\rangle = \frac{1}{2}\sum_{abmn} v_{abmn}\tilde{\rho}_{mnab} \tag{135}$$

If we substitute the all-order wave function $|\Psi\rangle$ into the Schrödinger equation (134), we obtain the following equations for the single- and double-excitation coefficients.

$$[\epsilon_a - \epsilon_m + \delta E]\rho_{ma} = \sum_{bn} \tilde{v}_{mban}\rho_{nb} + \sum_{bnr} v_{mbnr}\tilde{\rho}_{nrab} - \sum_{bcn} v_{bcan}\tilde{\rho}_{mnbc}, \tag{136}$$

$$[\epsilon_a+\epsilon_b-\epsilon_m-\epsilon_n+\delta E]\rho_{mnab}=v_{mnab}+\sum_{cd}v_{cdab}\rho_{mncd}+\sum_{rs}v_{mnrs}\rho_{rsab}$$
$$+\left[\sum_r v_{mnrb}\rho_{ra}-\sum_c v_{cnab}\rho_{mc}+\sum_{rc}\tilde{v}_{cnrb}\tilde{\rho}_{mrac}\right]+\left[\begin{array}{c}a\leftrightarrow b\\ m\leftrightarrow n\end{array}\right]. \quad (137)$$

These equations are reduced to radial form and solved iteratively.

To carry out the angular reduction of the SD equations, we write

$$\rho_{ma}=\delta_{ma}\,S(ma) \quad (138)$$

and let

$$\rho_{mnab}=\sum_k J_k(mnab)S_k(mnab)\,, \quad (139)$$

where $J_k(abcd)$ is the angular-momentum factor introduced in Eq. (95). With these substitutions, the equations for the single excitation coefficients become

$$[\epsilon_a-\epsilon_m+\delta E]\,S(ma)=\sum_{nb}\left[[b]R_0(mban)+\sum_k\frac{(-1)^{b+a+k}}{[a]}X_k(mbna)\right]\delta_{\kappa_n\kappa_b}\,S(nb)$$
$$+\sum_{knrb}\frac{(-1)^{a+b+n+r}}{[a][k]}X_k(mbnr)\tilde{S}_k(nrab)$$
$$-\sum_{knbc}\frac{(-1)^{a+b+c+n}}{[a][k]}X_k(bcan)\tilde{S}_k(mnbc)\,. \quad (140)$$

In this equation,

$$\tilde{S}_k(mnab)=S_k(mnab)+[k]\sum_{k'}\left\{\begin{array}{ccc}m&a&k\\ n&b&k'\end{array}\right\}S_{k'}(mnba)\,. \quad (141)$$

For the double excitation coefficient, we obtain

$$[\epsilon_a+\epsilon_b-\epsilon_m-\epsilon_n+\delta E_C]S_k(mnab)=X_k(mnab)$$
$$+\sum_{k'lcd}(-1)^{a+b+m+n}[k]\left\{\begin{array}{ccc}k'&l&k\\ a&m&c\end{array}\right\}\left\{\begin{array}{ccc}k'&l&k\\ b&n&d\end{array}\right\}X_l(cdab)S_{k'}(mncd)$$
$$+\sum_{k'lrs}(-1)^{a+b+m+n}[k]\left\{\begin{array}{ccc}k'&l&k\\ m&a&r\end{array}\right\}\left\{\begin{array}{ccc}k'&l&k\\ n&b&s\end{array}\right\}X_l(mnrs)S_{k'}(rsab)$$
$$+\left[\sum_r X_k(mnrb)\delta_{\kappa_r\kappa_a}S(ra)-\sum_c X_k(cnab)\delta_{\kappa_m\kappa_c}S(mc)\right.$$
$$-\sum_{rc}\frac{(-1)^{k+c+r}}{[k]}X_k(cnrb)\tilde{S}_k(mrac)$$
$$\left.-\sum_{lrc}(-1)^{k+c+r}\left\{\begin{array}{ccc}c&r&k\\ n&b&l\end{array}\right\}X_l(cnbr)\tilde{S}_k(mrac)\right]+\left[\begin{array}{c}m\leftrightarrow n\\ a\leftrightarrow b\end{array}\right]. \quad (142)$$

Table 3
Partial wave contributions (a.u.) to the all-order ground-state energy δE in helium.

L	$\delta E(L)$	δE
0	-0.0173678	-0.0173678
1	-0.0214896	-0.0388574
2	-0.0022208	-0.0410782
3	-0.0005576	-0.0416358
4	-0.0001991	-0.0418349
5	-0.0000876	-0.0419225
6	-0.0000443	-0.0419668
7	-0.0000247	-0.0419915
8–∞	-0.0000491	-0.0420406

The expression for the correlation energy δE becomes

$$\delta E = \frac{1}{2}\sum_{abmnk}\frac{(-1)^{a+b+m+n}}{[k]}X_k(abmn)\tilde{S}_k(mnab)\,. \tag{143}$$

We solve Eqs. (141–143) iteratively. As a first step, we restrict the virtual orbitals mn in the above radial equations to those with $L = 0$, namely, $s_{1/2}$ orbitals. The corresponding energy $\delta E(0)$ is listed in the first row of Table 3. In the next step, we include orbitals $p_{1/2}$ and $p_{3/2}$ with $L = 1$ and find the correction $\delta E(1)$ shown in the second row of Table 3. We continue this procedure through $L = 7$ as shown in the table. The partial-wave contributions $\delta E(L)$ again fall off as L^{-4} and can be extrapolated to give an all-order correlation energy $\delta E = -0.0420406$ a.u., listed on the last line of the table. Adding this to the HF binding energy brings theory into agreement with experiment to about 0.01%. The Breit interaction, QED, and recoil corrections, are responsible for the residual small difference.

Generalizations of this iterative scheme were developed and applied to evaluate energies of $(1s2p)$ triplet and $(1s2p)$ singlet states of helium-like ions in Refs. [40, 41]. These iterative all-order calculations lead to energies in close agreement with the configuration-interaction (CI) calculations discussed later in this chapter. It should be emphasized here that as Z increases along the isoelectronic sequence, Breit and QED corrections become more and more important.

3.9. Three-Electron Atoms

Now we turn to lithium and three-electron lithium-like ions. Again we start with the normally-ordered no-pair Hamiltonian given in Eq. (132), and choose the starting potential to be the Hartree-Fock potential of the $(1s)^2$ helium-like core. We expand the energy of an atomic state in powers of the interaction potential

$$E = E^{(0)} + E^{(1)} + E^{(2)} + \ldots,$$

and find that in each order of perturbation theory

$$E^{(k)} = E^{(k)}_{\rm core} + E^{(k)}_{v}.$$

The terms $E^{(k)}_{\rm core}$ give the k-th order contributions to the energy of the helium-like core, and are independent of the valence state. These are precisely the terms evaluated in the previous section. The terms $E^{(k)}_v$ are the k-th order contributions to the energy of the atom relative to the ionic core; in other words $-E^{(k)}_v$ is the k-th order contribution to the valence-electron removal energy. A straight forward application of Rayleigh-Schrödinger perturbation theory [42] gives,

$$E^{(0)}_v = \epsilon_v \tag{144}$$

$$E^{(1)}_v = 0 \tag{145}$$

$$E^{(2)}_v = -\sum_{amn} \frac{v_{vamn}\tilde{v}_{mnva}}{\epsilon_m + \epsilon_n - \epsilon_v - \epsilon_a} + \sum_{abm} \frac{v_{abmv}\tilde{v}_{mvab}}{\epsilon_m + \epsilon_v - \epsilon_a - \epsilon_b} \tag{146}$$

$$\begin{aligned} E^{(3)}_v = & \sum_{mrabc} \frac{\tilde{v}_{acrv}\tilde{v}_{vmba}\tilde{v}_{rbmc}}{(\epsilon_{vm} - \epsilon_{ab})(\epsilon_{rv} - \epsilon_{ac})} + \sum_{mnrac} \frac{\tilde{v}_{cvrm}\tilde{v}_{nmva}\tilde{v}_{ranc}}{(\epsilon_{mn} - \epsilon_{av})(\epsilon_{rn} - \epsilon_{cv})} \\ & + \sum_{mnabc} \frac{\tilde{v}_{camn}v_{nmba}\tilde{v}_{vbvc}}{(\epsilon_{mn} - \epsilon_{ab})(\epsilon_{nm} - \epsilon_{ac})} + \sum_{mnrab} \frac{\tilde{v}_{abnr}v_{nmba}\tilde{v}_{rvmv}}{(\epsilon_{mn} - \epsilon_{ab})(\epsilon_{rn} - \epsilon_{ab})} \\ & + \sum_{nabcd} \frac{\tilde{v}_{cdvn}v_{vnba}v_{badc}}{(\epsilon_{vn} - \epsilon_{ab})(\epsilon_{vn} - \epsilon_{cd})} + \sum_{mnrsa} \frac{\tilde{v}_{avsr}v_{nmva}v_{rsnm}}{(\epsilon_{mn} - \epsilon_{av})(\epsilon_{rs} - \epsilon_{av})} \\ & + \Bigg[\sum_{nrabc} \frac{\tilde{v}_{canr}\tilde{v}_{nvba}\tilde{v}_{rbvc}}{(\epsilon_{vn} - \epsilon_{ab})(\epsilon_{rn} - \epsilon_{ac})} + \sum_{mnrac} \frac{\tilde{v}_{acrm}\tilde{v}_{nmva}\tilde{v}_{rvnc}}{(\epsilon_{mn} - \epsilon_{av})(\epsilon_{rm} - \epsilon_{ac})} \\ & \quad + \sum_{mracd} \frac{\tilde{v}_{cdrm}\tilde{v}_{vmva}v_{radc}}{(\epsilon_m - \epsilon_a)(\epsilon_{rm} - \epsilon_{cd})} + \sum_{mrsac} \frac{\tilde{v}_{acsr}\tilde{v}_{mvva}v_{rsmc}}{(\epsilon_m - \epsilon_a)(\epsilon_{rs} - \epsilon_{ac})} \\ & \quad + \sum_{mrsab} \frac{\tilde{v}_{absr}v_{vmba}v_{rsmv}}{(\epsilon_{mv} - \epsilon_{ab})(\epsilon_{rs} - \epsilon_{ab})} + \sum_{mnacd} \frac{\tilde{v}_{cdmn}v_{nmva}v_{vadc}}{(\epsilon_{mn} - \epsilon_{av})(\epsilon_{mn} - \epsilon_{cd})} + \text{c.c.} \Bigg], \end{aligned} \tag{147}$$

where we have introduced the notation $\epsilon_{ij} = \epsilon_i + \epsilon_j$. Although we have in mind applications to Li and Li-like ions, the above equations are written for the more general case of an atom or ion with one valence electron outside of a closed core.

The lowest approximation to the removal energy is seen to be $-\epsilon_v$, where ϵ_v is the eigenvalue of the "frozen-core" Hartree-Fock equation. It should be emphasized that the valence orbital is not treated self consistently. The orbitals of the closed-shell core are determined self-consistently, then the valence electron HF equation is solved in the "frozen" potential of the core. From Eq. (145) it follows that there is no first-order correction to the removal energy in the frozen-core HF potential.

It is interesting to note that the second-order energy $E^{(2)}_v$ can be written as the diagonal matrix element of the second-order "self-energy" operator defined by

$$\Sigma^{(2)}_{ij}(\epsilon) = -\sum_{amn} \frac{v_{iamn}\tilde{v}_{mnja}}{\epsilon_m + \epsilon_n - \epsilon - \epsilon_a} + \sum_{abm} \frac{v_{abmi}\tilde{v}_{mjab}}{\epsilon_m + \epsilon - \epsilon_a - \epsilon_b}. \tag{148}$$

With this definition, $E^{(2)}_v = \left[\Sigma^{(2)}(\epsilon_v)\right]_{vv}$. It is an elementary exercise to show that, in configuration-space, the self-energy operator has the asymptotic form

$$\lim_{r\to\infty} \Sigma^{(2)}(\epsilon, \boldsymbol{r}, \boldsymbol{r'}) = -\frac{\alpha}{2r^4}\, \delta_{\boldsymbol{r}\boldsymbol{r'}},$$

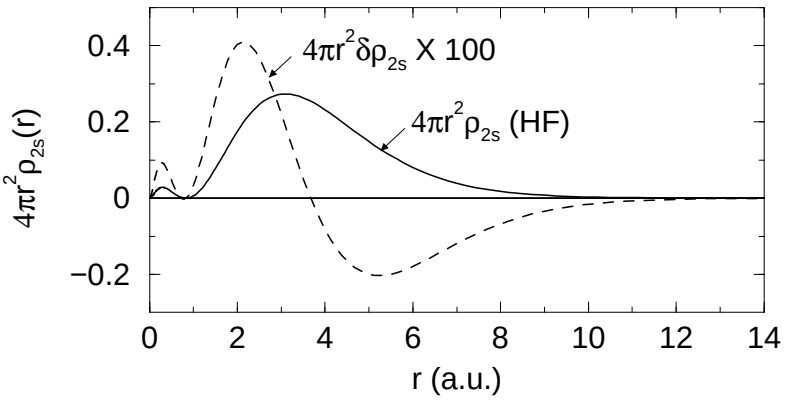

Figure 8. The radial density $4\pi r^2\rho_{2s}(r)$ given in the HF approximation is shown together with the modification $4\pi r^2\delta\rho_{2s}(r) \times 100$ to the radial density found in the Brueckner approximation.

where

$$\alpha = \frac{2}{3}\sum_{am}\frac{\langle m|z|a\rangle\langle a|z|m\rangle}{\epsilon_m - \epsilon_a} \tag{149}$$

is the Hartree-Fock approximation to the polarizability of the closed atomic core. Approximate calculations of high Rydberg levels of monovalent atoms and of electron-ion scattering are often based on a modified version of the Hartree-Fock equation [see 43, for example]

$$\left(h_0 + V_{\rm HF} - \frac{\alpha}{2r^4}\right)\psi = \epsilon\psi, \tag{150}$$

which accounts for the core polarizability and, consequently, accounts approximately for correlation corrections. In this spirit, one introduces Brueckner orbitals [44, 45] as solutions to

$$\left[h_0 + V_{\rm HF} + \Sigma(\epsilon)\right]\psi = \epsilon\psi, \tag{151}$$

To second-order, we may write $\psi \approx \phi_v + \delta\phi_v$, and $\epsilon = \epsilon_v + \delta\epsilon_v$ where

$$\left[h_0 + V_{\rm HF} - \epsilon_v\right]\phi_v = 0 \tag{152}$$

$$\left[h_0 + V_{\rm HF} - \epsilon_v\right]\delta\phi_v = \left[\delta\epsilon_v - \Sigma^{(2)}(\epsilon_v)\right]\phi_v \tag{153}$$

The inhomogeneous Eq. (153) has a nontrivial solution only if the right-hand side is orthogonal to ϕ_v, the solution to the homogeneous equation. This leads to the relation

$$\delta\epsilon_v = \left[\Sigma^{(2)}(\epsilon_v)\right]_{vv} = E_v^{(2)}. \tag{154}$$

The approximate Brueckner orbitals, $\phi_v + \delta\phi_v$ differ from Hartree-Fock orbitals ϕ_v in that the peaks in the radial wave functions are drawn in toward the nucleus by the attractive polarizability force. The attractive character of this force is illustrated in Fig. 8, where we plot the radial density of $2s$ valence electron in neutral lithium in the HF approximation together with the modification caused by the Brueckner-orbital correction.

Table 4
Contributions to the removal energy (a.u.) of lithium in perturbation theory.

Term	$2s_{1/2}$	$2p_{1/2}$	$2p_{3/2}$
$E^{(0)}$	-0.196320	-0.128638	-0.128636
$E^{(2)}$	-0.001649	-0.001375	-0.001375
$E^{(3)}$	-0.000125	-0.000145	-0.000145
Sum	-0.198114	-0.130158	-0.130156
Expt.	-0.198142	-0.130236	-0.130234

3.10. Angular Reduction

To put the MBPT formulas (146-147) into a form suitable for numerical evaluation, we carry out an angular momentum decomposition of the two-electron matrix element and sum over magnetic quantum numbers. This leads to

$$E_v^{(2)} = -\sum_{Lmna} \frac{X_L(mnva)Z_L(mnva)}{[L][j_v](\epsilon_m + \epsilon_n - \epsilon_v - \epsilon_a)} + \sum_{Lmab} \frac{X_L(mvab)Z_L(mvab)}{[L][j_v](\epsilon_m + \epsilon_v - \epsilon_a - \epsilon_b)} \tag{155}$$

The angular reduction of the third-order $E_v^{(3)}$, which is much more complicated, is relegated to the Appendix.

Let's look at specific results. For neutral lithium, the lowest-order Dirac-Hartree-Fock energies $E_v^{(0)} = \epsilon_v$ for the $2s$ and $2p$ states are given in the first row of Table 4. The Hartree-Fock energies are within 1–2% of the measured removal energies. Including second-order corrections accounts for the major part of the residual difference, while third-order corrections improve the differences with measurement to less than 0.1%, as shown in the table.

The Hartree-Fock energies increase roughly as Z^2 along the lithium isoelectronic sequence; the second-order energy $E^{(2)}$ increases rapidly at low Z and stays roughly constant at intermediate and high Z, and the third-order energy increases rapidly at low Z and falls off approximately as $1/Z$ at high Z. The contributions of $E^{(2)}$ and $E^{(3)}$ for $2s_{1/2}$, $2p_{1/2}$, and $2p_{3/2}$ states are plotted against nuclear charge Z for lithium-like ions in Fig. 9. Relativistic effects are apparent at large Z, where $E_v^{(2)}$ departs from constancy, and where differences between values of $E^{(2)}_{2p_{1/2}}$ and $E^{(2)}_{2p_{3/2}}$ and between $E^{(3)}_{2p_{1/2}}$ and $E^{(3)}_{2p_{3/2}}$ are seen.

3.11. Breit Interaction for Lithium-like Ions

As mentioned earlier, owing to its relatively small size, it is often sufficient to consider only those contributions to the energy that are linear in the Breit interaction. Such contributions may be obtained by replacing the Coulomb interaction in the MBPT expressions for $E^{(k)}$ by the sum of the Coulomb plus Breit interaction and linearizing in the Breit interaction. We let $B^{(k)}$ designate the contribution linear in the Breit interaction and of order $k-1$ in the Coulomb interaction. To simplify the resulting expressions, we introduce the notation

$$B_{ij} \stackrel{\text{def}}{=} \sum_a \tilde{b}_{aiaj} = -\sum_a b_{iaaj}.$$

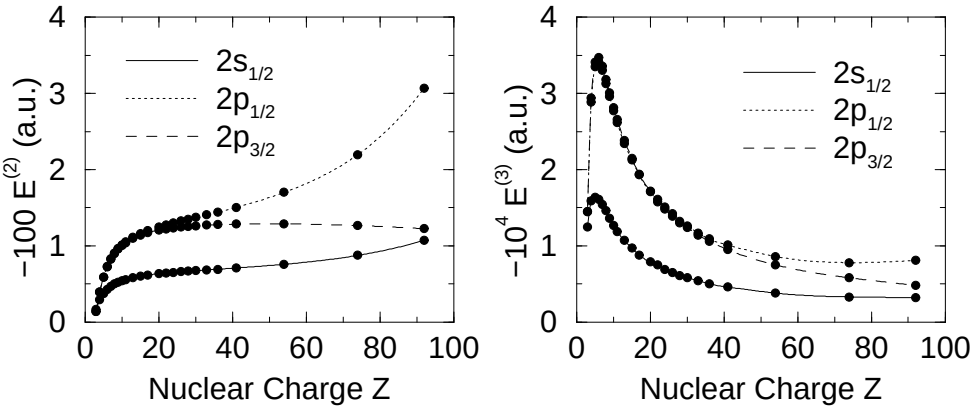

Figure 9. Second-order $E_v^{(2)}$ and third-order $E_v^{(3)}$ energies of $2s_{1/2}$, $2p_{1/2}$, and $2p_{3/2}$ states of lithium-like ions.

For atoms with one valence electron, we find

$$B_v^{(1)} = B_{vv} \tag{156}$$

$$B_v^{(2)} = -2\sum_{amn} \frac{b_{vamn}\tilde{v}_{mnva}}{\epsilon_{mn}-\epsilon_{va}} + 2\sum_{abm} \frac{b_{abmv}\tilde{v}_{mvab}}{\epsilon_{mv}-\epsilon_{ab}} + B_{\rm RPA}^{(2)} \tag{157}$$

$$B_{\rm RPA}^{(2)} = \sum_{am}\left[\frac{B_{am}\tilde{v}_{mvva}}{\epsilon_m-\epsilon_a} + \text{c.c.}\right] \tag{158}$$

$$B_v^{(3)} \approx B_{\rm BO}^{(3)} + B_{\rm RPA}^{(3)} \tag{159}$$

$$B_{\rm BO}^{(3)} = \sum_{i\neq v}\left\{\frac{B_{vi}}{\epsilon_i-\epsilon_v}\left[\sum_{amn}\frac{v_{mnav}\tilde{v}_{ianm}}{\epsilon_{mn}-\epsilon_{av}} + \sum_{abm}\frac{v_{abvm}\tilde{v}_{imba}}{\epsilon_{vm}-\epsilon_{ab}}\right] + \text{c.c.}\right\} \tag{160}$$

$$B_{\rm RPA}^{(3)} = \sum_{abmn}\left[\frac{B_{bn}\tilde{v}_{nmab}\tilde{v}_{avvm}}{(\epsilon_m-\epsilon_a)(\epsilon_n-\epsilon_b)} + \frac{B_{nb}\tilde{v}_{mbna}\tilde{v}_{avvm}}{(\epsilon_m-\epsilon_a)(\epsilon_n-\epsilon_b)} + \text{c.c.}\right], \tag{161}$$

where only the dominant subset of contributions to $B^{(3)}$ is given.

The first two terms in Eq. (157) are evaluated in exactly the same way as the second-order energy. The third term $B_{\rm RPA}^{(2)}$, the random-phase approximation contribution, is found to be an order of magnitude larger than the first two; it approximately equals in magnitude (and for neutral lithium almost cancels) the first-order Breit interaction $B_v^{(1)}$. Because the third term is so large, it is separated off and evaluated together with terms $B_{\rm RPA}^{(3)}$ from third-order that have the same denominator structure. Indeed, we can recover

the second- and third-order terms from the iterative solution to the RPA equations

$$B_{\rm RPA} = B_{vv} + \sum_{an} \frac{t_{an}\tilde{v}_{nvva}}{\epsilon_n - \epsilon_a} + \sum_{an} \frac{\tilde{v}_{avvn}t_{na}}{\epsilon_n - \epsilon_a} \tag{162}$$

$$t_{na} = B_{na} + \sum_{bm} \frac{t_{bm}\tilde{v}_{nmba}}{\epsilon_m - \epsilon_b} + \sum_{bm} \frac{\tilde{v}_{nbma}t_{mb}}{\epsilon_m - \epsilon_b} \tag{163}$$

$$t_{an} = B_{an} + \sum_{bm} \frac{t_{bm}\tilde{v}_{ambn}}{\epsilon_m - \epsilon_b} + \sum_{bm} \frac{\tilde{v}_{abmn}t_{mb}}{\epsilon_m - \epsilon_b}. \tag{164}$$

When we solve these equations iteratively, we recover the first-order Breit energy together with second-, third-, and higher-order RPA contributions. We plot $B_{\rm RPA}$ against Z for $n = 2$ states of lithium-like ions in the lower panel of Fig. 10.

The remaining third-order term $B^{(3)}_{\rm BO}$ is that associated with approximate Brueckner orbitals. Note that the solution to the approximate Brueckner orbital equation (153) can be written

$$\delta\phi_v = \sum_{i\neq v} \frac{|i\rangle\langle i\left|\Sigma^{(2)}(\epsilon_v)\right|v\rangle}{\epsilon_v - \epsilon_i}. \tag{165}$$

Comparing this with Eq. (160), we find

$$B^{(3)}_{\rm BO} = B_{(\delta v)\,v} + B_{v\,(\delta v)} = -2\sum_a b_{(\delta v)aav}. \tag{166}$$

We present the three contributions to the Breit interaction, $B_{\rm RPA}$, which includes the first-order term together with higher-order RPA corrections, the residual second-order Breit correction, and the third-order Brueckner correction for $2s$ and $2p$ states of lithium-like ions, in Fig. 10.

3.12. Reduced Mass and Mass Polarization

For many electron atoms, there are two further corrections associated with the finite mass of the nucleus. The first is the reduced-mass correction, discussed in Section 2.5 for one electron ions:

$$\Delta E_{\rm RM} \approx -\frac{m}{M+m}\,E, \tag{167}$$

where m is the electron mass and M is the nuclear mass. In this equation, E is the energy in atomic units, calculated assuming infinite nuclear mass.

The second correction, which is associated with nuclear recoil, is the mass-polarization correction,

$$\Delta E_{\rm MP} = \frac{M}{(M+m)^2}\Big\langle\Psi\Big|\sum_{i>j}\boldsymbol{p}_i{\cdot}\boldsymbol{p}_j\Big|\Psi\Big\rangle, \tag{168}$$

where $\boldsymbol{p}_k = \frac{1}{i}\boldsymbol{\nabla}_k$ is the electron momentum operator. The angle brackets designate the expectation value of the enclosed two-particle mass-polarization operator $P = \sum_{i>j}\boldsymbol{p}_i{\cdot}\boldsymbol{p}_j$.

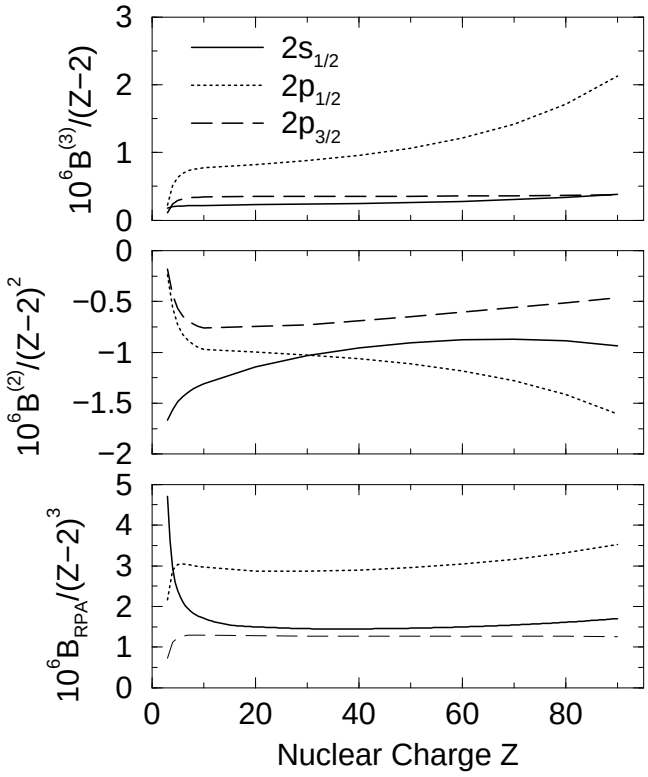

Figure 10. $B_{\rm RPA}$, the residual $B_v^{(2)}$ contribution, and the Brueckner-orbital contribution to $B_v^{(3)}$ are plotted against Z for $n = 2$ states of lithium-like ions. Notation: solid lines represent $2s_{1/2}$, dotted lines represent $2p_{1/2}$, and dashed lines represent $2p_{3/2}$. Units: a.u..

The reduced-mass and mass-polarization terms arise on transforming the many-electron plus nucleus Hamiltonian to center of mass coordinates.

In second-quantization the mass-polarization operator takes the form

$$P = \frac{1}{2}\sum_{ijkl} p_{ijkl} :a_i^\dagger a_j^\dagger a_l a_k: + \sum_{ij} p_{ij} :a_i^\dagger a_j: \,, \tag{169}$$

where $p_{ijkl} = \langle ij|\boldsymbol{p}_1\cdot\boldsymbol{p}_2|kl\rangle$ and $p_{ij} = -\sum_a p_{iaaj}$.

The angular decomposition of the two-particle matrix element p_{ijkl} is easily carried out and leads to

$$p_{ijkl} = \sum_L J_L(ijkl)\, P_L(ijkl) \equiv J_1(ijkl) P_1(ijkl), \tag{170}$$

where $J_L(ijkl)$ is the product of three-j coefficients defined in Eq. (95). The coefficient $P_1(ijkl)$, which is independent of magnetic quantum numbers, is given by

$$P_1(ijkl) = -\langle\kappa_i\|C_1\|\kappa_j\rangle\langle\kappa_j\|C_1\|\kappa_l\rangle P(ik)P(jl)\,, \tag{171}$$

where $P(ij)$ are radial matrix elements of the momentum operator. It is interesting to note that, by contrast to the decomposition of matrix elements of the Coulomb operator v_{ijkl} and the Breit operator b_{ijkl}, the sum over L in Eq. (170) reduces to a single term with $L = 1$. The radial part of the momentum operator in Dirac theory is

$$P(ba) = \frac{1}{i}\int_0^\infty dr \left[P_b(r)\left(\frac{dP_a}{dr} + \frac{\eta_a}{r}P_a\right) + Q_b(r)\left(\frac{dQ_a}{dr} + \frac{\zeta_a}{r}Q_a\right)\right], \tag{172}$$

with $\eta_a = l_a$ or $-l_a - 1$, for $l_b = l_a - 1$ or $l_b = l_a + 1$, respectively; and $\zeta_a = l'_a$ or $-l'_a - 1$ for $l'_b = l'_a - 1$ or $l'_b = l'_a + 1$, respectively. Here $l' = l(-\kappa)$. The rules for the two parameters η_a and ζ_a can be written in a somewhat simpler form by noting that only the values $\kappa_b = -\kappa_a$ or $\kappa_b = \kappa_a \pm 1$ are permitted by angular momentum selection rules; the corresponding values of η_a and ζ_a are given in the following small table.

κ_b	η_a	ζ_a
$\kappa_a + 1$	$-\kappa_b$	$-\kappa_a$
$\kappa_a - 1$ or $-\kappa_a$	κ_a	κ_b

It is easy to prove that $P(ab) = P(ba)^*$.

Owing to the similarity of the mass-polarization operator and the Breit operator, the mass-polarization corrections in MBPT can be classified using the scheme described for the Breit interaction in the previous subsection. Correspondingly, we write the valence contribution to the expectation value of P as

$$P_v \approx P_{\rm RPA} + P^{(2)} + P^{(3)}, \tag{173}$$

where $P_{\rm RPA}$ contains the lowest-order contribution and all higher-order iterates of the RPA equations, $P^{(2)}$ is the residual second-order correction, and $P^{(3)} \equiv P^{(3)}_{\rm BO}$ is the third-order Brueckner-orbital correction.

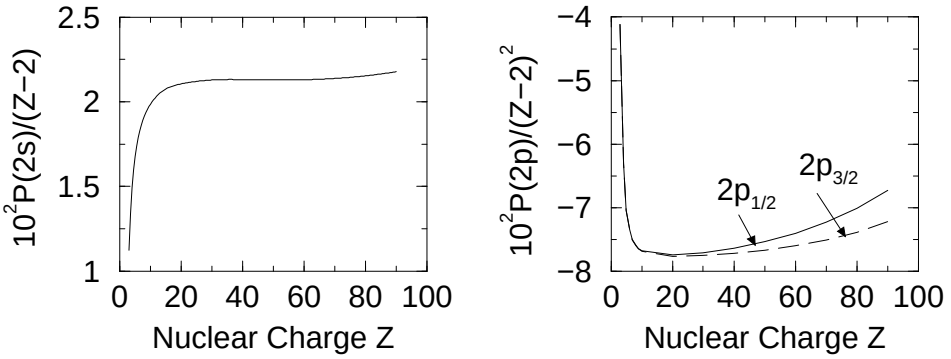

Figure 11. Scaled values of the mass-polarization operator $P(2s)/(Z-2)$ for the $2s$ state and $P(2p)/(Z-2)^2$ for $2p_{1/2}$ and $2p_{3/2}$ states are plotted against Z for $n=2$ states of lithium-like ions. Units: a.u..

The expectation value of the mass-polarization operator, calculated as described above, is presented for $2s$ and $2p$ states of lithium-like ions in Fig. 11. It should be mentioned that for the special case of lithium-like ions, with a $(1s)^2$ core, the RPA corrections to $P^{(1)}$ identically vanish. Therefore, for lithium-like ions, $P_{\rm RPA} \equiv P^{(1)}$. Moreover, for ns states of lithium-like ions, both $P^{(1)}$ and $P^{(3)}_{\rm BO}$ vanish. Thus, $P(2s) = P^{(2)}(2s)$ for lithium-like ions.

3.13. Lithium-like Uranium and the $2s_{1/2} - 2p_{1/2}$ Lamb Shift

As a specific example of the considerations in the previous subsections, let us consider the ion $^{238}U^{+89}$. This is a particularly interesting case since lithium-like uranium is the most highly charged ion for which both the $2s_{1/2} - 2p_{1/2}$ and $2s_{1/2} - 2p_{3/2}$ intervals have been precisely measured. The $2s_{1/2} - 2p_{1/2}$ energy interval, 280.59 (0.10) eV, was measured by Doppler-tuned spectrometry at Lawrence Berkeley Laboratory's Bevelac by Schweppe et al. [46] and the $2s_{1/2} - 2p_{3/2}$ interval, 4459.37 (0.21) eV, was measured by Doppler-free crystal spectrometry at Lawrence Livermore National Laboratory's high-energy electron beam ion trap by Beiersdorfer et al. [47, 48].

The charge form factor of the deformed ^{238}U nucleus is accurately known from the muonic x-ray measurements of Zumbro et al. [49] and can be parameterized by the deformed Fermi distribution

$$\rho(\boldsymbol{r}) = \frac{\rho_0}{1 + \exp\left[\frac{r - R(\hat{\boldsymbol{r}})}{a}\right]}, \tag{174}$$

where $a = 0.5046(9)$ fm and $R(\hat{\boldsymbol{r}}) = c\,[1 + \beta_2 Y_{20}(\hat{\boldsymbol{r}}) + \beta_4 Y_{40}(\hat{\boldsymbol{r}})]$, with $c = 7.0110(12)$ fm, $\beta_2 = 0.2653(19)$ and $\beta_4 = 0.0672(49)$. We average this distribution over angles and use the resulting radial distribution to determine the nuclear potential $V_{\rm nuc}(r)$. The resulting finite nuclear size corrections to the HF energies of the $2s_{1/2}$, $2p_{1/2}$ and $2p_{3/2}$ states are 1.3164, 0.1288, and -0.0082 a.u., respectively.

As seen in Table 5, the MBPT perturbation expansion of energies converges rapidly for $n = 2$ states of lithium-like uranium. The dominant corrections to the HF energies are

Table 5
Contributions to the binding energy (eV) of $n = 2$ states in Li-like ^{238}U and comparisons of residual differences with experiment with "screened" Lamb Shift calculations.

Term	$2s_{1/2}$	$2p_{1/2}$	$2p_{3/2}$
$E^{(0)}$	-32917.9662	-32631.2771	-28403.1054
$E^{(2)}$	-0.2915	-0.8342	-0.3339
$E^{(3)}$	-0.0009	-0.0022	-0.0013
$B_{\rm RPA}$	34.2164	71.0080	24.9497
$\Delta B(\omega)$	0.6513	0.2836	-6.4043
$B^{(2)}$	-0.2091	-0.3647	-0.0993
$B^{(3)}$	0.0010	0.0055	0.0009
RM	0.0758	0.0750	0.0654
MP	0.0001	-0.0339	-0.0365
$E_{\rm total}$	-32883.5232	-32561.1400	-28384.9646
Transition energy		$2s_{1/2} - 2p_{1/2}$	$2s_{1/2} - 2p_{3/2}$
MBPT		322.38	4498.56
Expt. (Refs. [46],[47])		280.59(10)	4459.37(21)
Expt. – MBPT		-41.79(10)	-39.19(21)
Lamb Shift (Refs. [50],[51])		-41.77	-39.13(5)

from $B_{\rm RPA}$, the frequency-dependence of the Breit interaction $\Delta B(\omega)$, and the second-order correlation corrections $E^{(2)}$ and $B^{(2)}$. Mass-polarization corrections are also found to be important in obtaining accurate values for $2s - 2p$ energy intervals.

From the table, we find that $E_{2p_{1/2}} - E_{2s_{1/2}} = 322.38$ eV and $E_{2p_{3/2}} - E_{2s_{1/2}} = 4498.56$ eV. The differences between the measured and theoretical values, -41.79±0.10 eV and -39.19 ±0.21 eV, for the $2s_{1/2} - 2p_{1/2}$ and $2s_{1/2} - 2p_{3/2}$ intervals, respectively, can be attributed to omitted QED corrections. Self-energy and vacuum polarization corrections to these intervals, including dominant contributions from higher-order diagrams associated with "screening" corrections, were calculated by Blundell [51] who gave a value of -41.68±0.05 eV for the Lamb-Shift correction to the $2s_{1/2} - 2p_{1/2}$ interval. However, the most completed screened QED calculations for this interval were carried out by Yerokhin et al. [50]. Their benchmark result of -41.77 eV for Li-like uranium is different from Blundell's value by 0.09 eV and is in better agreement with the deduced empirical QED energy. As for the $2s_{1/2} - 2p_{3/2}$ interval, the QED correction of -39.13±0.10 eV shown in Table 5 is obtained by extrapolation from Blundell's results at $Z = 60$, 70, 80 and 90, and the uncertainty of 0.05 eV at $Z = 90$ is quoted here, even though this estimate is likely to be too small. In Table 5, these theoretical and experimental values of the Lamb shift are seen to be in remarkably good agreement for both intervals. Nevertheless, many small corrections which are usually neglected cannot be ignored in these high-Z ions. Examples are higher-order Breit corrections, negative-energy state contributions and two-loop Lamb shifts. At the level of 0.1 eV or smaller, the good agreements shown here may be due in part to cancellation of errors. We shall revisit these comparisons in Sections 4.4 and 4.5.

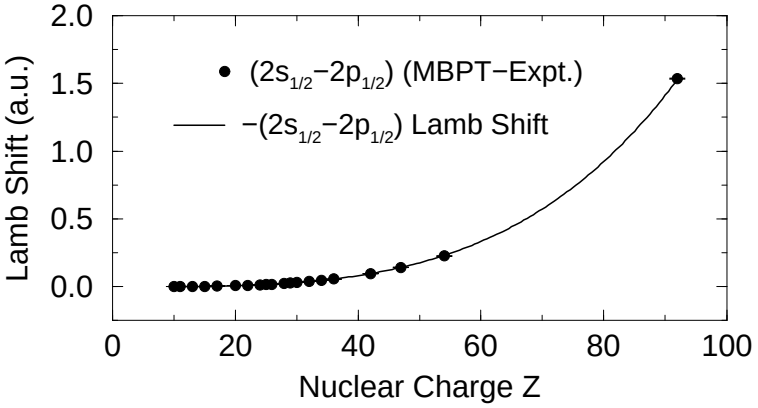

Figure 12. Experimental values of the $2s_{1/2} - 2p_{1/2}$ Lamb shift in lithium-like ions shown by the black dots are compared with theoretical values of the "screened" Lamb shift from Ref. [51].

Further comparisons of experimental and theoretical values of the $2s_{1/2} - 2p_{1/2}$ Lamb shift in lithium-like ions with nuclear charges ranging from 10 to 92 are shown in Fig. 12. The experimental values of the $2s_{1/2} - 2p_{1/2}$ intervals are taken from the review of Ph. Bosselmann et al. [52]. The corresponding MBPT values are calculated using the prescription given in Ref. [53]; the difference gives an "experimental" Lamb shift. The theoretical Lamb shift shown in the plot is from Ref. [51].

In these examples, the perturbation series converged rapidly and one was able to infer accurate values of the QED corrections from the difference between theory and experiment. For neutral lithium or light lithium-like ions, the convergence of MBPT is much slower and one must resort to all-order methods to obtain precise theoretical energies. We briefly describe the all-order single-double method for lithium and lithium-like ions in the next subsection.

3.14. Single-Double (SD) Equations for Lithium-like Ions

The relativistic SD equations for lithium-like ions have been discussed at length in [54] so we will give only a brief reprise of the equations here. In the SD approach, the wave function Ψ_v of an atomic system with one valence electron is represented as:

$$\begin{aligned}\Psi_v &= \left[1 + \sum_{ma} \rho_{ma} a_m^\dagger a_a + \frac{1}{2} \sum_{mnab} \rho_{mnab} a_m^\dagger a_n^\dagger a_b a_a \right. \\ &\left. + \sum_{m \neq v} \rho_{mv} a_m^\dagger a_v + \sum_{mna} \rho_{mnva} a_m^\dagger a_n^\dagger a_a a_v \right] \Phi_v, \end{aligned} \tag{175}$$

where Φ_v is the lowest-order atomic state function, which is taken to be the *frozen-core* Dirac-Hartree-Fock wave function of a state v.

The coefficients ρ_{ma} and ρ_{mnab} are amplitudes for single and double excitations from the core, respectively; ρ_{mv} is the amplitude for a single excitation of the valence electron,

and ρ_{mnva} is the amplitude for excitation of the valence electron and a core electron. Substituting the wave function (175) into the many-body Schrödinger equation, where the Hamiltonian is taken to be the relativistic *no-pair* Hamiltonian with Coulomb interactions, one obtains the coupled equations for single- and double-excitation coefficients [54]:

$$(\epsilon_a - \epsilon_m)\rho_{ma} = \sum_{bn} \tilde{v}_{mban}\rho_{nb} + \sum_{bnr} v_{mbnr}\tilde{\rho}_{nrab} - \sum_{bcn} v_{bcan}\tilde{\rho}_{mnbc}. \tag{176}$$

$$(\epsilon_a + \epsilon_b - \epsilon_m - \epsilon_n)\rho_{mnab} = v_{mnab} + \sum_{cd} v_{cdab}\rho_{mncd} + \sum_{rs} v_{mnrs}\rho_{rsab} + \left[\sum_{r} v_{mnrb}\rho_{ra} - \sum_{c} v_{cnab}\rho_{mc} + \sum_{rc} \tilde{v}_{cnrb}\tilde{\rho}_{mrac}\right] + \left[\begin{array}{c} a \leftrightarrow b \\ m \leftrightarrow n \end{array}\right] \tag{177}$$

As before, antisymmetrized excitation amplitudes are designated by $\tilde{\rho}_{ijkl} = \rho_{ijkl} - \rho_{ijlk}$. The correlation correction to the core energy is given in terms of the core excitation amplitudes by

$$\delta E_c = \frac{1}{2}\sum_{mnab} v_{abmn}\tilde{\rho}_{mnab}. \tag{178}$$

The equations governing the valence excitation amplitudes are:

$$(\epsilon_v - \epsilon_m + \delta E_v)\rho_{mv} = \sum_{bn} \tilde{v}_{mbvn}\rho_{nb} + \sum_{bnr} v_{mbnr}\tilde{\rho}_{nrvb} - \sum_{bcn} v_{bcvn}\tilde{\rho}_{mnbc}. \tag{179}$$

$$(\epsilon_v + \epsilon_b - \epsilon_m - \epsilon_n + \delta E_v)\rho_{mnvb} = v_{mnvb} + \sum_{cd} v_{cdvb}\rho_{mncd} + \sum_{rs} v_{mnrs}\rho_{rsvb} + \left[\sum_{r} v_{mnrb}\rho_{rv} - \sum_{c} v_{cnvb}\rho_{mc} + \sum_{rc} \tilde{v}_{cnrb}\tilde{\rho}_{mrvc}\right] + \left[\begin{array}{c} v \leftrightarrow b \\ m \leftrightarrow n \end{array}\right] \tag{180}$$

where δE_v is the correlation correction to the valence energy for the state v, which is given in terms of the excitation amplitudes by

$$\delta E_v = \sum_{ma} \tilde{v}_{vavm}\rho_{ma} + \sum_{mab} v_{abvm}\tilde{\rho}_{mvab} + \sum_{mna} v_{vbmn}\tilde{\rho}_{mnvb}. \tag{181}$$

To solve Eqs. (176–181), an angular momentum decomposition is first carried out and the equations are then reduced to coupled equations involving single-body radial wave functions only. The radial wave functions for states v, m, n, a, b, $\cdots$ are taken from a B-spline basis set [36] and the resulting coupled radial equations are solved iteratively. The core equations (176–177) are solved first and the valence equations (179–181) are then solved for valence states of interest using the converged core amplitudes.

3.15. Triple Excitations and Perturbation Theory

One can show that the core correlation energy δE_c obtained from Eq. (178) is complete through third order in perturbation theory. The valence correlation energy δE_v given in Eq. (181), by contrast, includes only part of the third-order correlation energy. Indeed, the

third-order contribution to the energy obtained by iterating Eqs. (176-177) and (179-180) once, substituting into Eq. (181), and omitting second- and fourth-order terms is

$$\begin{aligned}
\delta E_v^{(3)} = &\sum_{mabcd} \frac{\tilde{v}_{abvm} v_{cdab} v_{mvcd}}{(\epsilon_{ab} - \epsilon_{vm})(\epsilon_{cd} - \epsilon_{mv})} + \sum_{mabrs} \frac{\tilde{v}_{abvm} v_{mvrs} v_{rsab}}{(\epsilon_{ab} - \epsilon_{vm})(\epsilon_{ab} - \epsilon_{rs})} \\
&+ \sum_{mabcr} \frac{\tilde{v}_{abvm} \tilde{v}_{cvrb} \tilde{v}_{mrac}}{(\epsilon_{ab} - \epsilon_{vm})(\epsilon_{ac} - \epsilon_{mr})} + \sum_{mabcr} \frac{\tilde{v}_{abvm} \tilde{v}_{cmra} \tilde{v}_{vrbc}}{(\epsilon_{ab} - \epsilon_{vm})(\epsilon_{bc} - \epsilon_{vr})} \\
&+ \sum_{mabnr} \frac{\tilde{v}_{vavm} v_{mbnr} \tilde{v}_{nrab}}{(\epsilon_a - \epsilon_m)(\epsilon_{ab} - \epsilon_{nr})} - \sum_{mabcn} \frac{\tilde{v}_{vavm} v_{bcan} \tilde{v}_{mnbc}}{(\epsilon_a - \epsilon_m)(\epsilon_{bc} - \epsilon_{mn})} \\
&+ \sum_{mnbcd} \frac{\tilde{v}_{vbmn} v_{cdvb} v_{mncd}}{(\epsilon_{vb} - \epsilon_{mn})(\epsilon_{cd} - \epsilon_{mn})} + \sum_{mnbrs} \frac{\tilde{v}_{vbmn} v_{mnrs} v_{rsvb}}{(\epsilon_{vb} - \epsilon_{mn})(\epsilon_{vb} - \epsilon_{rs})} \\
&+ \sum_{mnbrc} \frac{\tilde{v}_{vbmn} \tilde{v}_{cnrb} \tilde{v}_{mrvc}}{(\epsilon_{vb} - \epsilon_{mn})(\epsilon_{vc} - \epsilon_{mr})} + \sum_{mnbrc} \frac{\tilde{v}_{vbmn} \tilde{v}_{cmrv} \tilde{v}_{nrbc}}{(\epsilon_{vb} - \epsilon_{mn})(\epsilon_{bc} - \epsilon_{nr})}, \qquad (182)
\end{aligned}$$

which differs from the results of third-order MBPT given in Eq. (147). The missing third-order terms are accounted for entirely by adding triple excitations of the form

$$\frac{1}{6} \sum_{abmnr} \rho_{mnrvab} a_m^\dagger a_n^\dagger a_r^\dagger a_v a_b a_a \, \Phi_v$$

to the right-hand side of the wave function in Eq. (175). The contribution of this term to the valence energy is

$$E_{v\,\mathrm{extra}} = \frac{1}{2} \sum_{mnab} \tilde{v}_{abmn} \rho_{mnvvab}. \qquad (183)$$

When this term is evaluated to lowest nonvanishing order (third order), it leads to the following contribution to the correlation energy:

$$\begin{aligned}
E_{v\,\mathrm{extra}}^{(3)} = &\sum_{mnabc} \frac{\tilde{v}_{abmn} \tilde{v}_{cmav} \tilde{v}_{nvbc}}{(\epsilon_{ab} - \epsilon_{mn})\,(\epsilon_{bc} - \epsilon_{nv})} + \sum_{mnabs} \frac{\tilde{v}_{abmn} \tilde{v}_{nvas} \tilde{v}_{msvb}}{(\epsilon_{ab} - \epsilon_{mn})\,(\epsilon_{vb} - \epsilon_{ms})} \\
&+ \sum_{mnabc} \frac{v_{abmn} \tilde{v}_{cvbv} \tilde{v}_{mnca}}{(\epsilon_{ab} - \epsilon_{mn})\,(\epsilon_{ca} - \epsilon_{mn})} + \sum_{mnabs} \frac{v_{abmn} \tilde{v}_{mvsv} \tilde{v}_{nsba}}{(\epsilon_{ab} - \epsilon_{mn})\,(\epsilon_{ab} - \epsilon_{ns})} \\
&+ \sum_{mnabs} \frac{v_{abmn} \tilde{v}_{mnvs} v_{vsba}}{(\epsilon_{ab} - \epsilon_{mn})\,(\epsilon_{ab} - \epsilon_{vs})} + \sum_{mnabc} \frac{v_{abmn} \tilde{v}_{cvba} v_{mnvc}}{(\epsilon_{ab} - \epsilon_{mn})\,(\epsilon_{vc} - \epsilon_{mn})} \\
&+ \sum_{mnabc} \frac{v_{abmn} \tilde{v}_{cmab} \tilde{v}_{vnvc}}{(\epsilon_{ab} - \epsilon_{mn})\,(\epsilon_c - \epsilon_n)} + \sum_{mnabs} \frac{v_{abmn} \tilde{v}_{mnas} \tilde{v}_{vsvb}}{(\epsilon_{ab} - \epsilon_{mn})\,(\epsilon_b - \epsilon_s)}. \qquad (184)
\end{aligned}$$

The sum $\delta E_v^{(3)} + E_{v\,\mathrm{extra}}^{(3)}$ gives the entire third-order valence correlation energy. In the examples below, we add $E_{v\,\mathrm{extra}}^{(3)}$ to the SD correlation energy δE_v to account for the missing third-order terms.

Table 6
Contributions to Li and Be^+ energy levels (a.u.). Both third-order MBPT and all-order SD values are given for comparison.

	Li			Be^+		
	$2s_{1/2}$	$2p_{1/2}$	$2p_{3/2}$	$2s_{1/2}$	$2p_{1/2}$	$2p_{3/2}$
HF	-0.196320	-0.128638	-0.128636	-0.666183	-0.519447	-0.519406
$E^{(2)}$	-0.001649	-0.001375	-0.001374	-0.002910	-0.003962	-0.003959
$E^{(3)}$	-0.000122	-0.000134	-0.000134	-0.000159	-0.000269	-0.000269
Breit	0.000003	0.000002	0.000001	0.000018	0.000022	0.000008
RM+MP	0.000016	0.000007	0.000007	0.000060	0.000016	0.000016
Total MBPT	-0.198072	-0.130139	-0.130137	-0.669174	-0.523640	-0.523610
δSD	-0.001853	-0.001608	-0.001607	-0.003143	-0.004369	-0.004366
$E^{(3)}_{\rm extra}$	0.000011	0.000010	0.000010	0.000011	0.000018	0.000018
Breit+RM+MP	0.000019	0.000009	0.000075	0.000078	0.000038	0.000024
Total SD	-0.198143	-0.130228	-0.130226	-0.669237	-0.523759	-0.523729
Expt.	-0.198142	-0.130236	-0.130235	-0.669242	-0.523764	-0.523734

3.16. Application to Li and Be^+

A typical application of the relativistic SD equations is given in Table 6, where we compare MBPT and SD calculations of energies (relative to the ionization threshold) of $2s_{1/2}$, $2p_{1/2}$, and $2p_{3/2}$ levels of lithium and singly ionized beryllium. The all-order calculations include partial waves through $l_{\rm max} = 7$. The second-order MBPT calculation is carried out in a large ($n = 100$) basis set and includes partial waves up to $l_{max} = 12$; The third-order values and $E^{(3)}_{\rm extra}$ are calculated with $n = 40$ spline basis set and $l_{\rm max} = 7$. Breit and reduced mass (RM) and mass polarization (MP) corrections values are taken from [54]. The SD value of the $2p_{3/2} - 2p_{1/2}$ fine structure interval for Li is 0.00000156 a.u. compared with the measured value 0.000001534(2) a.u.. The corresponding theoretical and experimental values for Be^+ are 0.00003001 a.u. and 0.00002998(3) a.u.. The tiny differences between the SD energies and experiment on the last line of Table 6 are probably dominated by the incomplete treatment of triple excitations.

4. RELATIVISTIC CONFIGURATION-INTERACTION METHOD

An alternative approach to the perturbation theory in treating many-electron systems is the configuration-interaction (CI) method which is based on the variational principle. Nonrelativistic CI techniques have been used extensively in atomic and molecular calculations. The generalization to relativistic configuration-interaction (RCI) calculations, however, presents theoretical as well as technical challenges. The problem originates from the many-electron Dirac Hamiltonian commonly used in RCI calculations:

$$H_{\rm Dirac} = \sum_i h_0(i) + \sum_{i>j} \Big[V_C(ij) + V_B(ij) \Big], \tag{185}$$

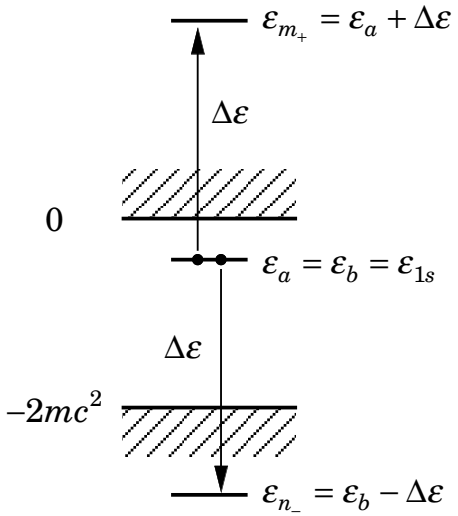

Figure 13. The continuum dissolution problem. An electron making a transition to an unoccupied negative-energy state imparts the resulting energy to the other electron.

where $h_0 = c\,\boldsymbol{\alpha}\cdot\boldsymbol{p} + (\beta - 1)c^2 + V_{\rm nuc}(r)$ is the one-electron Dirac Hamiltonian with the rest mass of the electron subtracted out, $V_C(ij) = 1/r_{ij}$ is the Coulomb interaction between the electrons, and $V_B(ij) = b_{ij}$ is the frequency-dependent/independent Breit interaction given in Eq. (85)/(86). This Hamiltonian is known to be problematic. Specifically in relativistic calculations, the existence of negative-energy states, which enter into sums over intermediate states in perturbation theory, results in the "continuum dissolution" problem, also known as the Brown-Ravenhall disease [1], in many-electron systems. Using the $1s^2$ ground state of helium-like ions as an example, this problem can be readily demonstrated with the second-order energy $E^{(2)}$ given in Eq. (90)

$$E^{(2)} = -\frac{1}{2}\sum_{abmn}\frac{v_{abmn}\tilde{v}_{mnab}}{\epsilon_m + \epsilon_n - \epsilon_a - \epsilon_b}.$$

If an intermediate state $|m_+ n_-\rangle$ consists of one $1s$ electron, denoted by a, being promoted to a positive-energy continuum state $|m_+\rangle$ with an energy $\epsilon_{m_+} = \epsilon_a + \Delta\epsilon > 0$, while the other $1s$ electron, denoted by b, being demoted to a negative-energy continuum state $|n_-\rangle$ with an energy $\epsilon_{n_-} = \epsilon_b - \Delta\epsilon < 2mc^2$, the denominator, $\epsilon_{m_+} + \epsilon_{n_-} - \epsilon_a - \epsilon_b$, in the above equation would vanish. In effect, any bound state in a many-electron system is degenerate in energy with an infinite number of electron-positron continuum states, as long as $\epsilon_{m_+} + \epsilon_{n_-} = \epsilon_a + \epsilon_b$. This situation is illustrated in Fig. 13.

However, the fact that the denominator can go to zero is not necessarily a problem. The same situation is encountered in the autoionization of atoms. Since an autoionizing state is embedded in the positive-energy continuum, second- and higher-order MBPT will also lead to vanishing denominators similar to those discussed above. In that case, an infinitesimal imaginary part must be added to the denominator, with the result that the principal part of the matrix elements leads to a real energy shift while the imaginary part

Table 7
Energies (eV) of the $1s^2$ ground state of helium-like uranium as calculated with basis functions generated in Coulomb (Coul) and Dirac-Kohn-Sham (DKS) potentials. $E_{\rm no-pair}$ and $E_{\rm Dirac}$ are RCI energies calculated without and with negative-energy states, respectively, and their differences are given by $\Delta E_{\rm Dirac}$. $E_{\rm QED}$ are energies from S-matrix calculations and $\Delta E_{\rm QED}$ are contributions from negative-energy states given by differences between $E_{\rm QED}$ and $E_{\rm no-pair}$.

Energy	Potential	$E_{\rm no-pair}$	$E_{\rm Dirac}$	$\Delta E_{\rm Dirac}$	$E_{\rm QED}$	$\Delta E_{\rm QED}$
Coulomb	Coul	-262235.48	-262235.10	0.38	-262235.18	0.30
	DKS	-262235.42	-262235.10	0.32	-262235.18	0.24
	ΔE	-0.06	0.00		0.00	
Breit	Coul	327.29	333.74	6.45		
	DKS	327.10	333.74	6.64		
	ΔE	0.19	0.00			

to an autoionization line width. But this is where the analogy ends. An autoionizing line width from the imaginary part of the energy denominator here would mean that there are no stable ground states for many-electron systems, as they can decay by "autoionizing" into the electron-positron continuum. The stability of atomic ground states is, of course, explained by the fact that the negative-energy sea is filled and that spontaneous pair production is prohibited by the Pauli exclusion principle. Here lies the real problem with the many-electron Dirac Hamiltonian: it has no provision to account for this fact and hence cannot prevent the decay of positive-energy electrons into the negative-energy continuum. The standard cure is to use the no-pair Hamiltonian which excludes negative-energy states entirely. This is the starting point of our MBPT calculations and is the starting point of our RCI calculations also.

Nevertheless, the use of the no-pair Hamiltonian does entail some compromises. Specifically in nonrelativistic CI calculations, eigenenergies saturated with large configuration expansions are independent of the basis functions used. Such is not the case here. By starting from the no-pair Hamiltonian and neglecting negative-energy states, relativistic basis sets are truncated and RCI as well as MBPT results are, in general, gauge and basis set dependent. Numerically, this has been demonstrated by Sapirstein et al. [55] who showed that the ground state RCI energy of helium-like uranium as calculated with the no-pair Hamiltonian depends on the potential used in generating the one-electron basis functions. These authors further showed that this potential dependence can be eliminated mathematically by completing the basis set to include both the positive- and negative-energy orbitals. Their results are shown in Table 7. It can be seen that negative-energy state contributions are substantial, especially for the Breit energies.

However, while the inclusion of negative-energy basis functions, which is equivalent to using the full Dirac Hamiltonian, does lead to potential independent results, it was also found that the $1s^2$ ground state is no longer the lowest eigenstate of the RCI matrix and is now surrounded by spurious energy levels characterized by configurations with one

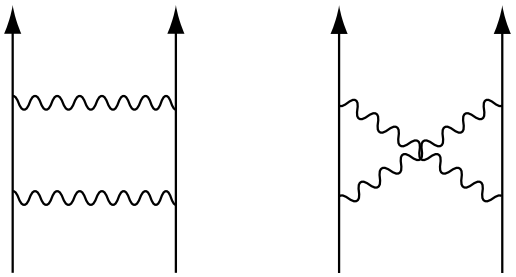

Figure 14. Ladder and crossed ladder diagrams for second-order correlation energies.

positive- and one negative-energy electrons. In effect, that was a numerical demonstration of the Brown-Ravenhall disease where the $1s^2$ ground state is embedded in a discrete representation of the (unphysical) electron-positron continuum when negative-energy basis functions are also used in RCI calculations. These results can be found in Table III of Ref. [55], along with more detailed discussions in that reference.

While there are no numerical disasters from vanishing denominators in RCI calculations when negative-energy basis functions are used, results of the full Dirac Hamiltonian, though potential independent, are nevertheless incorrect. To see this, we note that if the sum over intermediate states for the second-order energy is extended to included both positive- and negative-energy orbitals, $E^{(2)}$ can be rewritten as

$$\begin{aligned} E^{(2)}_{\rm Dirac} &= -\frac{1}{2}\sum_{abm_+n_+}\frac{v_{abm_+n_+}\tilde{v}_{m_+n_+ab}}{\epsilon_{m_+}+\epsilon_{n_+}-\epsilon_a-\epsilon_b} -\frac{1}{2}\sum_{abm_-n_-}\frac{v_{abm_-n_-}\tilde{v}_{m_-n_-ab}}{\epsilon_{m_-}+\epsilon_{n_-}-\epsilon_a-\epsilon_b} \\ &\quad -\frac{1}{2}\sum_{abm_+n_-}\frac{v_{abm_+n_-}\tilde{v}_{m_+n_-ab}}{\epsilon_{m_+}+\epsilon_{n_-}-\epsilon_a-\epsilon_b} -\frac{1}{2}\sum_{abm_-n_+}\frac{v_{abm_-n_+}\tilde{v}_{m_-n_+ab}}{\epsilon_{m_-}+\epsilon_{n_+}-\epsilon_a-\epsilon_b}\,. \end{aligned} \tag{187}$$

The first and second terms in the right-hand-side of Eq. (187) come from virtual electron-electron and positron-positron pairs in the intermediate states, respectively, while the third and fourth terms are from electron-positron pairs. $E^{(2)}_{\rm Dirac}$ can be compared with rigorous second-order correlation energy $E^{(2)}_{\rm QED}$ which have been calculated in the S-matrix formalism of QED from the ladder (L) and crossed ladder (X) diagrams shown in Fig. 14 [56, 57]. When these diagrams are taken together, $E^{(2)}_{\rm QED} = E_L + E_X$ have been shown to be gauge invariant [56]. Formulas for E_L and E_X in the Coulomb gauge with the exchange of two Coulomb photons have been given by Eqs. (16) and (17) in Ref. [55], respectively. In the notations used here, they can be written as

$$E_L = -\frac{1}{2}\sum_{abi_+j_+}\frac{v_{abi_+j_+}\tilde{v}_{i_+j_+ab}}{\epsilon_{i_+}+\epsilon_{j_+}-\epsilon_a-\epsilon_b} +\frac{1}{2}\sum_{abi_-j_-}\frac{v_{abi_-j_-}\tilde{v}_{i_-j_-ab}}{\epsilon_{i_-}+\epsilon_{j_-}-\epsilon_a-\epsilon_b}\,, \tag{188}$$

$$\begin{aligned} E_X &= -\frac{1}{2}\sum_{abi_+j_-}\frac{v_{aj_-i_+b}\,v_{bi_+j_-a}-v_{aj_-i_+a}\,v_{bi_+j_-b}}{\epsilon_{j_-}-\epsilon_{i_+}} \\ &\quad -\frac{1}{2}\sum_{abi_-j_+}\frac{v_{aj_+i_-b}\,v_{bi_-j_+a}-v_{aj_+i_-a}\,v_{bi_-j_+b}}{\epsilon_{i_-}-\epsilon_{j_+}}\,. \end{aligned} \tag{189}$$

It can be seen that the ladder diagram has the same electron-electron term as $E^{(2)}_{\rm Dirac}$, but its positron-positron term has an opposite sign. Moreover, electron-positron terms, which come from the crossed ladder diagram only, are very different from those in $E^{(2)}_{\rm Dirac}$ and their denominators, which are given by $\epsilon_{m_+} - \epsilon_{n_-}$, will not vanish. Thus, the correct QED treatment of relativistic correlation energies is shown to be free of the Brown-Ravenhall disease. S-matrix results of $E^{(2)}_{\rm QED}$ are shown in Table 7 and are clearly different from $E^{(2)}_{\rm Dirac}$.

When negative-energy states are excluded, both $E^{(2)}_{\rm Dirac}$ and $E^{(2)}_{\rm QED}$ reduce to the same no-pair energy[2]

$$E^{(2)}_{\rm no-pair} = -\frac{1}{2} \sum_{abm_+n_+} \frac{v_{abm_+n_+} \tilde{v}_{m_+n_+ab}}{\epsilon_{m_+} + \epsilon_{n_+} - \epsilon_a - \epsilon_b} \,, \tag{190}$$

which is a very good approximation to the true correlation energy. Residual contributions from negative-energy states are usually quite negligible except for very high-Z ions and can be treated as QED corrections from S-matrix calculations of the ladder and crossed ladder diagrams. We shall present an example of these corrections for high-Z Li-like ions later in this section. It should be noted that errors in $E_{\rm Dirac}$ from incorrect treatments of electron-positron and positron-positron terms can be very subtle and $E_{\rm Dirac}$ may look perfectly normal in RCI calculations when negative-energy basis functions are also included. Nevertheless, it is very difficult, if not impossible, to identify and correct the intrinsic errors in $E_{\rm Dirac}$ and the use of the many-electron Dirac Hamiltonian without the projection operators should be avoided even if it does not appear to be giving nonsensical results.

Before we proceed to discuss specific RCI calculations, we would like to clarify a common confusion regarding the no-pair calculation. The purpose of the projection operator is to filter out negative-energy states. But as the solutions of the homogeneous one-electron Dirac equation form a complete basis set, positive-energy Dirac orbitals will invariably include some admixtures of negative-energy orbitals from another potential through an unitary transformation. This raises some doubts about the no-pair calculation since it appears that there is no way of turning the effect of negative-energy states completely off even with the use of projection operators. To address this concern, let us re-emphasize that the intrinsic problem with the many-electron Dirac Hamiltonian is not that negative-energy states exist but that it is unable to prevent the appearance of the unphysical electron-positron pairs. To exclude these spurious pair contributions, it is sufficient to project out the negative-energy states which come from the same potential as the bound and positive-energy states currently in use. There is nothing wrong with contributions from the negative-energy states of a different potential *implicitly* mixed-in through an

[2]Note that Eqs. (188) and (189) are derived with the background potential U set to zero and sums over intermediate states i_+ and j_+ include unoccupied as well as occupied states. Limiting these sums to unoccupied states m_+ and n_+ leads to an additional term $\sum_{m_+}(V_{\rm HF})_{am_+}(V_{\rm HF})_{m_+a}/(\epsilon_a - \epsilon_{m_+})$ in Eq. (190) from the remaining sums over occupied states in E_L, but the same term will also show up from the electron-electron pair term in $E^{(2)}_{\rm Dirac}$ if U is set to zero instead of to $V_{\rm HF}$. The bottom line is that the no-pair limit of $E^{(2)}_{\rm Dirac}$ and $E^{(2)}_{\rm QED}$ will remain the same as long as the same local background potential $U(r)$ is used in both cases.

unitary transformation which involves only linear superpositions of Dirac orbitals. Indeed, it is well known that S-matrix calculations can be carried out in the Furry representation [58] with an external local potential as long as the correct background potential $U(r)$ is used to counter any change in the representation. The same is true with no-pair calculations, even though no-pair results will, in general, be gauge and potential dependent as we have mentioned earlier. Note, however, that the analogy with S-matrix calculations breaks down if the basis functions are individually optimized and do not correspond to a common local potential. While there may not be any serious numerical problems associated with these mixed-representation calculations, their intrinsic accuracy will be all but impossible to assess.

4.1. Finite Basis Functions

The choice of basis functions can be critical to RCI calculations. Finite basis sets such as the Slater-type and Gaussian-type orbitals have been used extensively in nonrelativistic atomic and molecular CI calculations. Relativistically, since the energy functional is not bounded from below due to the existence of the negative-energy states, expansions of the 4-component spinor wave functions in terms of finite basis sets is known to lead to variational instabilities in RCI calculations and to drastic problems such as the appearance of spurious eigenstates and the "variational collapse" of eigenenergies. These problems are not limited to many-electron systems and can affect the simple hydrogenic ions also. Signs of trouble in Dirac-Fock calculations readily showed up in the first finite basis set expansion attempt by Kim [59]. In most cases, additional constraints must be imposed on the basis functions to bring these problems under control.

As an example, one of more well-known constraints on the basis functions is the so-called "kinetic balance" condition [60, 61]. Specifically, most of the finite basis functions do not form complete basis sets in the Hilbert space. If the large- and small-component radial wave functions are expanded in terms of one of these orthonormal basis sets $\{\varphi_k\}$ such that $P(r) = \sum_i a_i \varphi_i(r)$ and $Q(r) = \sum_j b_j \varphi_j(r)$, then the operator identity $(\boldsymbol{\sigma}\cdot\boldsymbol{p})(\boldsymbol{\sigma}\cdot\boldsymbol{p}) = \boldsymbol{p}^2$ will not necessarily translate into the matrix identity

$$\sum_k \langle i|(\boldsymbol{\sigma}\cdot\boldsymbol{p})|k\rangle\langle k|(\boldsymbol{\sigma}\cdot\boldsymbol{p})|j\rangle = \langle i|\boldsymbol{p}^2|j\rangle \tag{191}$$

because $\sum_k |k\rangle\langle k| = \mathbf{I}$ holds only approximately. This leads to wrong kinetic energies in the nonrelativistic limit when $c \to \infty$ which persist in relativistic calculations when c is finite. To "balance" this effect, the expansion coefficients $\{a_i\}$ and $\{b_j\}$ should not be varied independently but should be adjusted in such a way that $P(r)$ and $Q(r)$ satisfy the condition

$$Q(r) = -\frac{1}{2mc}\Big(\frac{d}{dr} + \frac{\kappa}{r}\Big)P(r) \tag{192}$$

in the nonrelativistic limit. Even so, additional constraints may still be needed to maintain variational stabilities [61]. Detailed discussions of the criteria that physically acceptable basis functions should satisfy and on the common types of finite basis sets used in RCI calculations can be found in an article by Grant [62].

It should be mentioned that problems in RCI calculations are not limited to finite basis set expansions of one-electron radial wave functions and can occur even if $P(r)$ and $Q(r)$

are generated numerically. Examples are the multiconfiguration Dirac-Fock (MCDF) orbitals which are obtained by solving a set of coupled differential equations in a self-consistent approximation. The trouble is that the inhomogeneous configuration-mixing terms in MCDF equations do not necessarily have the correct nonrelativistic limit and can lead to incorrect fine structure results. In some cases, *ad hoc* corrections have to be made by explicitly subtracting out the spurious contributions that remain in the nonrelativistic limit [see 63, for example]. MCDF orbitals are free of the variational instability problem and, being highly optimized, are very efficient for RCI calculations, but they should be used with care, especially in high-precision calculations.

While the numerical problems in relativistic basis set expansion calculations are largely under control by now, the construction of positive-energy projection operators for the no-pair Hamiltonian remains a very difficult task and is thus frequently ignored. Here, we again use the B-spline basis sets described in Section 3.5 for RCI calculations. Expansions of the radial wave functions $P(r)$ and $Q(r)$ in terms of the piecewise polynomial B-spline functions $B_i(r)$ shown in Eq. (118) are free of the problems mentioned above, and the resulting one-electron B-spline orbitals cleanly separated into positive- and negative-energy states so that the projection operators can be implemented by using only positive-energy B-spline orbitals which readily provide an accurate, discrete representation of the bound and continuum states for high-precision correlation energy calculations. Furthermore, B-spline orbitals are solutions of the homogeneous one-electron Dirac equation and form completed basis sets as confirmed by sum rule calculations [36]. They thus satisfy the kinetic balance condition implicitly and are not known to lead to the appearance of spurious eigenstates nor to variational instability problems. The only down side is that the B-spline basis functions are not highly optimized and typical RCI calculations can include up to a few hundreds of these functions in the basis set, resulting in very large-scale CI expansions. These RCI calculations were once limited to run on mainframe supercomputers. However, with advances in computing power, they can now be carried out on fast workstations. In the following, we shall describe some of the high-precision RCI calculations with B-spline basis functions for few-electron systems.

4.2. RCI Equation

For RCI calculations, it is more convenient to work in the configuration space. Our starting point is the no-pair Hamiltonian given before with the Coulomb interaction only in Eq. (71). Here, we rewrite it as

$$H^{(n.p.)} = \sum_i h_0(i) + \sum_{i>j} \Lambda_+(ij)\Big[V_C(ij) + V_B(ij)\Big]\Lambda_+(ij), \tag{193}$$

which is the same as the many-electron Dirac Hamiltonian shown in Eq. (185) but with the positive-energy projection operators $\Lambda_+(ij)$ added. The effects of finite nuclear size are taken into account by using the Fermi charge distribution of the nucleus which are built into the nuclear potential $V_{\rm nuc}$ in the one-electron Dirac Hamiltonian h_0. For simplicity, we shall use H to represent the no-pair Hamiltonian in the following.

The construction of a trial wave function $\Psi(JM)$ for a N-electron atomic system starts with a set of one-electron basis functions $\{a_i\}$. B-spline orbitals here. The N-electron configuration-state function $\phi(\gamma JM)$ is a simultaneous eigenfunction of the angular mo-

mentum operators J^2 and J_Z obtained from anti-symmetrized Slater determinant wave functions $|a_1, a_2, \ldots, a_N\rangle$ such that

$$\phi(\gamma JM) = \sum_{\{m_{a_i}\}} |a_1, a_2, \ldots, a_N\rangle \, \langle j_{a_1} m_{a_1}, j_{a_2} m_{a_2}, \ldots, j_{a_N} m_{a_N} | \gamma JM\rangle, \tag{194}$$

where $\gamma = \{a_1, a_2, \ldots, a_N\}$ is a set of quantum numbers representing different electronic configurations and $\langle j_{a_1} m_{a_1}, j_{a_2} m_{a_2}, \ldots, j_{a_N} m_{a_N} | \gamma JM\rangle$ is a generalized Clebsch-Gordon coefficient. The atomic-state function $\Psi(JM)$ with angular momentum (J, M) and parity π is then expressed as a linear superpositions of configuration-state functions with the same angular momentum and parity quantum numbers

$$\Psi(JM) = \sum_i c_i \, \phi(\gamma_i JM). \tag{195}$$

In terms of the expansion coefficients c_i, the energy functional is given by

$$E = \langle \Psi | H | \Psi \rangle = \sum_{i,j} c_i c_j \langle \phi_i | H | \phi_j \rangle = \sum_{i,j} c_i c_j H_{ij}. \tag{196}$$

Variation of the energy functional with respect to c_i, subject to the wave function normalization condition

$$\langle \Psi | \Psi \rangle = \sum_{i,j} c_i c_j \langle \phi_i | \phi_j \rangle = \sum_i c_i^2 = 1 \tag{197}$$

leads to the CI equation

$$\sum_j (H_{ij} - \lambda \delta_{ij}) c_j = 0. \tag{198}$$

The calculation is thus reduced to an eigenvalue problem in term of the real, symmetric matrix H_{ij}. Resulting atomic-state functions $\Psi(JM)$ are simultaneous eigenfunctions of H, J^2 and J_Z. These are large-scale calculations involving very big matrices and the lowest-few eigenstates are determined using an implementation of the Davidson method [64] by Stathopoulos and Fischer [65]. This is an iterative scheme based on the perturbation theory and is very efficient for diagonally dominated CI matrices with fast rates of convergence and modest demands on computer resources. In general, most of our computer time is spent in setting up the Coulomb and, especially, the Breit matrices and efficient algorithms have been developed to speed up these calculations. By comparison, the computer time used in solving the matrix equation is relatively insignificant.

4.3. Two-Electron Systems

In this subsection, we deal with RCI calculations for helium-like ions B-spline basis functions [66–68]. Two-electron configuration-state functions (CSF) are constructed from positive-energy B-spline orbitals and are given by

$$\phi(\gamma JM) = |j_a j_b JM\rangle = \eta_{ab} \sum_{m_a, m_b} C(j_a, j_b, J; m_a, m_b, M) |j_a m_a, j_b m_b\rangle, \tag{199}$$

where $\eta_{ab} = \eta_{ba}$ is a normalization constants such that

$$\eta_{ab} = \begin{cases} 1 & \text{for } a \neq b \\ \frac{1}{\sqrt{2}} & \text{for } a = b \end{cases} . \tag{200}$$

From the interchange symmetry of the Clebsch-Gordan coefficient, we have

$$|j_a j_b JM\rangle = (-1)^{j_a+j_b+J+1} |j_b j_a JM\rangle. \tag{201}$$

It follows that for two identical particles, $|j_a j_a JM\rangle = 0$ unless J is even.

The atomic state function $\Psi(JM)$ is given by a linear combination of CSFs as shown in Eq. (195). Let $\gamma_i = \{ab\}$ and $\gamma_j = \{cd\}$, the Hamiltonian matrix element H_{ij} defined in Eq. (196) is given by

$$H_{ij} = K_{ij} + V_{ij}, \tag{202}$$

where K_{ij} is the matrix element of the one-electron Hamiltonian operator and V_{ij} is that of the two-electron Coulomb and Breit operators. Here,

$$K_{ij} = \eta_{ab}\eta_{cd}\big[I_{ac}\delta_{bd} + I_{bd}\delta_{ac} + (-1)^{j_a+j_b+J+1}\big(I_{ad}\delta_{bc} + I_{bc}\delta_{ad}\big)\big], \tag{203}$$

with

$$\begin{aligned} I_{ab} &= \langle a|h_0|b\rangle = \langle b|h_0|a\rangle = I_{ba} \\ &= \int dr \Big\{ c\Big[P_a\Big(\frac{d}{dr} - \frac{\kappa_b}{r}\Big)Q_b - Q_a\Big(\frac{d}{dr} + \frac{\kappa_b}{r}\Big)P_b\Big] \\ &\quad + V_{\rm nuc}(r)\big[P_aP_b + Q_aQ_b\big] - 2mc^2 Q_aQ_b\Big\}\delta_{\kappa_a\kappa_b}\delta_{m_am_b}. \end{aligned} \tag{204}$$

If Coulomb basis functions are used such that $h_0|a\rangle = \epsilon_a|a\rangle$, as is the case here for two-electron systems, K_{ij} is reduced to

$$K_{ij} = (\epsilon_a + \epsilon_b)\delta_{ij}. \tag{205}$$

As for the two-electron matrix element,

$$\begin{aligned} V_{ij} &= \eta_{ab}\eta_{cd}\sum_L \Bigg[(-1)^{j_b+j_c+J+L} \begin{Bmatrix} j_a & j_b & J \\ j_d & j_c & L \end{Bmatrix} X_L(abcd) \\ &\qquad + (-1)^{j_b+j_c+L} \begin{Bmatrix} j_a & j_b & J \\ j_c & j_d & L \end{Bmatrix} X_L(abdc)\Bigg], \end{aligned} \tag{206}$$

where the Coulomb matrix element $X_L(abcd)$ has already been given by Eq. (96). When frequency-independent Breit interaction is also included, V_{ij} is still given by the above expression, but the Coulomb matrix element $X_L(abcd)$ is replaced by

$$X_L(abcd) \to X_L(abcd) + M_L(abcd) + N_L(abcd) + O_L(abcd), \tag{207}$$

where the unretarded Breit matrix elements $M_L(abcd)$ and $N_L(abcd)$ are given by Eqs. (106) and (107), respectively, while the retarded Breit matrix element $O_L(abcd)$ is given by

Table 8
Contributions to the ionization energy (a.u.) of the $1s2p\,^3P_0$ state of helium-like neon. $E_{\rm Coul}$, $E_{\rm Breit}$, $E_{B\times B}$ and $E_{\rm no\text{-}pair}$ are the Coulomb, first-order Breit, high-order Breit and no-pair energies, respectively, and higher-ℓ contributions are from partial wave extrapolations. RCI results are from [66]. MBPT results are from [41].

Configuration	$E_{\rm Coul}$	$E_{\rm Breit}$	$E_{B\times B}$	$E_{\rm no\text{-}pair}$
$s_{1/2}p_{1/2}$	-10.329953	0.004024	-0.000003	-10.325932
$p_{3/2}d_{3/2}$	-0.002003	-0.000053	0.000000	-0.002056
$d_{5/2}f_{5/2}$	-0.000151	-0.000006	0.000000	-0.000157
$f_{7/2}g_{7/2}$	-0.000026	-0.000002	0.000000	-0.000028
$g_{9/2}h_{9/2}$	-0.000007	-0.000001	0.000000	-0.000008
higher-ℓ	-0.000004	-0.000001	0.000000	-0.000005
Total	-10.332143	0.003962	-0.000004	-10.328185
MBPT	-10.332144	0.003962	-0.000005	-10.328187

Eq. (113). For frequency-dependent Breit interaction, these Breit matrix elements are modified according to the recipe shown in Section 3.4. Furthermore, off-diagonal matrix elements are calculated with the frequency-symmetrized Breit operator shown in Eq. (87).

For He-like ions, the CI expansion for an atomic state $\Psi(JM)$ includes CSFs from two-electron excitations $(n\ell n'\ell')$ with the same total angular momentum (J, M) and parity π. Our basis sets typically consist of 40 positive-energy B-spline functions for each of the angular momentum states $s_{1/2},\ p_{1/2},\ p_{3/2},\ \ldots$ We include orbitals up to $\ell,\ \ell' = 5$ or 6 and use the first 20 to 25 basis functions of each angular symmetry in our calculations. Contributions from the remaining higher-energy basis functions are insignificant and can be neglected. Those from higher-ℓ states are also small and can be obtained by partial wave extrapolations. The number of configurations used here ranges from 2000 to 10 000. Resulting RCI matrices are dense and the first few eigenstates are solved by the Davidson method as mentioned in the previous section. Mass polarization corrections discussed in Section 3.12 are then calculated as expectation values of the operator $P = \frac{1}{M}\sum_{i>j}\boldsymbol{p}_i\cdot\boldsymbol{p}_j$ using eigenvectors from the RCI calculations.

A typical convergent pattern as a function of the angular symmetry for the ionization energy of the $1s2p\,^3P_0$ state of He-like neon is shown in Table 8. Coulomb energies $E_{\rm Coul}$ listed in the second column are eigenenergies of the Hamiltonian matrices with Coulomb interaction only. First-order Breit energies $E_{\rm Breit}$ listed in the third column are calculated as expectation values of the Breit operator with corresponding Coulomb eigenvectors. No-pair energies $E_{\rm no\text{-}pair}$ listed in the last column are eigenvalues of the full no-pair Hamiltonian including both Coulomb and Breit interactions. Differences between $E_{\rm no\text{-}pair}$ and $E_{\rm Coul} + E_{\rm Breit}$ give higher-order Breit corrections $E_{B\times B}$ listed in the fourth column. In the first row of this table, results are calculated with basis set expansions including ns and np orbitals only. In the second to fifth rows, increments to the Coulomb, first-order Breit, higher-order Breit and no-pair energies are shown by successively adding configurations with basis functions of increasing angular momenta. Extrapolations of these partial-wave

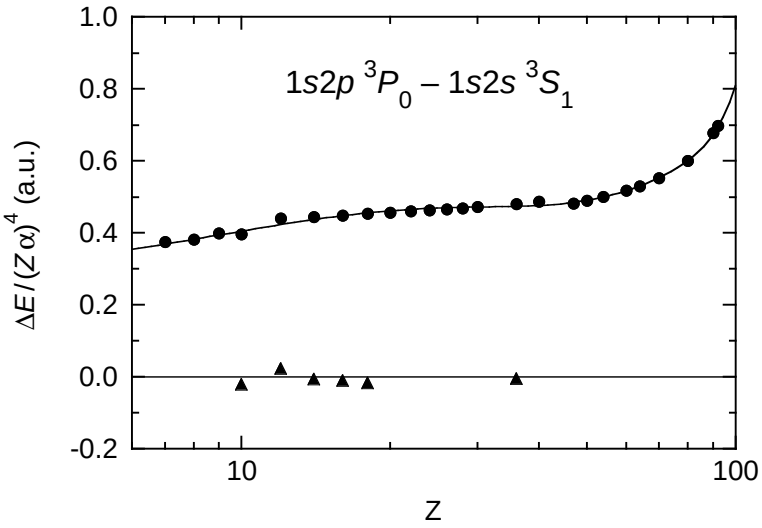

Figure 15. Correlation energies (a.u.) of the $1s2p\,^3P_0 - 1s2s\,^3S_1$ transition in He-like ions relative to the RCI values [66] are scaled by $(Z\alpha)^4$ and plotted as functions of the atomic number Z. Solid circles are results of the unified theory [69]. Solid triangles are results of MBPT [41].

series to $\ell \to \infty$, assuming that they decrease as $1/(\ell+1/2)^n$ with $n = 6.5$ for both $E_{\rm Coul}$ and $E_{\rm no\text{-}pair}$ and $n = 4.5$ for $E_{\rm Breit}$, lead to the higher-ℓ corrections listed in the sixth row. Final RCI results, shown in the seventh row, are in excellent agreement with the all-order MBPT results of Plante et al. [41].

Drake [69] updated and extended the benchmark work of Accad et al. [70] on the term values of the $n = 1$ and 2 states of He-like ions with $Z = 2 - 100$ by combining variational methods and the relativistic $1/Z$ expansion approach. Drake's unified theory accounts for electron correlation energies precisely at low Z and includes the dominant relativistic, QED and recoil corrections. Systematic comparisons have been made between the correlation energy results of the unified theory and those of RCI [66–68] and all-order MBPT [41]. While RCI and MBPT are found to be in excellent agreement with each other, both of them disagree slightly with the unified theory and these differences are due mainly to relativistic correlation corrections of orders $(Z\alpha)^4$ and higher which are not included in the unified theory. An example of these comparisons on the correlation energies of the $1s2p\,^3P_0 - 1s2s\,^3S_1$ transition in He-like ions is displayed in Fig. 15. It is evident that the results of RCI and MBPT are in very good agreement while those of the unified theory are off by about $0.5\,(Z\alpha)^4$ a.u..

RCI calculations have provided very accurate no-pair energies for the low-lying states of He-like ions [66–68]. Resulting eigenenergies and eigenvectors have also been used in high-precision radiative transition [71], atomic polarizability [72], and hyperfine structure [73] calculations. As we have mentioned before, negative-energy states are important for restoring the potential independence of the no-pair energies. It is interesting to note that they are also responsible for the gauge invariance of the radiative transitions [71, 74, 75].

4.4. Many-Electron Systems

For atomic systems with more than two electrons, CI expansions in terms of CSFs can be prohibitively large and steps have to be taken to keep the computation manageable. We begin by choosing a reference state to represent an atomic system. Leading correlation effects are then calculated from CSFs that arise from single and double excitations from this reference state, and residual corrections can be obtained from the dominant triple and quadruple excitations. Single and double excitations can be further classified by valence-valence, core-valence and core-core correlations, depending on whether one or two electrons are excited from the valence or core states of the atomic system. These breakdowns not only provide a systematic way of improving correlation energies but also permit different parts of the calculation to be carried out with varying degree of sophistication, depending on the importance of their contributions. Thus, dominant correlation energies from valence-valence and core-valence excitations are typically calculated with as complete a CI expansion as possible, while smaller corrections from core-core, triple and quadruple excitations can be evaluated with smaller basis set expansions for more tractable calculations.

The reference state is usually chosen to be consisted of the dominant configurations of the atomic state in question. Using the 4-electron Be-like ion as an example, the reference state for the $2s^2\ {}^1S_0$ ground state is taken to be $(1s^22s^2 + 1s^22p^2)_{J=0}$ and the CSFs for the valence-valence, core-valence and core-core correlations are then given by $1s^2n\ell n'\ell'$, $1s2sn\ell n'\ell' + 1s2pn\ell n'\ell'$, and $2s^2n\ell n'\ell' + 2p^2n\ell n'\ell'$, respectively. As for the $2s2p\ {}^3P_0$, ${}^3P_1$, ${}^3P_2$, and ${}^1P_1$ excited states, the reference states are $(1s^22s2p)_{J=0,1,2}$ and CSFs from single and double excitations are $1s^2n\ell n'\ell'$, $1s2sn\ell n'\ell' + 1s2pn\ell n'\ell'$, and $2s2pn\ell n'\ell'$. Since the same configuration can come from different excitations, for example $1s2s2p3d$ can come from both $1s2sn\ell n'\ell'$ and $1s2pn\ell n'\ell'$, care must be taken to ensure that no configuration is doubly counted. We note that individual contributions to the correlation energy (valence-valence, core-valence, etc.) depend on the choice of the reference state. Should the reference state of the $2s^2\ {}^1S_0$ ground state be represented by the single $(1s^22s^2)_{J=0}$ configuration, for example, the CSFs for core-valence and core-core correlations would consist only of the $1s2sn\ell n'\ell'$ and $2s^2n\ell n'\ell'$ configurations, and a substantial amount of correlation energy from the $1s2pn\ell n'\ell'$ and $2p^2n\ell n'\ell'$ configurations will be missing from single- and double-excitation calculations. These configurations can still be included in the calculation, but only as triple and quadruple excitations.

RCI calculations have been carried out for three-electron Li-like [76, 77], four-electron Be-like [78] and twelve-electron Mg-like [79] ions, and for Li-like to F-like [80] and Na-like to Si-like [81] uranium ions. In these calculations, B-spline basis functions are generated in Dirac-Kohn-Sham (DKS) potentials to better account for screening effects. Typically, 30 positive-energy B-spline orbitals are generated for each orbital angular momentum up to $\ell = 5$ or 6 and the first 20 - 24 orbitals are used as basis functions. The construction of the N-electron CSF $\phi(\gamma JM)$ and the reduction of the Hamiltonian matrix elements $H_{ij} = \langle\phi_i|H|\phi_j\rangle$ into terms involving one-electron integrals I_{ab} and two-electron Coulomb and Breit integrals $X_L(abcd)$, $M_L(abcd)$, $N_L(abcd)$ and $O_L(abcd)$ can, in principle, be carried out analytically as in the case of He-like ions, but with the availability of general-purpose, angular-recoupling code packages [82–84], these tedious tasks are best left to be tackled numerically. Here, we use the angular package in GRASP [83] for this purpose.

Table 9
No-pair energies (eV) of the $2s - 2p_{3/2}$ transition in Li-like uranium. B_0 and B_ω are first-order frequency-independent and frequency-dependent Breit energies, respectively. $B_0 \times B_0$ and $B_\omega \times B_\omega$ are corresponding higher-order Breit energies, respectively.

Contribution		RCI	MBPT
Coulomb		4514.79	4514.81
Breit	B_0	-9.17	-9.16
	B_ω	-6.91	-7.06
	$B_0 \times B_0$	0.16	
	$B_\omega \times B_\omega$	0.05	
	Sum	-15.88	-16.22
Mass Polarization		-0.04	-0.04
$E_{\text{no-pair}}$		4498.87	4498.56

The sizes of our CI expansions range from 10 000 to 300 000 configurations. Resulting Hamiltonian matrices are sparse and diagonally dominated. As in the case of He-like ions, the first few eigenstates are obtained using the Davidson's method, and corresponding eigenvectors are used to evaluate the mass polarization corrections.

Three-Electron Li-like Ions

In Table 9, no-pair energies of the $2s - 2p_{3/2}$ transition in Li-like uranium ($Z = 92$) are compared between RCI [77] and MBPT [85]. Here, Breit energies are broken down into first-order (B) and higher-order ($B \times B$) contributions, both of which are further divided into frequency-independent (B_0) and frequency-dependent (B_ω) corrections. As mentioned in Section 4.3, first-order RCI Breit energies are calculated as expectation values of the Breit operator with Coulomb eigenvectors, while higher-order RCI Breit energies are additional contributions from diagonalizing the Coulomb + Breit matrices. From the perturbation theory point of view, first-order RCI Breit energies are equivalent to the sums of all terms with the exchange of exactly one transverse (Breit) photon along with the possible exchanges of one or more longitudinal (Coulomb) photons (B, $B \times C$, $B \times C \times C$, etc.), while higher-order RCI Breit corrections are from the sums of all terms involving the exchanges of more than one transverse photons ($B \times B$, $B \times B \times C$, etc.). It can be seen that the discrepancy on the order of 0.34 eV in Breit energy is due partly to differences in the frequency-dependent terms and partly to higher-order contributions which are included in RCI but not in MBPT. Thus, these normally small corrections can no longer be ignored at high Z, as they can easily change the deduced empirical QED corrections for this transition from -39.19±0.21 eV shown in Table 5 to a new value of -39.50±0.21 eV, which is more consistent with the systematic trend of these QED corrections as discussed in Ref. [77].

In Table 10, RCI [76] and MBPT [85] energies on the $2s-2p_{1/2}$ and $2s-2p_{3/2}$ transitions in Li-like ions are compared with experiment. For these low- to mid-Z ions, higher-order Breit corrections are quite negligible and RCI and MBPT are in very good agreement

Table 10
Theoretical and experimental energies (eV) for the $2s - 2p_{1/2}$ and $2s - 2p_{3/2}$ transitions in Li-like ions. References to these results can be found in [76].

Z	$2s - 2p_{1/2}$			$2s - 2p_{3/2}$		
	RCI	MBPT	Experiment	RCI	MBPT	Experiment
10	15.8888	15.8885	15.8887(2)	16.0933	16.0931	16.0932(2)
15	25.813	25.812	25.814(3)	27.205	27.205	27.206(3)
20	35.963	35.964	35.962(2)	41.028	41.028	41.029(2)
26	48.600	48.602	48.599(1)	64.567	64.568	64.566(2)
32	61.907	61.911	61.902(4)	101.051	101.055	101.043(12)
42	86.11	86.12	86.10(1)	211.99	211.99	211.94(7)
54	119.82	119.84	119.97(10)	492.21	492.22	492.34(62)

with each other and with experiment. Experimental data exist for some higher-Z ions ($Z = 83$, 90 and 92), but QED corrections must also be included when comparing theory with experiment. In some cases, differences from higher-order Breit corrections mentioned in the previous paragraph are partially canceled out by those from QED energies, resulting in smaller apparent differences between RCI and MBPT. We shall present some of these high-Z comparisons in the next subsection when we discuss QED corrections in many-electron systems. More detailed comparison between theory and experiment along the lithium isoelectronic sequence can be found in [76, 77].

Four-Electron Be-like Ions

The strength of the RCI method is that it is intrinsically an all-order method as long as the CI expansion is saturated with enough configurations. This is further demonstrated in Fig. 16 which shows another comparison with MBPT on the energies of the $2s^2\,{}^1S_0 - 2s2p\,{}^1P_1$ transition in Be-like ions. In the nonrelativistic Z-expansion theory, the transition energy between levels of the same principal quantum numbers ($\Delta n = 0$) are given by a $1/Z$ expansion series

$$E = a_1 Z + a_0 + a_{-1}/Z + a_{-2}/Z^2 + \ldots, \tag{208}$$

where the leading Z^2 term cancels between the initial and final states. While RCI results [78] should be accurate to all orders in $1/Z$, second-order MBPT results [86] are exact only up to the a_0 term. At low Z, differences between RCI and MBPT clearly show an $1/Z$ trend. At high Z, they are dominated by relativistic correlation corrections of the order of $(1/Z)(Z\alpha)^4$ and the change in the systematic trend to a Z^3 behavior is quite obvious at around $Z = 40$. Also shown in this figure are the nonrelativistic full-core-plus-correlation (FCPC) results by Zhu and Chung [87] which are in very good agreement with RCI at low Z. But as relativistic corrections are included as first-order perturbations only, FCPC calculations were not extended to high-Z ions.

In Fig. 17, comparisons are made between theory and experiment on the energies of the same $2s^2\,{}^1S_0 - 2s2p\,{}^1P_1$ transition in Be-like ions. Results from RCI [78] are consistently

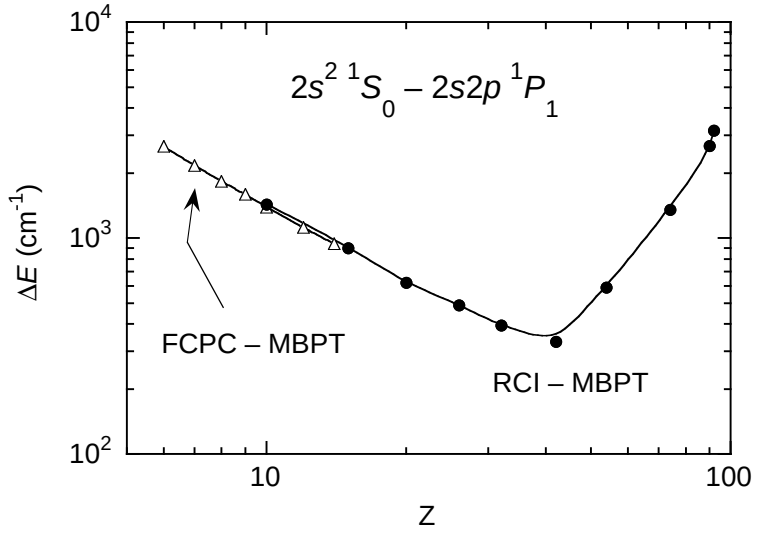

Figure 16. Correlation energies (cm^{-1}) of the $2s^2\,{}^1S_0 - 2s2p\,{}^1P_1$ transition in Be-like ions relative to the MBPT values are plotted as functions of the atomic number Z. Solid circles are results of RCI. Open triangles are results of FCPC.

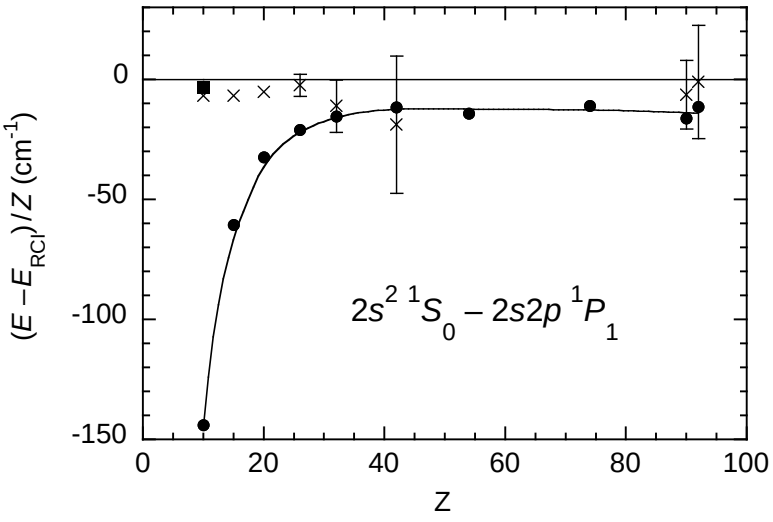

Figure 17. The $2s^2\,{}^1S_0 - 2s2p\,{}^1P_1$ transition energies (cm^{-1}) for Be-like ions relative to the RCI values [78] are scaled by the atomic number Z and shown as functions of Z. Solid circles are results of MBPT [86]. The Solid square is the result of FCPC [87]. Crosses with error bars are experimental measurements and references can be found in [78].

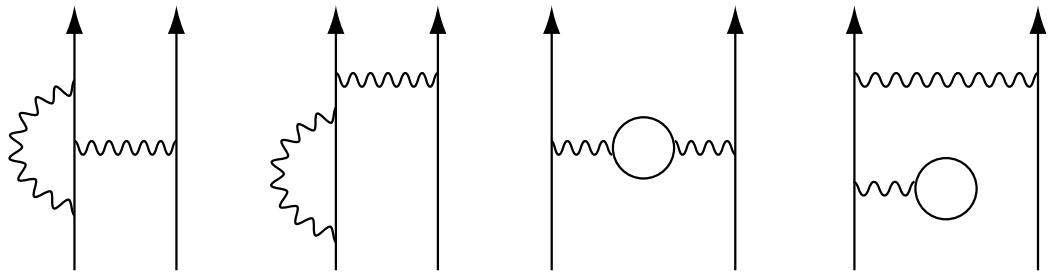

Figure 18. Typical higher-order radiative diagrams for the screening corrections to the self-energy and vacuum polarization.

in good agreement with experiment along the isoelectronic sequence, while second-order MBPT [86] deviates considerably from experiment at low Z due to an inadequate treatment of electron correlation. At high Z, QED corrections are important and account for some of the discrepancies between RCI and MBPT.

4.5. QED Corrections in Many-Electron System

QED corrections are important for high-Z, few-electron ions. They are dominated by the one-loop self-energy and vacuum polarization diagrams shown in Fig. 1. At present, self-energies can be calculated nonperturbatively to all orders in $Z\alpha$ with numerical bound-state Green's functions in a non-Coulomb model potential using the method of Cheng et al. [88, 89]. Leading vacuum polarization corrections can also be obtained from the expectation values of the Uehling potential using screened wavefunctions from the same model potential. As for the Wichmann-Kroll corrections, while they can be estimated from existing hydrogenic $n = 1$ and 2 results [90–92] by assuming an $1/n^3$ scaling and by choosing reasonable effective nuclear charges $Z_{\rm eff}$ to account for the screening effects, their accuracies are hard to gauge even though high precision is not required for these small corrections. Instead, they can now be calculated directly in the same way as the self-energies using numerical bound-state Green's functions [93]. Total QED corrections to many-electron ions are then given by the sum of one-electron QED contributions, weighted by the fractional occupation number of each valence orbital as obtained from the eigenvectors of RCI calculations.

In the calculation of one-loop radiative diagrams, model potentials are commonly used to account for screening corrections which can be quite significant, and results are potential dependent unless higher-order correlation diagrams such as those shown in Fig. 18 are also evaluated. Blundell made the first attempt to evaluate these screening diagrams for the $ns - np$ transitions in alkali-like ions [47]. To date, the most complete, screened QED calculations are available for the $1s^2$ ground state of He-like ions by Persson et al. [94] and Yerokhin et al. [95], for the $2s - 2p_{1/2}$ transition in Li-like ions by Yerokhin et al. [50] and for both the $2s - 2p_{1/2}$ and $2s - 2p_{3/2}$ transitions in Li-like bismuth ($Z = 83$) by Sapirstein and Cheng [96]. These calculations are extremely complicated and are not yet available for other many-electron systems. In most cases, a suitable choice of model potential in calculating the 1-loop diagrams remains the best way to get good estimates

Table 11
Energies (eV) of the $3s - 3p_{3/2}$ transitions in Na-like to Al-like uranium [81]. Na-1 is the $3s - 3p_{3/2}$ line. Mg-1 is the $(3s^2)_{J=0} - (3s3p_{3/2})_{J=1}$ line. Al-1 is the $(3s^23p_{1/2})_{J=1/2} - (3s3p_{1/2}3p_{3/2})_{J=1/2}$ line. VV, CV and CC are valence-valence, core-valence and core-core contributions to the Coulomb energies, respectively. B_0 and B_ω are frequency-independent and frequency-dependent contributions to the Breit energies, respectively.

Contributions		Na-1	Mg-1	Al-1
RCI	VV	1318.12	1329.58	1332.55
	CV	0.09	-0.06	-0.20
	CC	-0.07	-0.04	-0.10
	Coulomb	1318.14	1329.48	1332.25
	B_0	-1.05	-1.03	-0.62
	B_ω	-1.74	-1.72	-1.67
	Breit	-2.79	-2.75	-2.29
	Mass polarization	-0.01	-0.01	-0.01
	Sum	1315.34(2)	1326.72(2)	1329.95(2)
QED	Self-energy	-14.21	-13.99	-13.98
	Uehling	4.10	4.04	4.03
	Wichmann-Kroll	-0.20	-0.20	-0.20
	Core relaxation	0.08	0.08	0.08
	Sum	-10.23(7)	-10.07(7)	-10.07(7)
Total theory		1305.11(7)	1316.65(7)	1319.88(7)
Experiment		1305.12(2)	1316.64(1)	1319.86(2)

of QED corrections.

For consistency with RCI calculations, we also use DKS potentials for screened QED calculations. DKS potentials have been shown in Ref. [77] to give very good QED results for high-Z Li-like and Be-like ions and they appear to work just as well for Na-like to Si-like uranium [81]. Typically, QED corrections to transition energies are carried out in a frozen-core approximation where contributions from the valence electrons are considered but not those from the core electrons which cancel exactly between the initial and final states. In [77] and [81], however, it was found that core-relaxation effects are important and that they can be accounted for by summing the differences in QED energies of the core electrons as calculated with two different DKS potentials specific to the electronic configurations of the initial and final states of the transition.

An example of these QED calculations is shown in Table 11 where comparisons are made between theory and experiment for the $3s - 3p_{3/2}$ transition energies in Na-like to Al-like uranium. In this table, RCI Coulomb energies are broken down into valence-valence (VV), core-valence (CV) and core-core (CC) contributions, with the reference states taken to be consisted of the dominant $n = 3$ configurations of the atomic states. While CV results do not appear to be any larger than the CC results, that is largely due to cancellations between the initial and final states and CV contributions have to

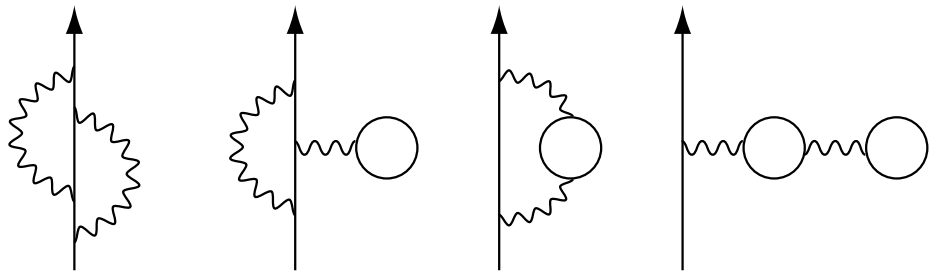

Figure 19. Typical two-loop Lamb shift diagrams.

be calculated very accurately to avoid errors from incomplete cancellations. The Breit energies shown here include higher-order effects. For simplicity, they are not separated into VV, CV and CC results. Instead, they are separated into frequency-independent (B_0) and frequency-dependent (B_ω) contributions. The main uncertainties in the resulting RCI energies are from the missing triple and quadruple excitations which are estimated to be no more than 0.02 eV. As for the QED corrections, they are consistently given by about -10 eV here and is dominated by the electron self-energies as expected. It is interesting to note that at -0.20 eV, Wichmann-Kroll corrections are about 10 times larger than experimental uncertainties and are very significant. Even core-relaxation corrections to the QED energies, though small at 0.08 eV, are important in bringing theory into good agreement with experiment. Uncertainties in QED corrections, of the order of 0.07 eV, are due mainly to the use of DKS potentials to account for screening corrections, and as we shall discuss in the following paragraphs, to higher-order 2-loop Lamb shifts and negative-energy state contributions to the correlation energies. Theoretical results as given by the sums of RCI and QED energies are seen to be in excellent agreement with the high-precision EBIT measurements carried out at the Lawrence Livermore National Laboratory. All data shown in Table 11 are from Ref. [81]. More detailed discussions of these results can also be found there.

Besides the one-loop radiative corrections, there are other small contributions to the QED energies. One of them is the high-order QED corrections from 2-loop Lamb shifts which have been studied indirectly in [96]. In that work, the $2s - 2p_{3/2}$ transition energy for Li-like bismuth is calculated from pure QED theory in the S-matrix formalism by evaluating a complete set of correlation and radiative diagrams involving the exchange of one and two virtual photons, with the exception of the 2-loop Lamb shift diagrams such as those shown in Fig. 19. The screened self-energy and vacuum polarization corrections are calculated to be -34.333 eV and 7.985 eV, respectively, for a total 1-loop QED value of -26.348 eV. Along with the correlation energy which is calculated to be 2814.312 eV, the transition energy is given by 2787.964 eV. Comparing this result with the high-precision EBIT measurement of 2788.139±0.039 eV [97], a difference of 0.175 eV is found which can be attributed to the uncalculated 2-loop Lamb shifts. By taking the usual scaling rules into account, the size of this correction is consistent with the value of 1.57(31) eV for the $1s$ state of hydrogen-like uranium from direct 2-loop Lamb shift calculations by Mallampalli and Sapirstein [98] and Yerokhin and Shabaev [99]. The search for two-loop Lamb shifts

in hydrogen-like uranium is currently limited by the uncertainty of the measured $1s$ Lamb shift of 468±13 eV [100]. With advances in atomic structure and screened 1-loop QED calculations, it may actually be better to search for 2-loop Lamb shifts in high-Z, few-electron ions. Another QED correction which is usually ignored is the contribution from negative-energy states to the correlation energies. As we have mentioned before, S-matrix calculations of the correlation energies include contributions from the negative-energy states correctly and are not affected by the continuum dissolution problem. Comparing the 2814.312 eV correlation energy shown in Ref. [96] with the RCI no-pair energy of 2814.47 eV shown in Ref. [77], a difference of -0.16 eV is found which should be due mainly to contributions from negative-energy states. We thus see that both the 2-loop Lamb shift and negative-energy state contributions are very sizable (about four times the experimental uncertainties) but almost completely cancel each other. As a result, summing the RCI no-pair energy of 2814.47 eV [77] and the screened 1-loop QED energy of -26.348 eV [96] gives a transition energy of 2788.12 eV which is in excellent agreement with the measured value of 2788.139±0.039 eV [97]. Indeed, the good agreement between theory and experiment shown in Table 11 may also be due in part to cancellations of errors, even though the 2-loop lamb shifts and negative-energy state contributions for the $n = 3$ states should be a lot smaller at about 0.05 eV in magnitude based on an $1/n^3$ scaling.

In conclusion, relativistic atomic structure calculations based on the MBPT and RCI methods are now accurate enough to make precision tests of QED theory in many-electron systems. Tests of parity non-conserving effects in heavy, neutral atoms have also been carried out and this topic is covered in another chapter of this book series.

Acknowledgments

The work of WRJ was supported in part by NSF Grant No. PHY-0139928. The work of KTC and MHC were performed under the auspices of the U.S. Department of Energy by the University of California, Lawrence Livermore National Laboratory under Contract No. W-7405-Eng-48.

Appendix

Equation (147) for the third-order valence energy of an atom with a single valence electron reduces to the following form after decomposing in an angular momentum basis and summing over magnetic quantum numbers.

$$
\begin{aligned}
E_v^{(3)} = & \sum_{mnabc}\sum_{kk'} \delta_{j_b j_c} \frac{(-1)^{j_a+j_m+j_n+j_v+k'}}{[k][j_b][j_v]} \frac{X_k(nmba) Z_k(acmn) Z_{k'}(vbcv)}{(\epsilon_{ab}-\epsilon_{mn})(\epsilon_{ac}-\epsilon_{mn})} \\
& - \sum_{mnrab}\sum_{kk'} \delta_{j_m j_r} \frac{(-1)^{j_a+j_b+j_n+j_v+k'}}{[k][j_r][j_v]} \frac{X_k(nmba) Z_k(abrn) Z_{k'}(vrmv)}{(\epsilon_{ab}-\epsilon_{mn})(\epsilon_{ba}-\epsilon_{nr})} \\
& + 2 \sum_{mracd}\sum_{kk'} \delta_{j_m j_a} \frac{(-1)^{j_c+j_d+j_r+j_v+k'}}{[k][j_a][j_v]} \frac{Z_k(dcrm) X_k(radc) Z_{k'}(mvva)}{(\epsilon_{cd}-\epsilon_{mr})(\epsilon_{a}-\epsilon_{m})} \\
& - 2 \sum_{acmrs}\sum_{kk'} \delta_{j_a j_m} \frac{(-1)^{j_c+j_r+j_s+j_v+k'}}{[k][j_a][j_v]} \frac{Z_k(casr) X_k(rsmc) Z_{k'}(mvva)}{(\epsilon_{ac}-\epsilon_{rs})(\epsilon_{a}-\epsilon_{m})} \\
& - 2 \sum_{acmnr}\sum_{k} \frac{(-1)^{j_c+j_r+k}}{[k]^2[j_v]} \frac{Z_k(carm) Z_k(vrnc) Z_k(vanm)}{(\epsilon_{ac}-\epsilon_{mr})(\epsilon_{av}-\epsilon_{mn})} \\
& - \sum_{acmnr}\sum_{k} \frac{(-1)^{j_c+j_r+k}}{[k]^2[j_v]} \frac{Z_k(vamn) Z_k(arnc) Z_k(cvrm)}{(\epsilon_{va}-\epsilon_{mn})(\epsilon_{vc}-\epsilon_{mr})} \\
& + 2 \sum_{abcnr}\sum_{k} \frac{(-1)^{j_c+j_r+k}}{[k]^2[j_v]} \frac{Z_k(acnr) Z_k(rbcv) Z_k(abnv)}{(\epsilon_{ac}-\epsilon_{nr})(\epsilon_{ab}-\epsilon_{nv})} \\
& + \sum_{mrabc}\sum_{k} \frac{(-1)^{j_c+j_r+k}}{[k]^2[j_v]} \frac{Z_k(bamv) Z_k(rbcm) Z_k(carv)}{(\epsilon_{ab}-\epsilon_{mv})(\epsilon_{ac}-\epsilon_{vr})} \\
& + 2 \sum_{mnacd}\sum_{kk'k''} \frac{1}{[j_v]} \begin{Bmatrix} k & k' & k'' \\ j_a & j_c & j_m \end{Bmatrix} \begin{Bmatrix} k & k' & k'' \\ j_v & j_d & j_n \end{Bmatrix} \frac{Z_k(cdmn) X_{k'}(nmva) X_{k''}(vadc)}{(\epsilon_{cd}-\epsilon_{mn})(\epsilon_{va}-\epsilon_{mn})} \\
& - 2 \sum_{abmrs}\sum_{kk'k''} \frac{1}{[j_v]} \begin{Bmatrix} k & k' & k'' \\ j_v & j_b & j_s \end{Bmatrix} \begin{Bmatrix} k & k' & k'' \\ j_m & j_a & j_r \end{Bmatrix} \frac{Z_k(basr) X_{k'}(rsmv) X_{k''}(vmba)}{(\epsilon_{ab}-\epsilon_{rs})(\epsilon_{ba}-\epsilon_{vm})} \\
& - \sum_{nabcd}\sum_{kk'k''} \frac{1}{[j_v]} \begin{Bmatrix} k & k' & k'' \\ j_n & j_a & j_c \end{Bmatrix} \begin{Bmatrix} k & k' & k'' \\ j_v & j_b & j_d \end{Bmatrix} \frac{X_k(badc) Z_{k'}(dcvn) X_{k''}(vnba)}{(\epsilon_{ab}-\epsilon_{nv})(\epsilon_{cd}-\epsilon_{nv})} \\
& + \sum_{amnrs}\sum_{kk'k''} \frac{1}{[j_v]} \begin{Bmatrix} k & k' & k'' \\ j_m & j_s & j_a \end{Bmatrix} \begin{Bmatrix} k & k' & k'' \\ j_n & j_r & j_v \end{Bmatrix} \frac{Z_k(avsr) X_{k'}(nmva) X_{k''}(rsnm)}{(\epsilon_{va}-\epsilon_{mn})(\epsilon_{va}-\epsilon_{rs})}.
\end{aligned}
\tag{209}
$$

References

[1] G. E. Brown and D. G. Ravenhall, Proc. Roy. Soc. A **208**, 552 (1951).

[2] M. H. Mittleman, Phys. Rev. A **4**, 893 (1971).

[3] M. H. Mittleman, Phys. Rev. A **5**, 2395 (1972).

[4] M. H. Mittleman, Phys. Rev. A **24**, 1167 (1981).

[5] J. Sucher, Phys. Rev. A **22**, 348 (1980).

[6] A. R. Edmonds, *Angular Momentum in Quantum Mechanics* (Princeton University Press, Princeton, New Jersey, 1974).

[7] W. Magnus and F. Oberhettinger, *Formulas and Theorems for the Functions of Mathematical Physics* (Chelsea, New York, 1949).

[8] U. D. Jentschura, P. J. Mohr, and G. Soff, Phys. Rev. A **63**, 042512 (2001).

[9] P. J. Mohr, Ann. Phy. (N.Y.) **88**, 26 (1974).

[10] P. J. Mohr, Ann. Phy. (N.Y.) **88**, 52 (1974).

[11] P. J. Mohr, Phy. Rev. A **26**, 2338 (1982).

[12] P. J. Mohr, Phy. Rev. A **46**, 4421 (1992).

[13] P. J. Mohr and Y. Kim, Phy. Rev. A **45**, 2727 (1992).

[14] P. J. Mohr and G. Soff, Phys. Rev. Lett. **70**, 158 (1993).

[15] K. Pachucki, D. Leibfreid, M. Weitz, A. Huber, W. König, and T. W. Hänsch, J. Phys. B **29**, 177 (1996).

[16] M. I. Eides, H. Grotch, and A. Shelyuto, Phys. Rep. **342**, 63 (2001).

[17] E. A. Uehling, Phys. Rev. **48**, 55 (1935).

[18] E. H. Wichmann and N. H. Kroll, Phys. Rev. **101**, 843 (1956).

[19] M. Baranger, F. J. Dyson, and E. E. Salpeter, Phys. Rev. **88**, 680 (1952).

[20] K. Bechert and J. Meixner, Ann. Physik **22**, 525 (1935).

[21] G. Breit and G. E. Brown, Phys. Rev. **74**, 1278 (1948).

[22] W. A. Baker and F. N. Glover, Phys. Rev. **99**, 317 (1955).

[23] J. R. Sapirstein and D. R. Yennie, in *Quantum Electrodynamics*, edited by T. Kinoshita (World Scientific, Singapore, 1990).

[24] B. E. Lathrup, A. Peterman, and E. de Rafael, Phys. Rep. **3**, 193 (1972).

[25] G. W. Erickson and D. R. Yennie, Ann. Phys. (N.Y.) **35**, 271 (1965).

[26] H. Grotch and D. R. Yennie, Rev. Mod. Phys. **41**, 350 (1969).

[27] W. R. Johnson and G. Soff, At. Data & Nucl. Data Tables **33**, 405 (1985).

[28] H. F. Beyer, H.-J. Kluge, and V. P. Shevelko, *X-Ray Radiation of Highly Charged Ions* (Springer-Verlag, Berlin, 1997).

[29] H. A. Bethe and E. E. Salpeter, *Quantum Mechanics of One- ans Two-Electron Atoms* (Academic Press, New York, 1957).

[30] I. Lindgren and J. Morrison, *Atomic Many-Body Theory* (Springer-Verlag, 1986), 2nd ed.

[31] W. R. Johnson, S. A. Blundell, and J. Sapirstein, Phys. Rev. A **37**, 2767 (1988).

[32] J. B. Mann and W. R. Johnson, Phys. Rev. A **4**, 44 (1971).

[33] C. deBoor, *A Practical Guide to Splines* (Springer, New York, 1978).

[34] A. Chodos, R. L. Jaffe, K. Johnson, C. B. Thorn, and V. W. Weisskopf, Phys. Rev. D **9**, 3471 (1974).

[35] J. J. Sakurai, *Advanced Quantum Mechanics* (Addison-Wesley, Reading, MA, 1967).

[36] W. R. Johnson, S. A. Blundell, and J. Sapirstein, Phys. Rev. A **37**, 307 (1988).

[37] E. Anderson, Z. Bai, C. Bischof, S. Blackford, J. Demmel, J. Dongarra, J. Du Croz, A. Greenbaum, S. Hammarling, A. McKenney, et al., *LAPACK User's Guide* (SIAM, Philadelphia, 1999).

[38] E. Lindroth, Phys. Rev. A **37**, 316 (1986).

[39] S. A. Blundell, W. R. Johnson, Z. W. Liu, and J. Sapirstein, Phys. Rev. A **39**, 3768 (1989).

[40] W. R. Johnson and J. Sapirstein, Phys. Rev. A **46**, R2197 (1992).

[41] D. Plante, W. R. Johnson, and J. Sapirstein, Phys. Rev. A **49**, 3519 (1994).

[42] S. A. Blundell, D. S. Guo, W. R. Johnson, and J. Sapirstein, At. Data & Nucl. Data Tables **37**, 103 (1987).

[43] J. E. Sienkwicz and W. E. Baylis, J. Phys. B **25**, 2081 (1992).

[44] K. A. Brueckner, Phys. Rev. **96**, 508 (1954).

[45] R. K. Nesbet, Phys. Rev. **109**, 1632 (1958).

[46] J. Schweppe, A. Belkacem, L. Blumenfeld, N. Claytor, B. Feinberg, H. Gould, V. E. Kostroun, L. Levy, S. Misawa, J. R. Mowat, et al., Phys. Rev. Lett. **66**, 1434 (1991).

[47] P. Beiersdorfer, D. Knapp, R. E. Marrs, S. R. Elliott, and M. H. Chen, Phys. Rev. Lett. **71**, 3939 (1993).

[48] P. Beiersdorfer, Nucl. Instrum. Methods Phys. Res. B **99**, 114 (1995).

[49] J. D. Zumbro, E. B. Shera, Y. Tanaka, C. E. Bemis, Jr., R. A. Naumann, M. V. Hoehn, W. Reuter, and R. M. Steffen, Phys. Rev. Lett. **53**, 1888 (1984).

[50] V. A. Yerokhin, A. N. Artemyev, T. Beier, G. Plunien, V. M. Shabaev, and G. Soff, Phys. Rev. A **60**, 3522 (1999).

[51] S. A. Blundell, Phys. Rev. A **47**, 1790 (1993).

[52] Ph. Bosselmann, U. Staude, D. Horn, K.-H. Schartner, F. Folkmann, A. E. Livingston, and P. H. Mokler, Phys. Rev. A **59**, 1874 (1999).

[53] S. A. Blundell, W. R. Johnson, and J. Sapirstein, Phys. Rev. A **37**, 2764 (1988).

[54] S. A. Blundell, W. R. Johnson, Z. W. Liu, and J. Sapirstein, Phys. Rev. A **40**, 2233 (1989).

[55] J. Sapirstein, K. T. Cheng, and M. H. Chen, Phys. Rev. A **59**, 259 (2001).

[56] S. A. Blundell, P. J. Mohr, W. R. Johnson, and J. Sapirstein, Phys. Rev. A **48**, 2615 (1993).

[57] I. Lindgren, H. Persson, S. Salomonson, and L. Labzowski, Phys. Rev. A **51**, 1167 (1995).

[58] W. H. Furry, Phys. Rev. **81**, 115 (1951).

[59] Y. K. Kim, Phys. Rev. **154**, 17 (1967).

[60] F. Mark and W. H. E. Schwarz, Phys. Rev. Lett. **48**, 673 (1982).

[61] R. E. Stanton and S. Havriliak, J. Chem. Phys. **81**, 1910 (1984).

[62] I. P. Grant, in *Atomic, Molecular and Optical Physics Hankbook*, edited by G. W. F. Drake (AIP Press, Woodbury, New York, 1996), chap. 22.

[63] Y. K. Kim, F. Parente, J. P. Marques, P. Indelicato, and J. P. Desclaux, Phys. Rev. A **58**, 1885 (1998).

[64] E. R. Davidson, J. Comput. Phys. **17**, 87 (1975).

[65] A. Stathopoulos and C. F. Fischer, Comput. Phys. Commum. **79**, 1 (1994).

[66] M. H. Chen, K. T. Cheng, and W. R. Johnson, Phys. Rev. A **47**, 3692 (1993).

[67] K. T. Cheng, M. H. Chen, W. R. Johnson, and J. Sapirstein, Phys. Rev. A **50**, 247 (1994).

[68] K. T. Cheng and M. H. Chen, Phys. Rev. A **61**, 044503 (2000).

[69] G. W. F. Drake, Can. J. Phys. **66**, 586 (1988).

[70] Y. Accad, C. L. Pekeris, and B. Schiff, Phys. Rev. A **4**, 516 (1971).

[71] W. R. Johnson, D. R. Plante, and J. Sapirstein, in *Advances in Atomic, Molecular, and Optical Physics*, edited by B. Bederson and H. Walther (Academic Press, San Diego, 1995), p. 251.

[72] W. R. Johnson and K. T. Cheng, Phys. Rev. A **53**, 1375 (1996).

[73] W. R. Johnson, K. T. Cheng, and D. R. Plante, Phys. Rev. A **55**, 2728 (1997).

[74] A. Derevianko, I. M. Savukov, W. R. Johnson, and D. R. Plante, Phys. Rev. A **58**, 4453 (1998).

[75] I. M. Savukov and W. R. Johnson, Phys. Rev. A **62**, 052506 (2000).

[76] M. H. Chen, K. T. Cheng, W. R. Johnson, and S. Sapirstein, Phys. Rev. A **52**, 266 (1995).

[77] K. T. Cheng, M. H. Chen, and S. Sapirstein, Phys. Rev. A **62**, 054501 (2000).

[78] M. H. Chen and K. T. Cheng, Phys. Rev. A **55**, 166 (1997).

[79] M. H. Chen and K. T. Cheng, Phys. Rev. A **55**, 3440 (1997).

[80] K. T. Cheng and M. H. Chen, Phys. Rev. A **53**, 2206 (1996).

[81] M. H. Chen, K. T. Cheng, P. Beiersdorfer, and J. Sapirstein, Phys. Rev. A (2003), in press.

[82] A. Bar-Shalom and M. Klapisch, Comput. Phys. Commun. **50**, 375 (1988).

[83] K. G. Dyall, I. P. Grant, C. T. Johnson, F. A. Parpia, and E. P. Plummer, Comput. Phys. Commun. **55**, 425 (1989).

[84] G. Gaigalas, S. Fritzsche, and I. P. Grant, Comput. Phys. Commun. **139**, 263 (2001).

[85] S. A. Blundell, W. R. Johnson, and J. Sapirstein, Phys. Rev. A **41**, 1698 (1990).

[86] M. S. Safronova, W. R. Johnson, and U. I. Safronova, Phys. Rev. A **53**, 4036 (1996).

[87] X. W. Zhu and K. T. Chung, Phys. Rev. A **50**, 3818 (1994).

[88] K. T. Cheng, W. R. Johnson, and J. Sapirstein, Phys. Rev. Lett. **66**, 2960 (1991).

[89] K. T. Cheng, W. R. Johnson, and J. Sapirstein, Phys. Rev. A **47**, 1817 (1993).

[90] G. Soff and P. J. Mohr, Phys. Rev. A **38**, 5066 (1988).

[91] H. Persson, I. Lindgren, S. Salomonson, and P. Sunnergren, Phys. Rev. A **48**, 2772 (1993).

[92] T. Beier, G. Plunien, M. Greiner, and G. Soff, J. Phys. B **30**, 2761 (1997).

[93] J. Sapirstein and K. T. Cheng, Phys. Rev. A (2003), to be published.

[94] H. Persson, S. Salomonson, P. Sunnergren, and I. Lindgren, Phys. Rev. Lett. **76**, 204 (1996).

[95] V. A. Yerokhin, A. N. Artemyerv, and V. M. Shabaev, Phys. Lett. A **234**, 361 (1997).

[96] J. Sapirstein and K. T. Cheng, Phys. Rev. A **64**, 022502 (2001).

[97] P. Beiersdorfer, A. L. Osterheld, J. H. Scofield, J. R. C. López-Urrutia, and K. Widmann, Phys. Rev. Lett. **80**, 3022 (1998).

[98] S. Mallampalli and J. Sapirstein, Phys. Lett. A **57**, 1548 (1998).

[99] V. A. Yerokhin and V. M. Shabaev, Phys. Rev. A **64**, 062507 (2001).

[100] T. Stöhlker, P. H. Mokler, F. Bosch, R. W. Dunford, F. Franzke, O. Klepper, C. Kozhuharov, T. Ludziejewski, F. Nolden, H. Reich, et al., Phys. Rev. Lett. **85**, 3109 (2000).

Index